The *Planck* satellite: from the first astrophysical results to cosmological promises

Carlo Burigana @ INAF/IASF Bologna

in collaboration with
Alessandro Gruppuso, Nazzareno Mandolesi,
Paolo Natoli, Pietro Procopio

On behalf of the *Planck* Collaboration

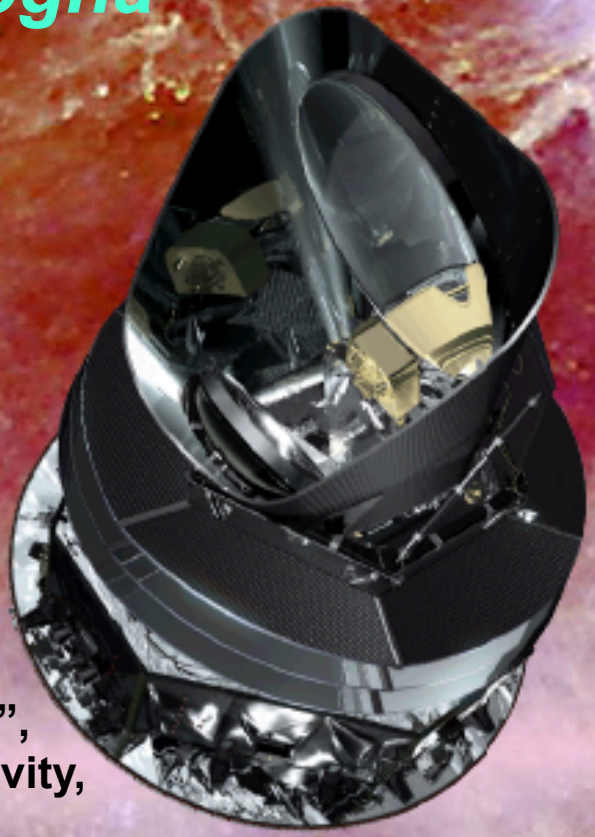

The 15th Paris Cosmology Colloquium 2011
"From Cold Dark Matter to Warm Dark Matter in the Standard Model of the Universe: Theory and Observations",
The International School Daniel Chalonge: 20 Years of Activity,
Observatoire de Paris, Paris campus, 20-22 July 2011

Cosmic Microwave Background Radiation Overview

The oldest light or the first light of the Universe

1965 — Penzias and Wilson

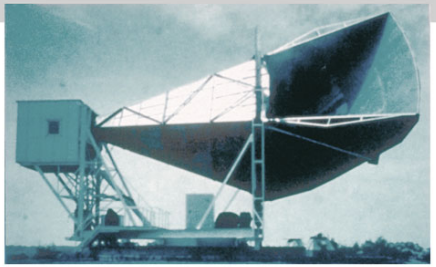

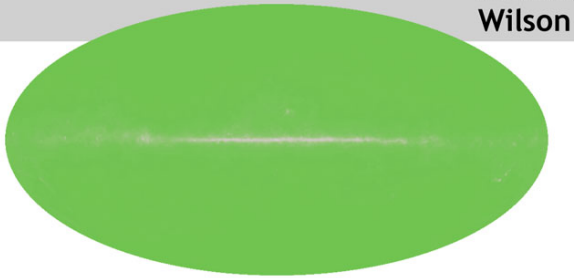

Discovered the remnant afterglow from the **Big Bang**.
→ **2.7 K**

1992 — COBE

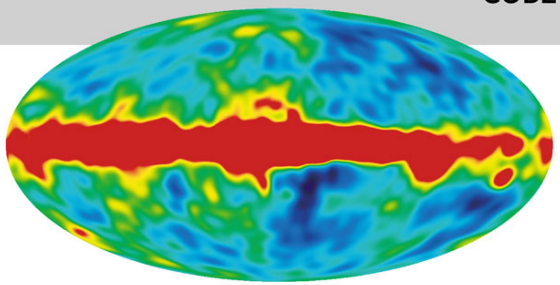

Blackbody radiation,
Discovered the patterns (**anisotropy**) in the afterglow.
→ **angular scale ~ 7°** at a level ΔT/T of 10^{-5}

2003 — WMAP

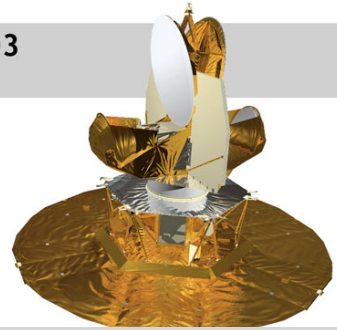

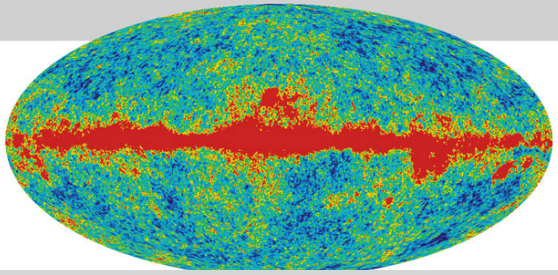

(Wilkinson Microwave Anisotropy Probe):
→ **angular scale ~ 15'**

2009 — Planck

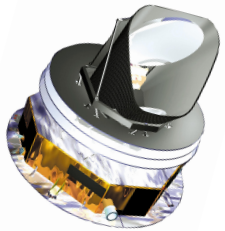

→ **angular scale ~ 5',**
ΔT/T ~ 2×10^{-6}, 30~867 Hz

Why Planck?

COBE - 1989

4-years data

WMAP - 2001

7-years data

PLANCK - 2009

6-months data

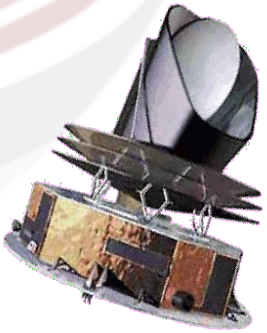

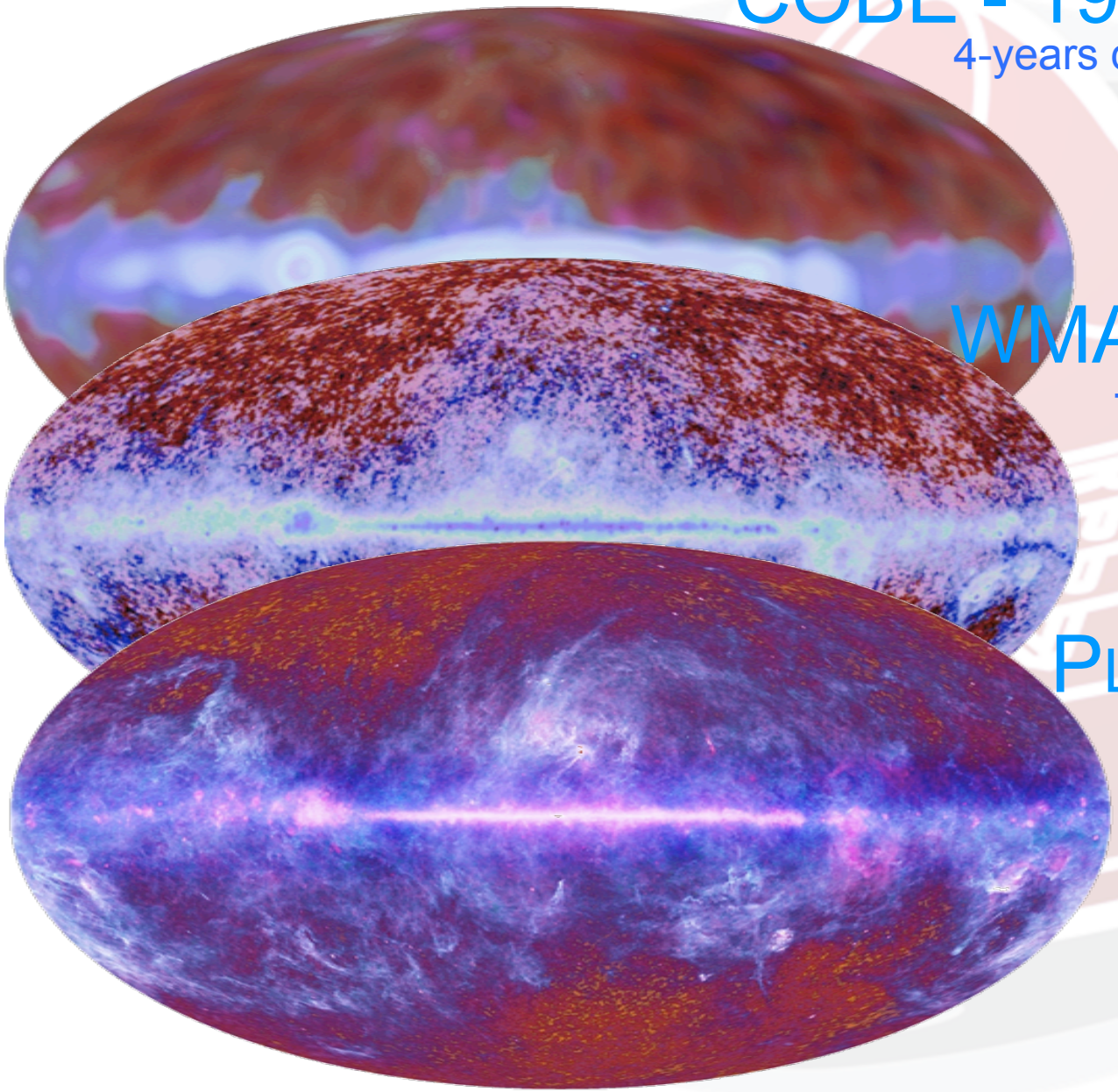

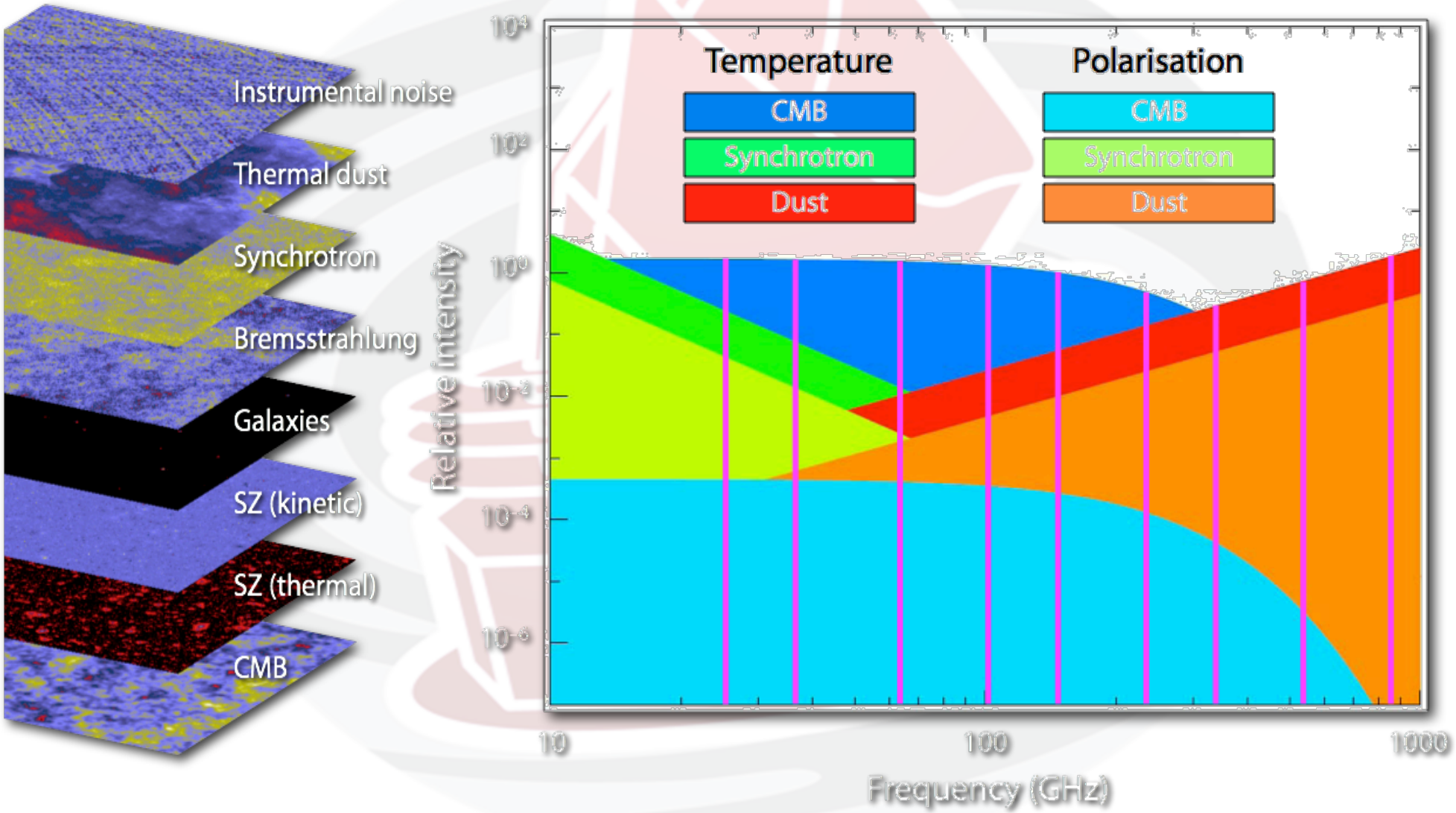
Instrumental noise
Thermal dust
Synchrotron
Bremsstrahlung
Galaxies
SZ (kinetic)
SZ (thermal)
CMB
Temperature
CMB
Synchrotron
Dust
Polarisation
CMB
Synchrotron
Dust
Relative intensity
10
100
1000
Frequency (GHz)

Expected results from simulations

30, 44, 70, 100, 143, 217, 353, 545, 857 GHz – I, Q, U at all channels
Except 545 & 857 GHz

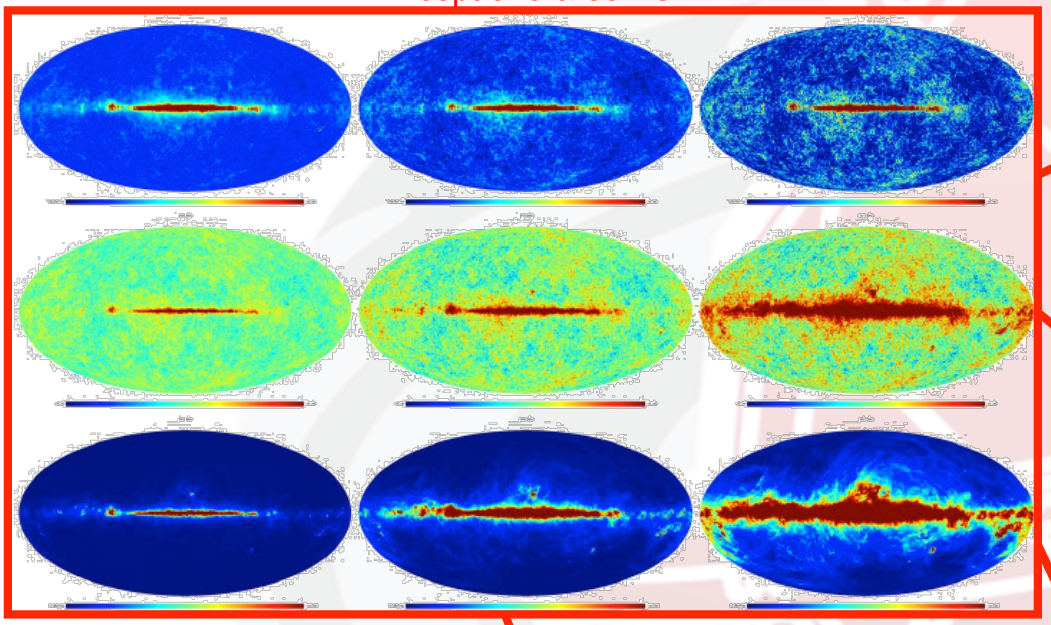

Cosmic Microwave Background

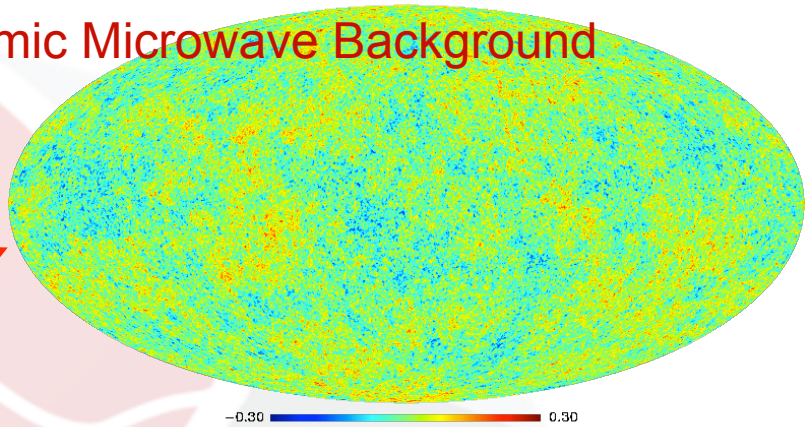

Sunyaev-Zeldovich

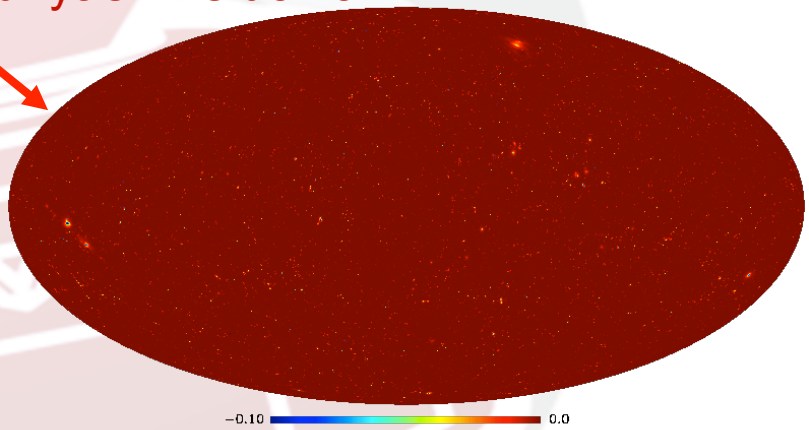

The Milky Way

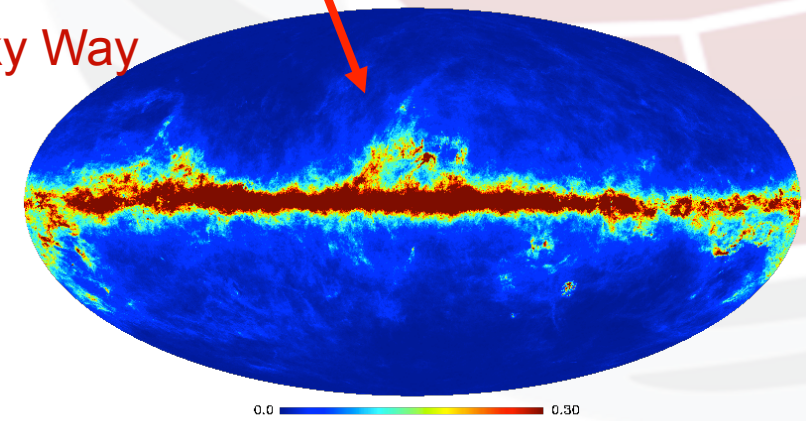

Point & Compact sources

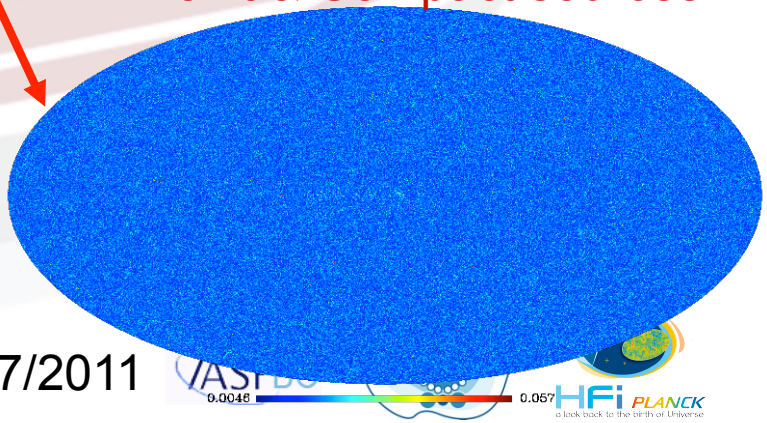

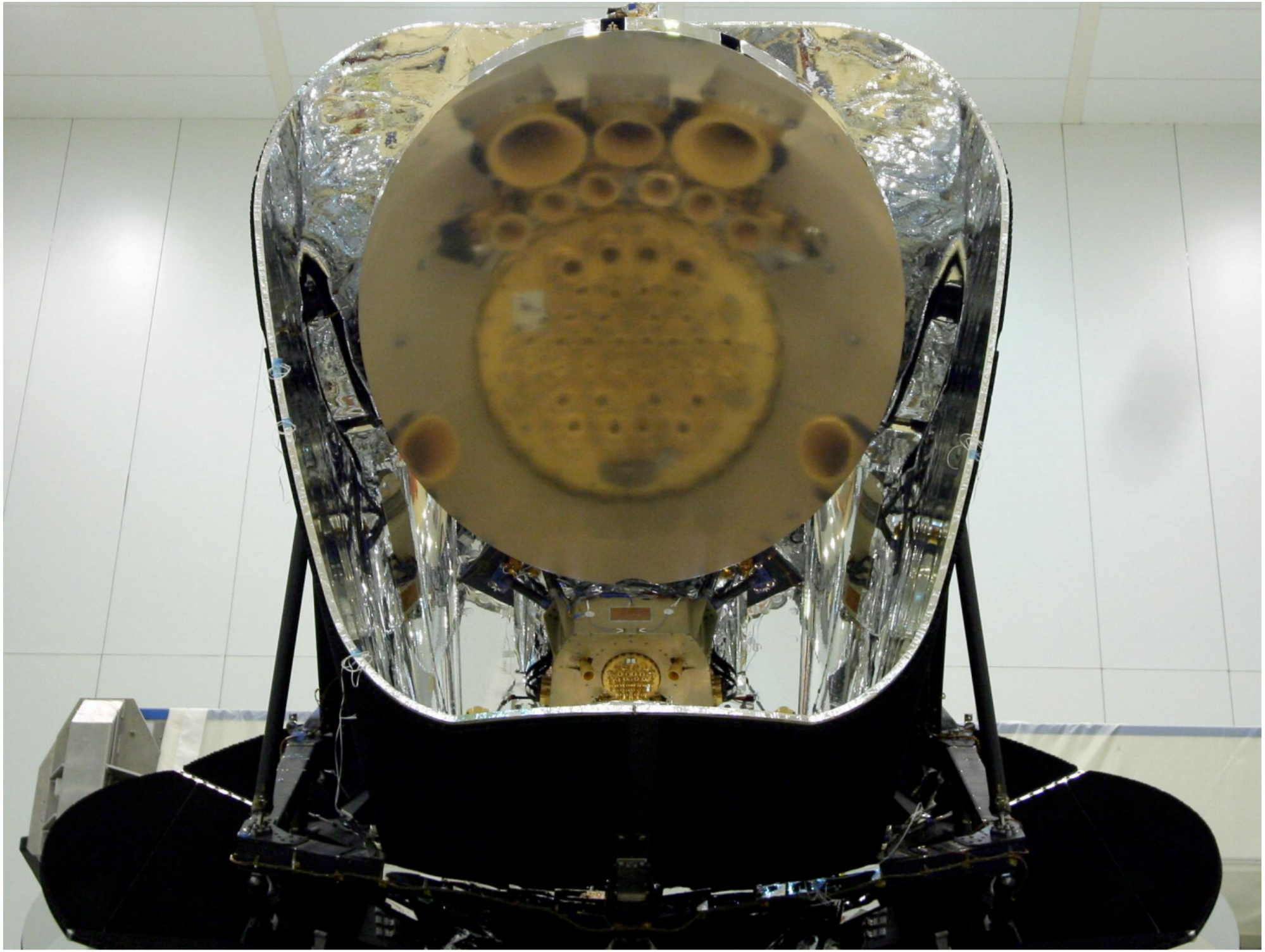

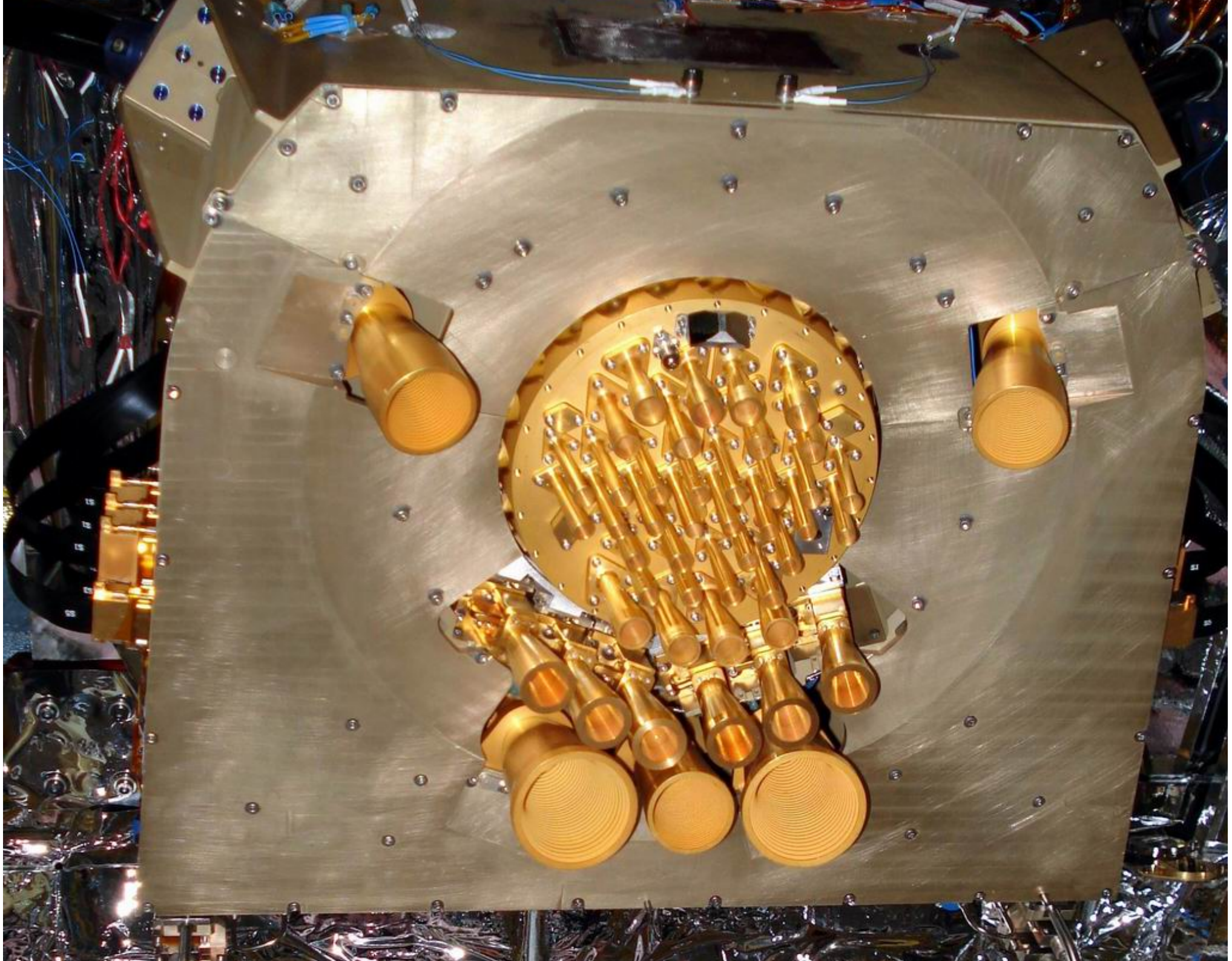

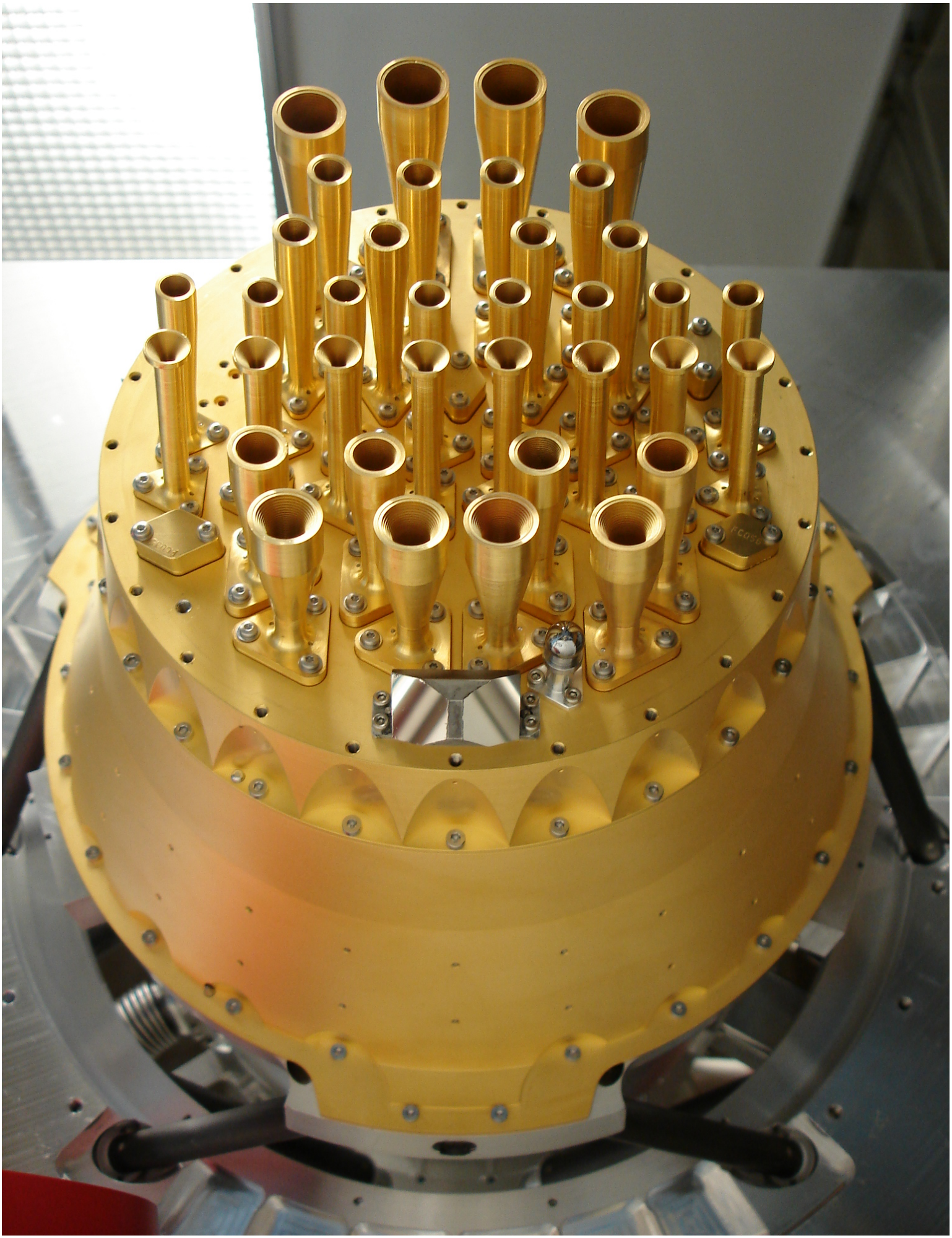

Observing strategy

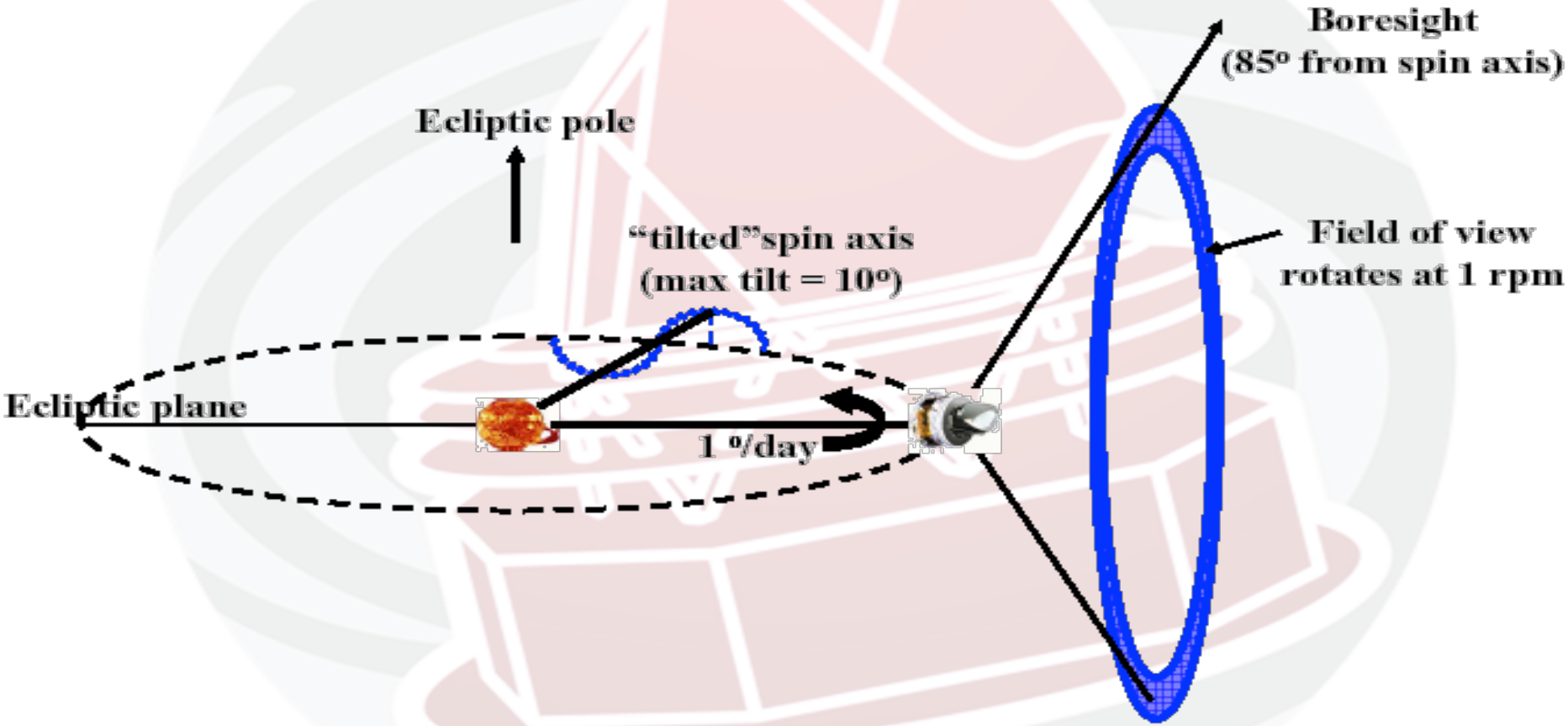

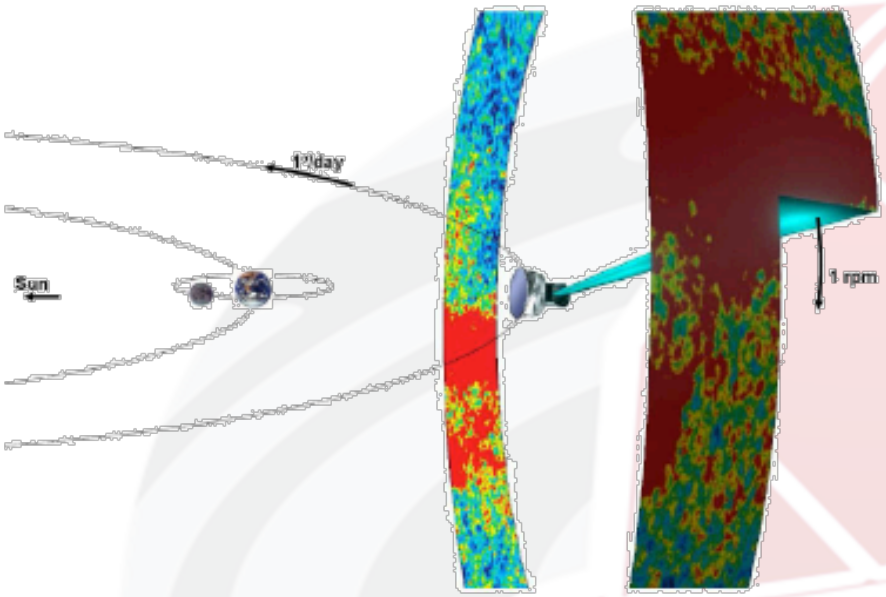

Planck is a survey mission

About 6 months are needed to cover ~95% of the sky.

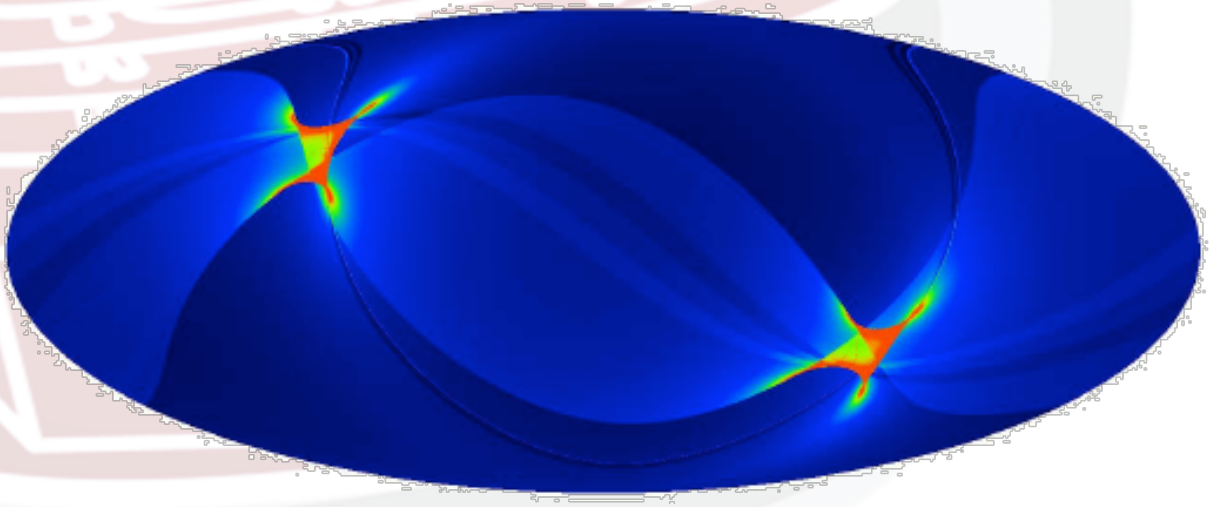

Current Status

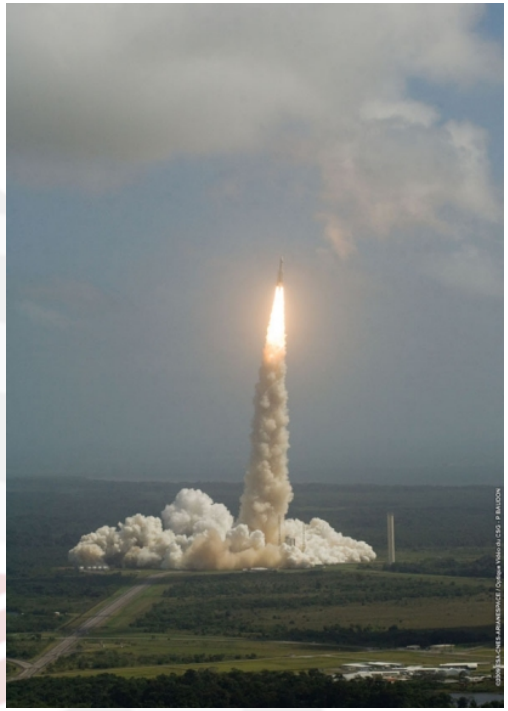

- @ 22 July 2011: 799 days since launch.
- Satellite and instruments working nominally and continuously since start of sky surveys (mid August 2009)
- Sky coverage is 100%
  - **All the sky has been surveyed for about 23.5 months, i.e. about four times.**
  - The currently approved mission operation (to end Nov 2011) will do over > four sky surveys, until the end of the cold phase (end January 2012) with two instruments: HFI + LFI
  - A further 12 months extension has been approved with LFI only

Planck-LFI: the Instrument

Sensitivity, stability & low systematics

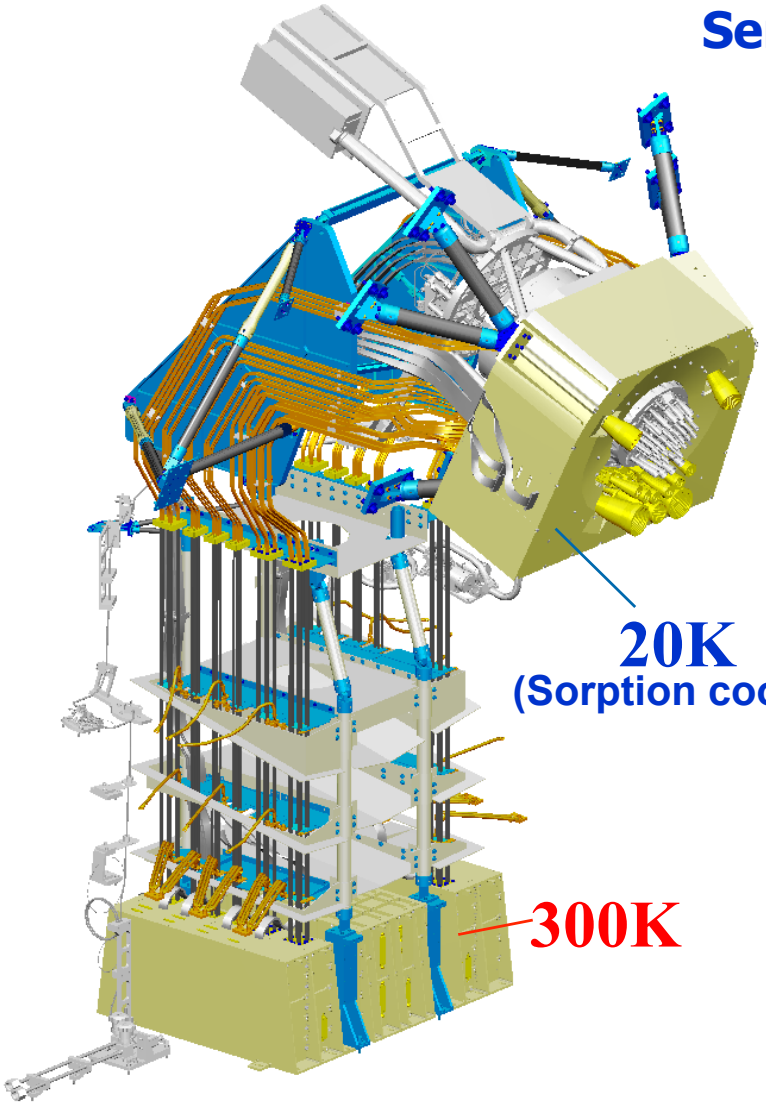

(MB et al 2010, Mandolesi et al 2010)

Sensitivity ($\Delta T/T \sim 3 \times 10^{-6}$/pix)

- State-of-the-art InP LNA technology
- Cryo operation
  20K Sorption Cooler
- 22-element array

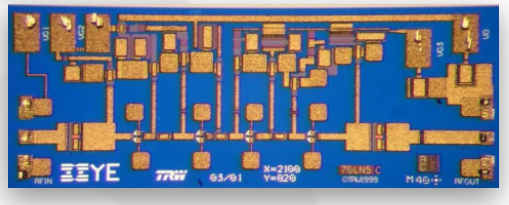

70 GHz MMIC HEMT

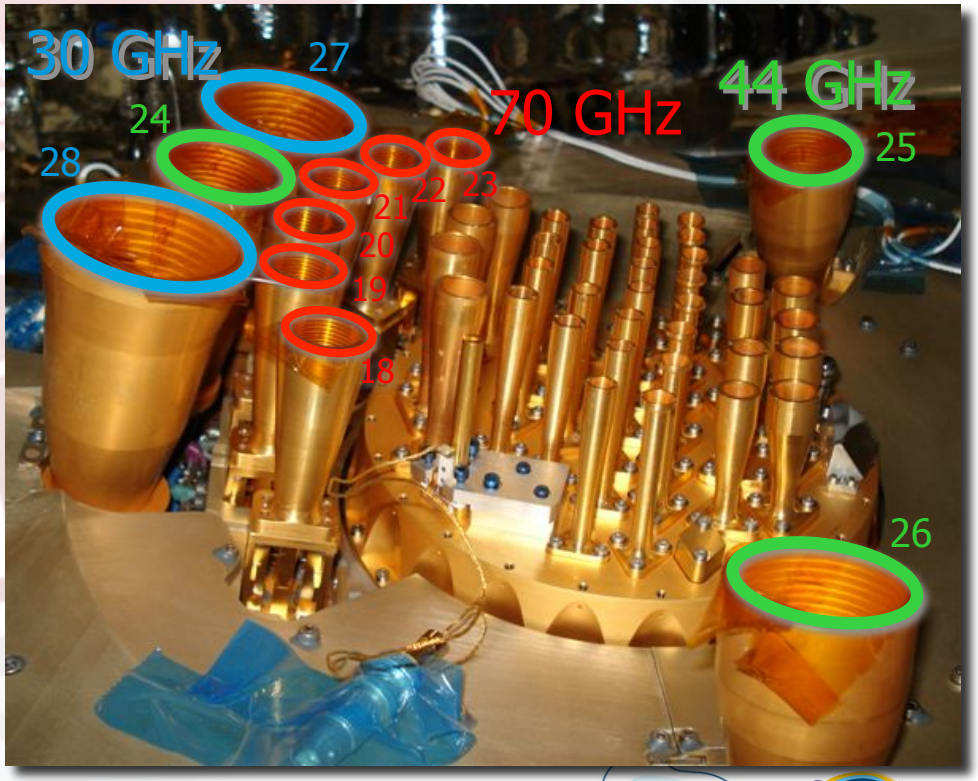

Planck-LFI: the Instrument

Sensitivity, stability & low systematics

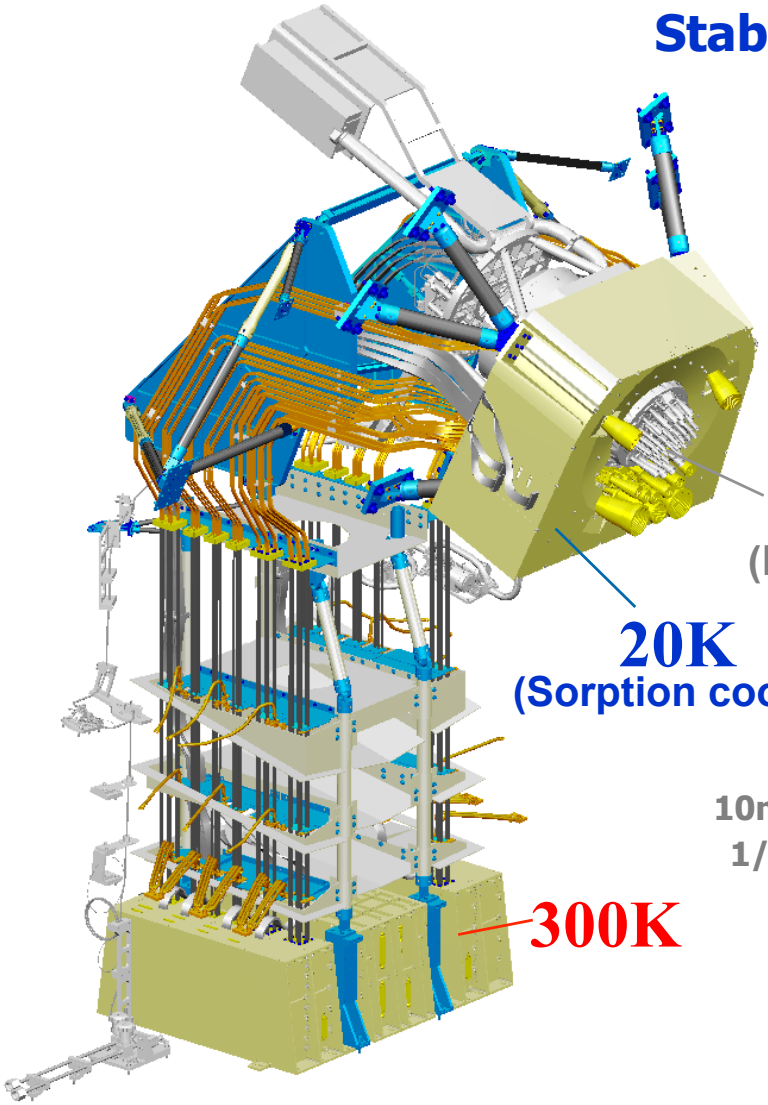

(MB et al 2010, Mandolesi et al 2010)

Stability (f_K < 50 mHz) & Low systematics (~1μK)

- Pseudo-correlation radiometer design
- Refs cooled to 4K

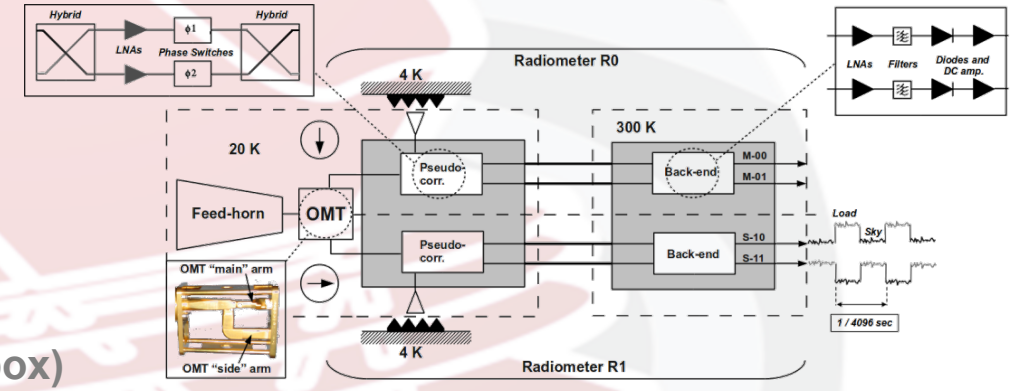

10min of flight data
1/44 LFI detectors
(LFI27S-11)

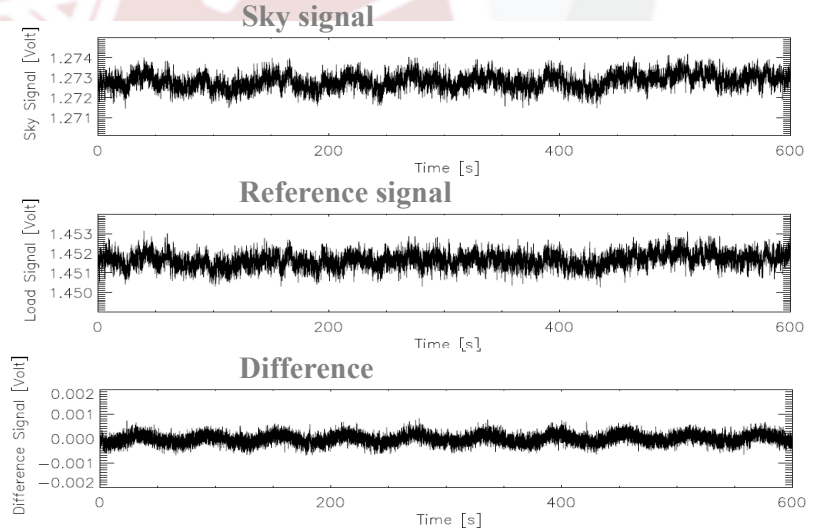

Planck-LFI: Data Processing

(Zacchei, Maino, et al. 2011)

- Beginning of Nominal Survey: 13/08/2009
- *11 Jan 2011 release based on OD's 91-389*
- No significant problems detected, no missed OD's

Percentage of missed data

		30 GHz	44 GHz	70 GHz
Missing	[%]	0.00016	0.00027	0.00039
Anomalies	[%]	0.41412	0.69726	0.41025
Maneuvers	[%]	8.29798	8.29798	8.29798
Usable	[%]	91.28774	91.0049	91.29138

Real gaps

Data flagged as not suitable for science
- Occasional Idrain steps
- DAE gain changes

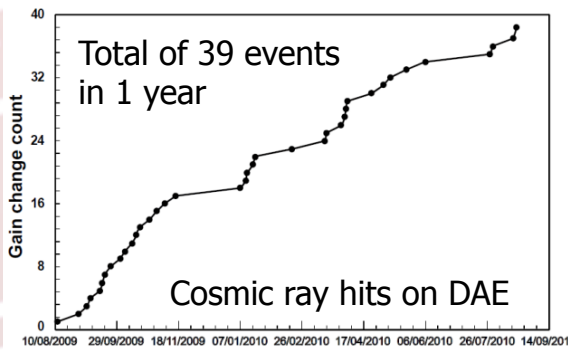

Science data acquired during re-pointing
- Currently not usable by pipeline
- In principle recoverable with full pointing information

- The stability of the pipeline contributed to the creation of ERCSC (first public product from Planck) with high quality

LFI Beams

(Sandri, Villa et al. 2010, 2011)

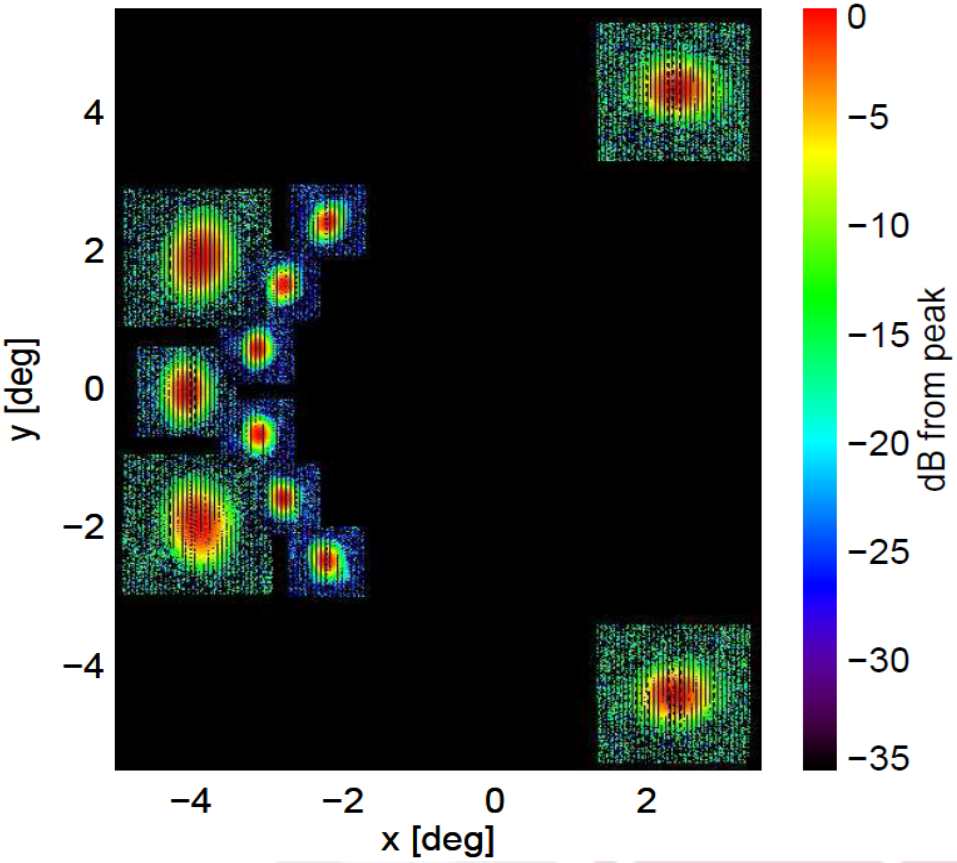

- χ^2 fit of beam model (bivariate Gaussian)
  (Burigana et al. 2001)

- Uncertainty on FWHM ~0.1′-1.3′

- Ellipticity ~1.3, as expected

Good match with model predictions…

- Jupiter is by far best beam calibrator for LFI
  (in LFI beams: 24 Oct – 1 Nov, 2009)
- Use calibrated, differenced TOD's
  → Measure M and S radiometers independently
- 1/f fluctuations removed by destriping (Madam)

Beam ID	FWHM	FWHM Uncertainty
70 GHz		
Ave FWHM: 13′.01; ave e: 1.27		
LFI18	13′.39	0.170′
LFI19	13′.01	0.174′
LFI20	12′.75	0.170′
LFI21	12′.74	0.156′
LFI22	12′.87	0.164′
LFI23	13′.27	0.171′
44 GH		
Ave FWHM: 27′.92		ave e: 1.26
LFI24	22′.98	0.652′
LFI25	30′.46	1.075′
LFI26	30′.31	1.131′
30 GHz		
Ave FWHM: 32′.65		ave$e$: 1.38
LFI27	32′.65	1.266′
LFI28	32′.66	1.287′

Planck-LFI eyes in the sky

Model

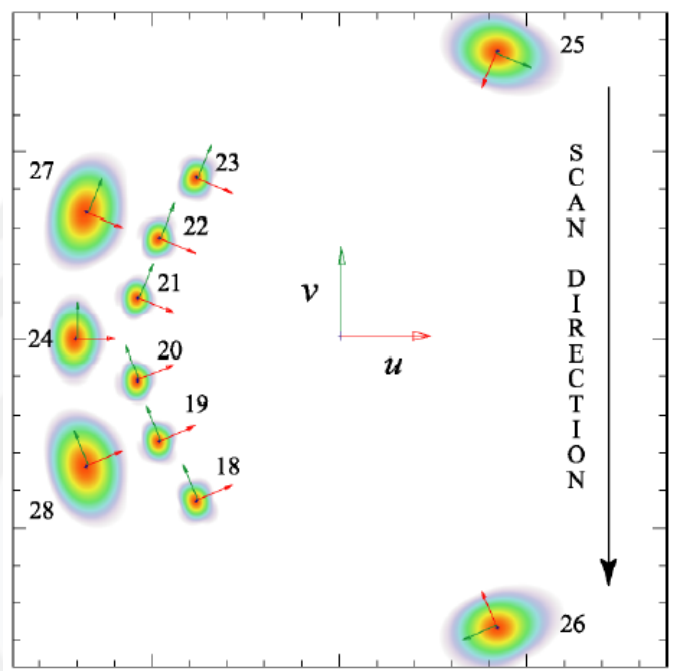

Measurement

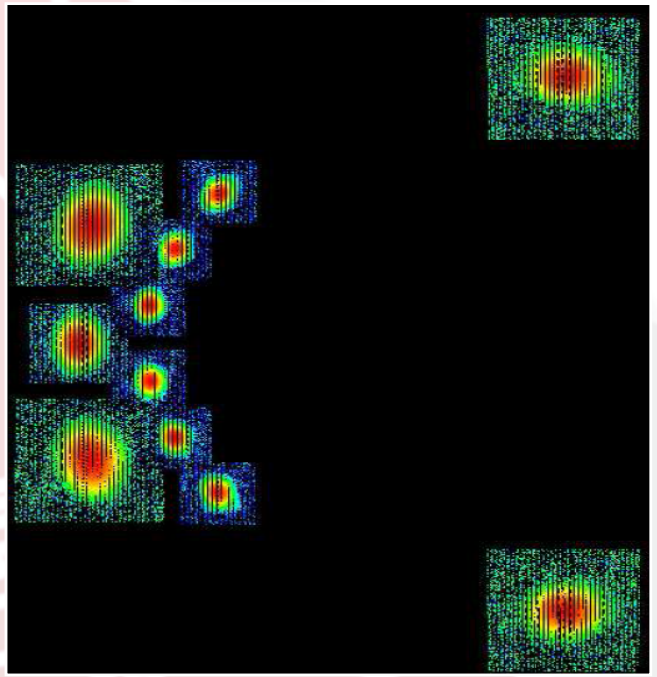

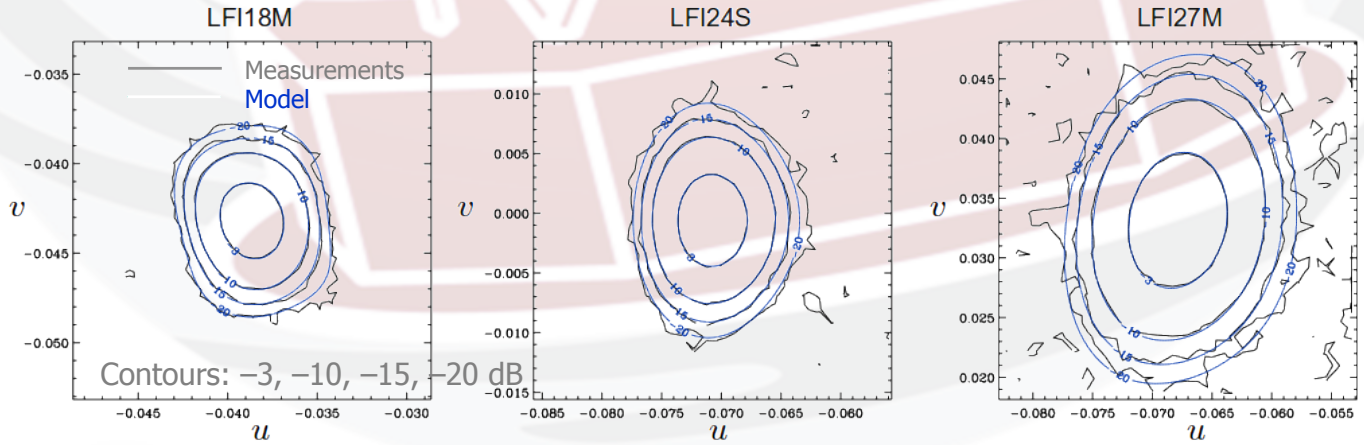

Noise properties

- Noise spectra well described by 2-component (3-parameter) model (of all 22 LFI radiometers)

- Fit to noise power spectra

(Natoli et al. 2001)
(de Gasperis et al. 2005)

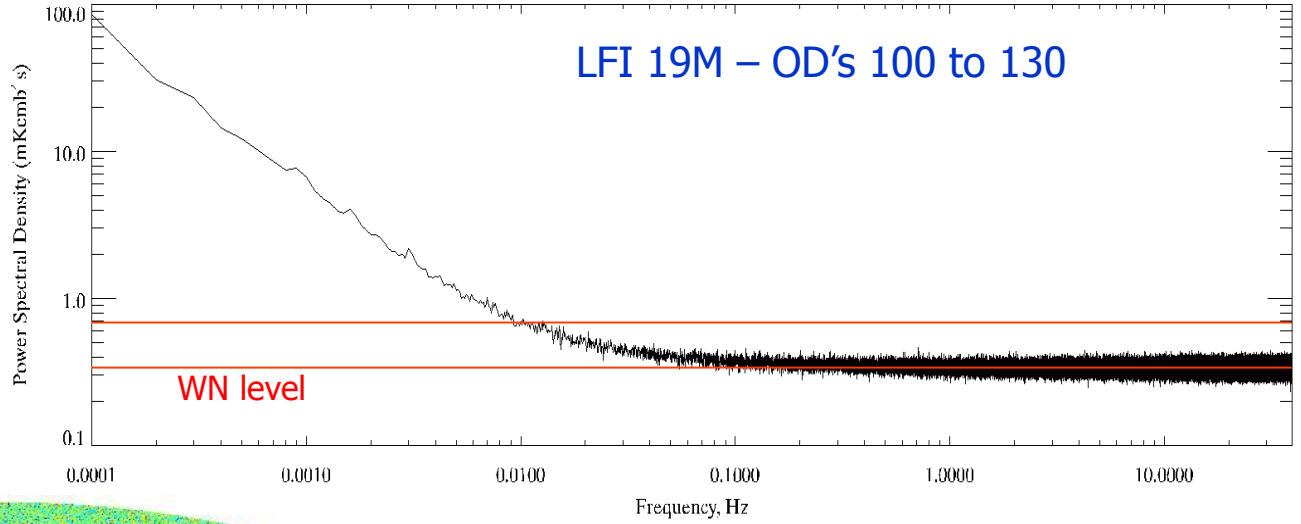

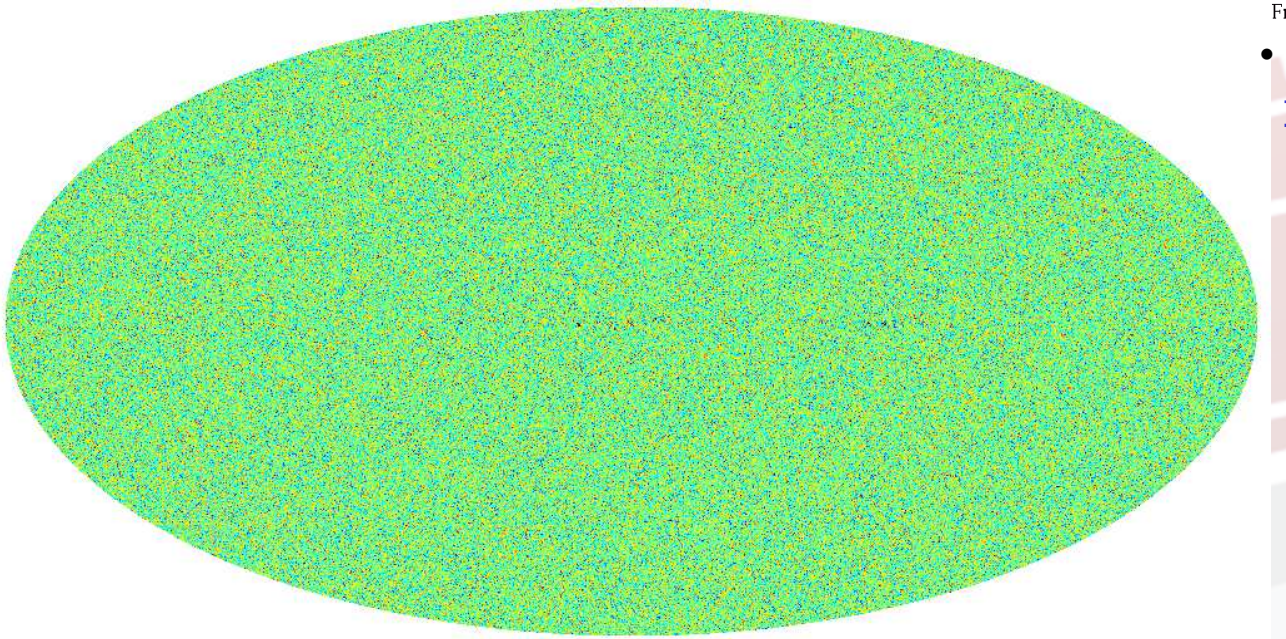

- Map from Jack-knife timelines:
  1st – 2nd half of each pointing period
  - Structure-less map
  - Small residuals on galactic plane due to beam ellipticity

Contribution of residual 1/f to white noise:
4.0% at 30 GHz
1.6% at 44 GHz
0.2% at 70 GHz

Requirement: < 12%

Planck-LFI: rough data

10min of flight data – 1/44 LFI detectors

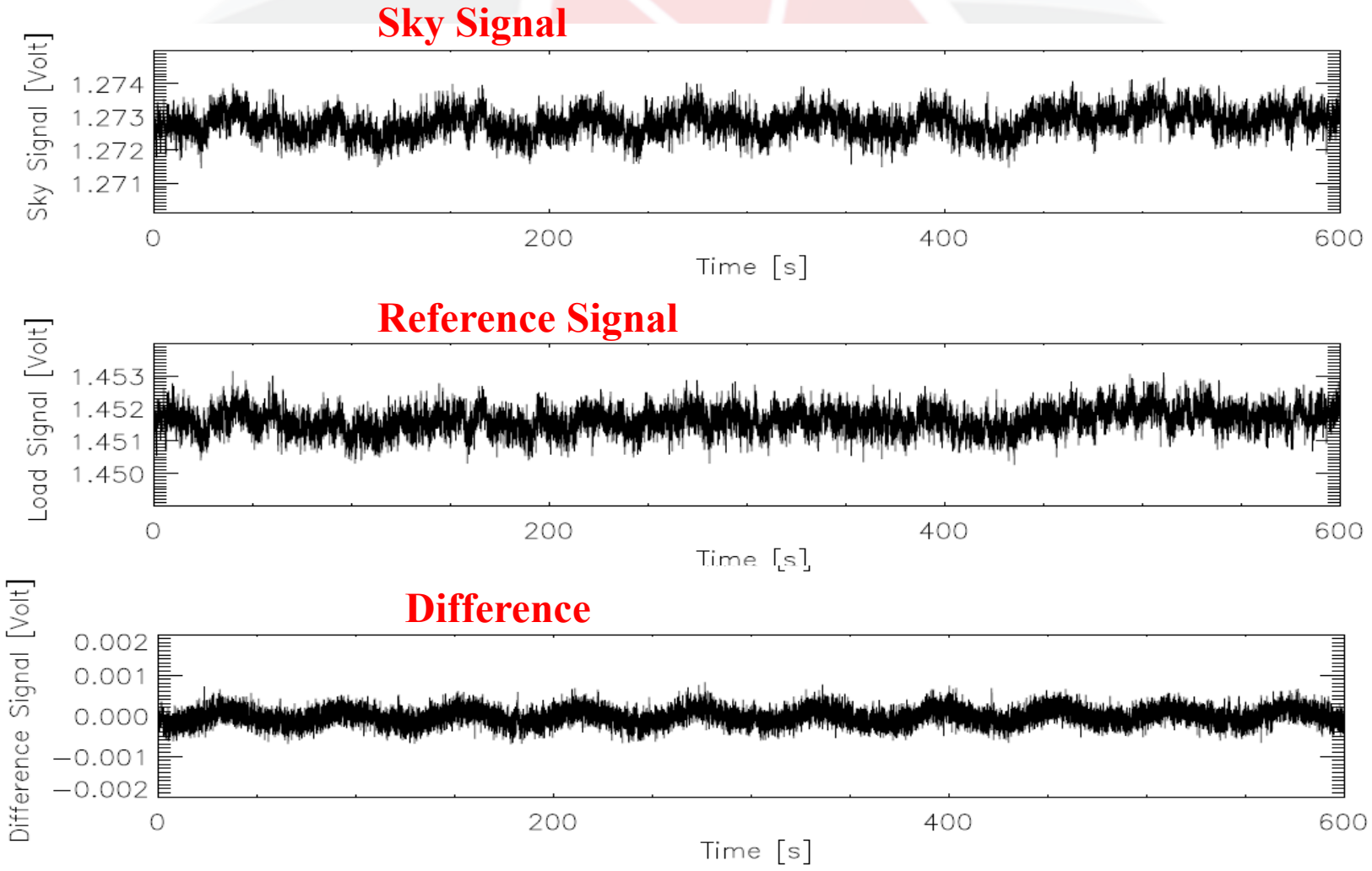

Planck-HFI: rough data

3min of flight data – 1/54 HFI detectors

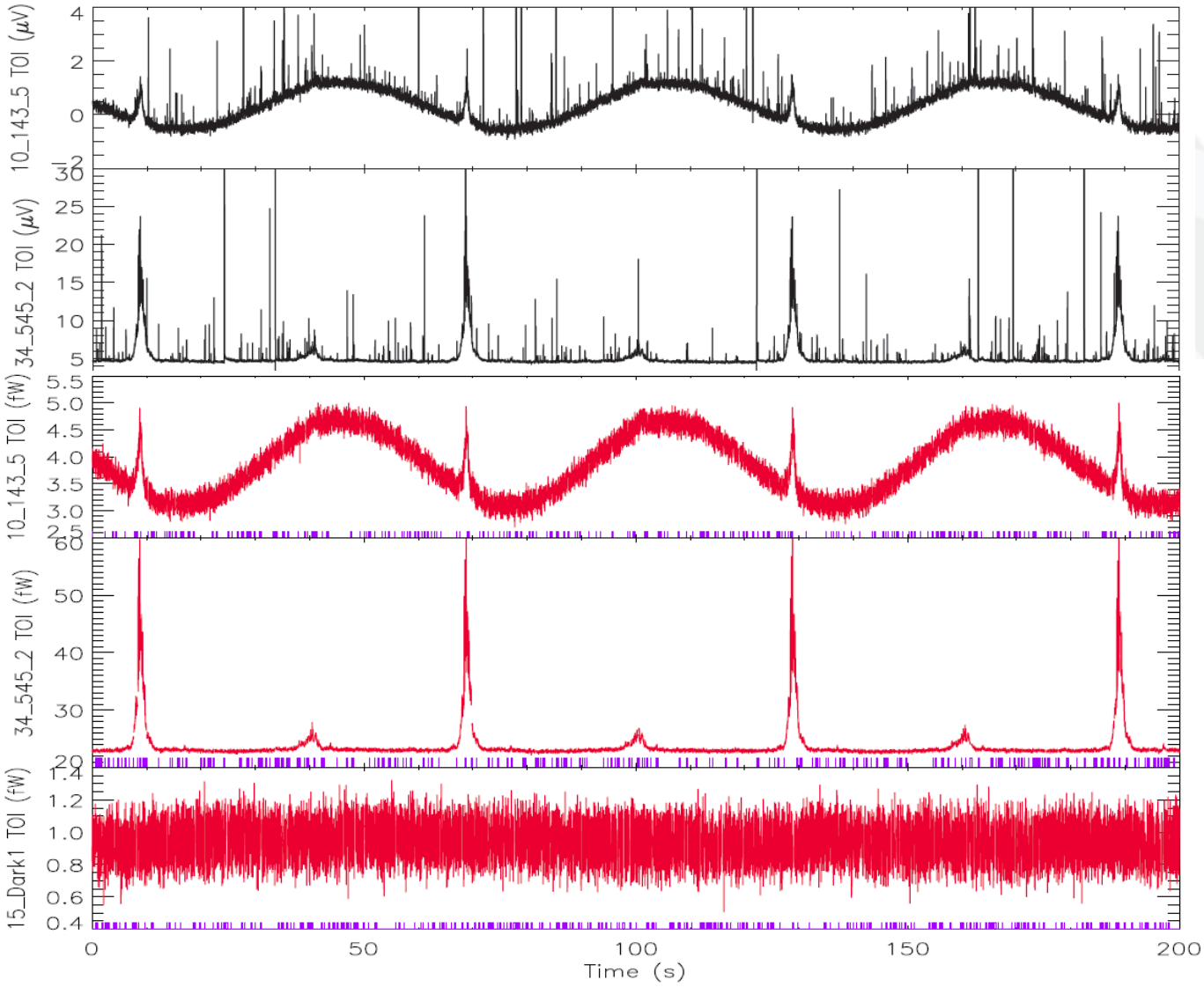

From simulations to reality!

The Planck view of the sky after almost one year of operations (CMB removed)

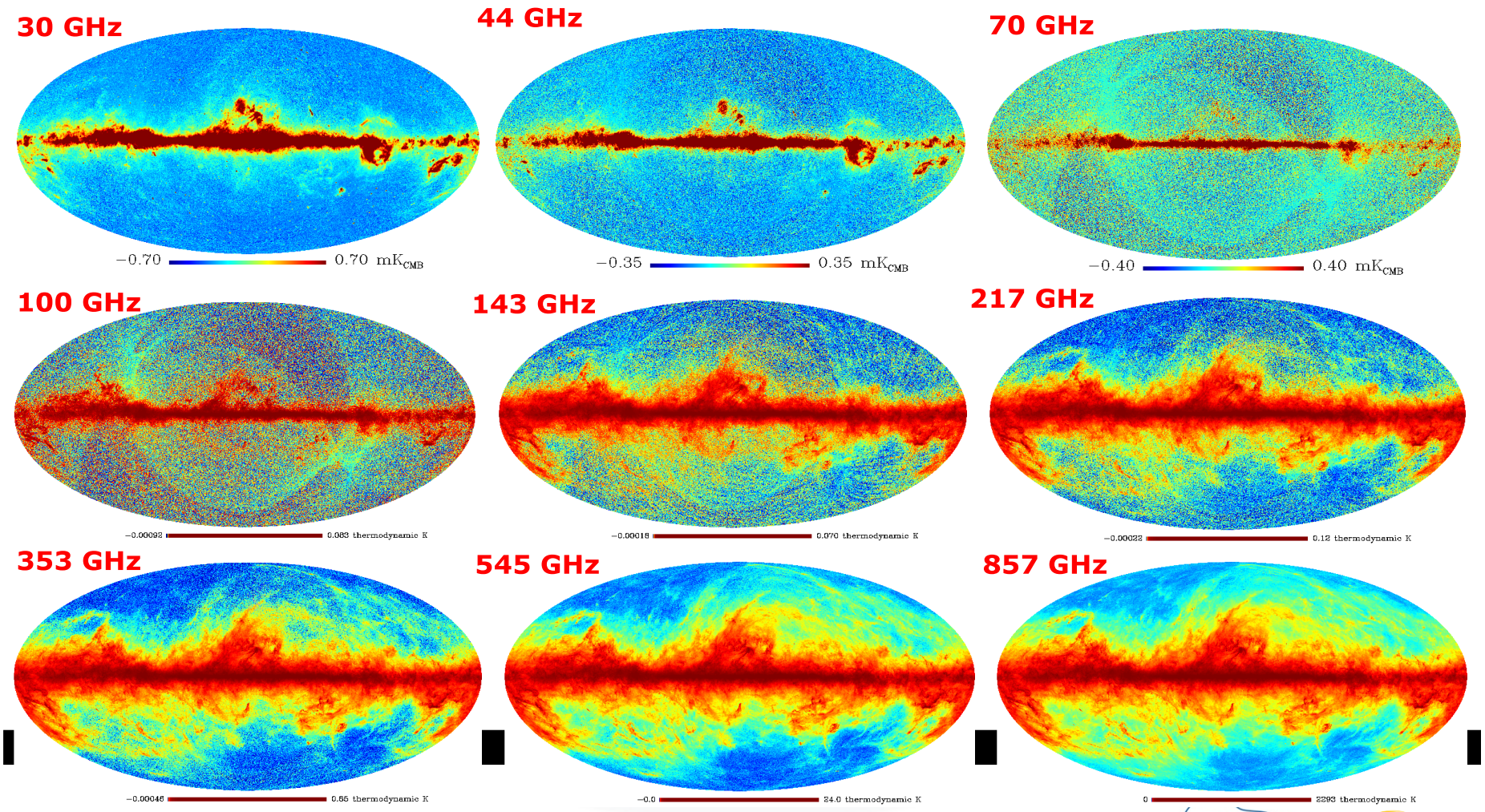

ERCSC

ERCSC arXiv papers

- Planck Early Results: The Early Release Compact Source Catalogue 1101.2041
- The Explanatory Supplement to the Planck Early Release Compact Source Catalogue,

  Planck Collaboration 2011 ESA,

  available @ Planck esa web site

  http://www.rssd.esa.int/Planck

- The catalogue is based on the entire sky once and 60% of the sky a second time
- A Monte-Carlo algorithm based on the injection and extraction of artificial sources into the Planck maps was implemented to select reliable sources among all extracted candidates such that the cumulative reliability of the catalogue is >=90%.
- As a result of the Monte-Carlo assessment of the reliability of sources from different techniques, the PowellSnakes source extraction technique was used at the 5 frequencies between 30 and 143 GHz while the SExtractor technique was used between 217 and 857 GHz.
- The 10 sigma photometric flux density limit of the catalogue at |b|>30 deg is 0.49, 1.0, 0.67, 0.5, 0.33, 0.28, 0.25, 0.47 and 0.82 Jy at each of the nine frequencies between 30 and 857 GHz. Sources which are up to a factor of 2 fainter than this limit, and which are present in "clean" regions of the Galaxy where the sky background due to emission from the interstellar medium is low, are included in the ERCSC if they meet the high reliability criterion
- The Planck ERCSC provides a robust list of stars with dust shells, stellar cores, radio galaxies, blazars, infrared luminous galaxies, Galactic interstellar medium features, 915 cold molecular cloud core candidates, 189 SZ cluster candidates as well as unclassified sources from the first high sensitivity radio/submillimetre observations of the entire sky.

The Planck ERCSC in brief

Freq [GHz]	30	44	70	100	143	217	353	545	857
$\lambda(\mu m)$	10000	6818	4286	3000	2098	1382	850	550	350
Sky Coverage (%)	99.96	99.98	99.99	99.97	99.82	99.88	99.88	99.80	99.79
Beam FWHM $(')^a$	32.65	27.00	13.01	9.94	7.04	4.66	4.41	4.47	4.23
# of Sources	705	452	599	1381	1764	5470	6984	7223	8988
# of $\|b\| > 30°$ Sources	307	143	157	332	420	691	1123	2535	4513
$10\sigma^b$ (mJy)	1173	2286	2250	1061	750	807	1613	2074	2961
$10\sigma^c$ (mJy)	487	1023	673	500	328	280	249	471	813
Flux Density Limit^d (mJy)	480	585	481	344	206	183	198	381	655

Notes. $^{(a)}$ The precise beam values are presented in Planck Collaboration (2011e) and Planck Collaboration (2011f). This table shows the values which were adopted for the ERCSC. $^{(b)}$ Flux density of the median $>10\sigma$ source at $|b| > 30°$ in the ERCSC where σ is the photometric uncertainty of the source. $^{(c)}$ Flux density of the faintest $>10\sigma$ source at $|b| > 30°$ in the ERCSC. $^{(d)}$ Faintest source at $|b| > 30°$ in the ERCSC.

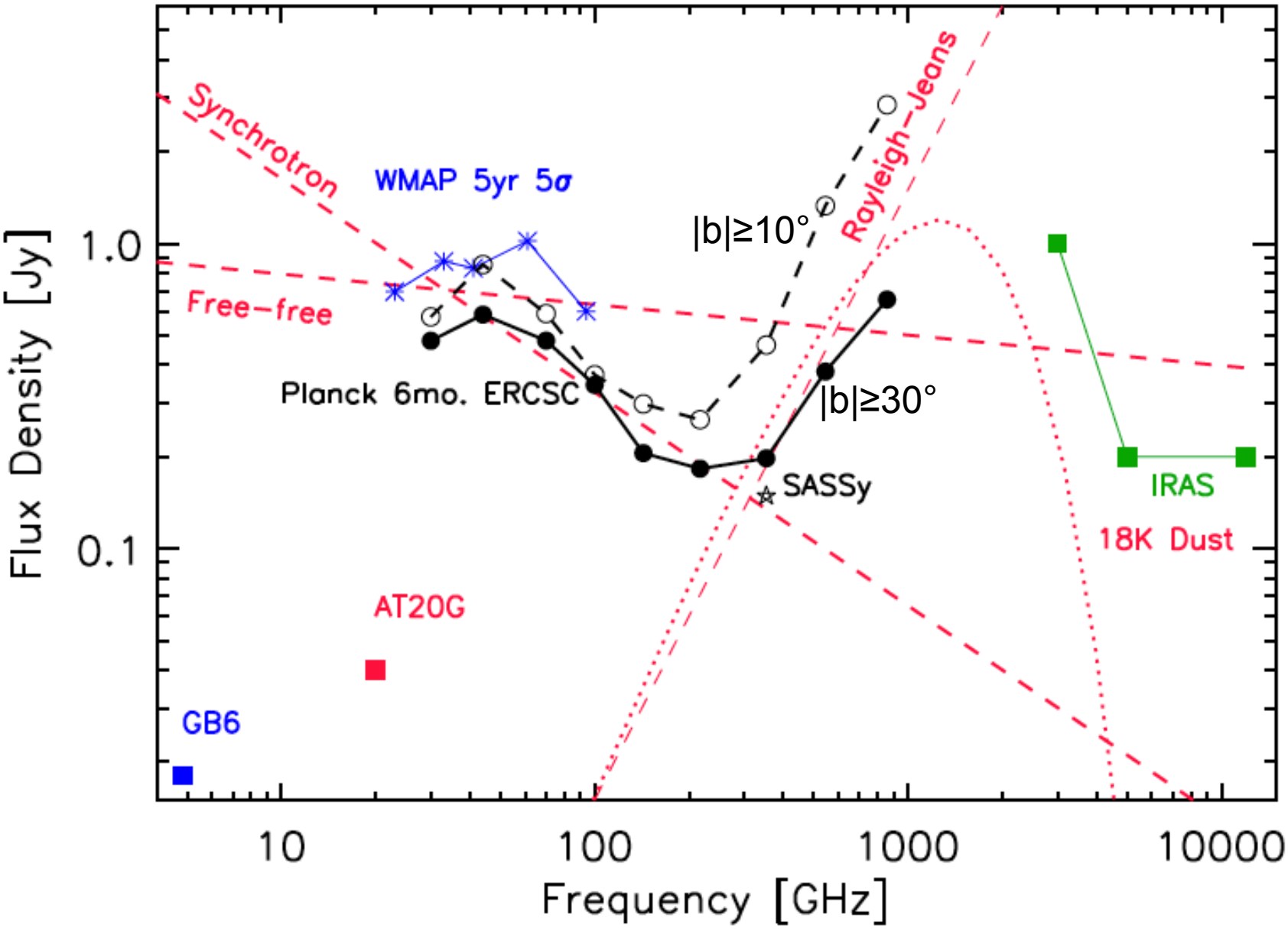
Synchrotron
WMAP 5yr 5σ
Rayleigh–Jeans
|b|≥10°
Free–free
Planck 6mo. ERCSC
|b|≥30°
SASSy
IRAS
18K Dust
AT20G
GB6
Flux Density [Jy]
1.0
0.1
10
100
1000
10000
Frequency [GHz]

Table 2. ERCSC Catalogue Columns

Column Name	Description
	Identification
NAME	Source name
FLUX	Flux density (mJy)
FLUX_ERR	Flux density error (mJy)
CMBSUBTRACT	Flag indicating detection of source in CMB subtracted maps
EXTENDED	Flag indicating that source is extended
DATESOBS	UTC dates at which this source was observed
NUMOBS	Number of days this source observed
CIRRUS	Cirrus flag based on 857 GHz source counts
	Source Position
GLON	Galactic longitude (deg) based on extraction algorithm
GLAT	Galactic latitude (deg) based on extraction algorithm
POS_ERR	Standard deviation of positional offsets for sources with this SNR (arcminute)
RA	Right Ascension (J2000) in degrees transformed from (GLON,GLAT)
DEC	Declination (J2000) in degrees transformed from (GLON,GLAT)
	Effective beam
BEAM_FWHMMAJ	Elliptical Gaussian beam FWHM along major axis (arcmin)
BEAM_FWHMMIN	Elliptical Gaussian beam FWHM along minor axis (arcmin)
BEAM_THETA	Orientation of Elliptical Gaussian major axis (measured East of Galactic North)
	Morphology
ELONGATION	Ratio of major to minor axis lengths
	Source Extraction Results
FLUXDET	Flux density of source as determined by detection method (mJy)
FLUXDET_ERR	Uncertainty (1 sigma) of FLUXDET (mJy)
MX1	First moment in X (arcmin)
MY1	First moment in Y (arcmin)
MX2	Second moment in X ($arcmin^2$)
MXY	Cross moment in X and Y ($arcmin^2$)
MY2	Second moment in Y ($arcmin^2$)
PSFFLUX	Flux density of source as determined from PSF fitting (mJy)
PSFFLUX_ERR	Uncertainty (1 sigma) of PSFFLUX (mJy)
GAUFLUX	Flux density of source as determined from 2-D Gaussian fitting (mJy)
GAUFLUX_ERR	Uncertainty (1 sigma) of GAUFLUX (mJy)
GAU_FWHMMAJ	Gaussian fit FWHM along major axis (arcmin)
GAU_FWHMMIN	Gaussian fit FWHM along minor axis (arcmin)
GAU_THETA	Orientation of Gaussian fit major axis
	Quality Assurance
RELIABILITY	Fraction of MC sources that are matched and have photometric errors < 30%
RELIABILITY_ERR	Uncertainty (1 sigma) in reliabiliy based on Poisson statistics
MCQA_FLUX_ERR	Standard deviation of photometric error for sources with this SNR
MCQA_FLUX_BIAS	Median photometric error for sources with this SNR
BACKGROUND_RMS	Background point source RMS obtained from threshold maps (mJy)
	Bandfilling (857 GHz catalog only)
BANDFILL217	217 GHz Aperture Photometry Flux Density at 857 GHz Source Position (mJy)
BANDFILL217_ERR	Uncertainty in BANDFILL217
BANDFILL353	353 GHz Aperture Photometry Flux Density at 857 GHz Source Position (mJy)
BANDFILL353_ERR	Uncertainty in BANDFILL353
BANDFILL545	545 GHz Aperture Photometry Flux Density at 857 GHz Source Position (mJy)
BANDFILL54_SERR	Uncertainty in BANDFILL545

ERCSC_f030.fits
ERCSC_f044.fits
ERCSC_f070.fits
ERCSC_f100.fits
ERCSC_f143.fits
ERCSC_f217.fits
ERCSC_f353.fits
ERCSC_f545.fits
ERCSC_f857.fits

ESZ.fits
ECC.fits

Table 6. ESZ Catalogue Columns

Keyword	Type
INDEX	Index of clusters i.e., 1, 2, 3...
NAME	*Planck* name of cluster candidate
GLON	Galactic Longitude from *Planck* (deg)
GLAT	Galactic Latitude from *Planck* (deg)
RA	Right Ascension (deg) from *Planck* (J2000)
DEC	Declination (deg) from *Planck* (J2000)
SNR	Signal-to-noise ratio returned by the matched multi-filter (MMF3)
ID	External identifier of cluster e.g., Coma, Abell etc.
REDSHIFT	Redshift of cluster from the MCXC X-ray cluster compilation (Piffaretti et al. 2010) unless stated otherwise in the notes
GLON_X	Galactic Longitude of the associated X-ray cluster (deg)
GLAT_X	Galactic Latitude of the associated X-ray cluster (deg)
RA_X	Right Ascension (deg) of the associated X-ray cluster (J2000)
DEC_X	Declination (deg) of the associated X-ray cluster (J2000)
THETA_X	Angular size (arcmin) at 5R500 from X-ray data.
Y_PSX	Integrated Compton-Y (arcmin^2) at X-ray position and within 5R500 (THETA_X)
Y_PSX_ERR	Uncertainty in Y_PSX
THETA	Estimated angular size (arcmin) from matched multi-filter (MMF3)
THETA_ERR	Uncertainty in THETA
Y	Integrated Compton-Y (arcmin^2) at *Planck* position and within THETA from matched multi-filter (MMF3)
Y_ERR	Uncertainty in Y

Table 7. ECC Catalogue Columns

Keyword	Type
NAME	Source name
SNR	Signal to Noise ratio of detection
GLON	Galactic longitude (deg) based on bandmerge algorithm
GLAT	Galactic latitude (deg) based on bandmerge algorithm
RA	Right Ascension in degrees (J2000)
DEC	Declination in degrees (J2000)
APFLUX353	Aperture flux density at 353 GHz (mJy)
APFLUX545	Aperture flux density at 545 GHz (mJy)
APFLUX857	Aperture flux density at 857 GHz (mJy)
APFLUX3000	Aperture flux density at 3000 GHz (mJy)
APFLUX353_ERR	Uncertainty (1 sigma) in APFLUX353
APFLUX545_ERR	Uncertainty (1 sigma) in APFLUX545
APFLUX857_ERR	Uncertainty (1 sigma) in APFLUX857
APFLUX3000_ERR	Uncertainty (1 sigma) in APFLUX3000
TEMPERATURE	Temperature from greybody fit (K)
BETA	Emissivity index from greybody fit
S857	Flux density at 857 GHz from greybody fit (mJy)
TEMPERATURE_ERR	Uncertainty (1 sigma) in TEMPERATURE (K)
BETA_ERR	Uncertainty (1 sigma) in BETA
S857_ERR	Uncertainty (1 sigma) in S857
BESTNORM	Summed squared residuals for best fit (mJy^2)
TEMPERATURE_CORE	Core Temperature from greybody fit to cold residual emission (K)
BETA_CORE	Emissivity index from greybody fit to cold residual emission
MAJ_AXIS_FWHM_CORE	Ellipse major axis of cold residual emission (arcmin)
MIN_AXIS_FWHM_CORE	Ellipse minor axis of cold residual emission (arcmin)
TEMPERATURE_CORE_ERR	Uncertainty (1 sigma) TEMPERATURE_CORE (K)
BETA_CORE_ERR	Uncertainty (1 sigma) BETA_CORE
MAJ_AXIS_FWHM_CORE_ERR	Uncertainty (1 sigma) MAJ_AXIS_FWHM_CORE
MIN_AXIS_FWHM_CORE_ERR	Uncertainty (1 sigma) MIN_AXIS_FWHM_CORE

Planck Early Release Compact Source Catalogue

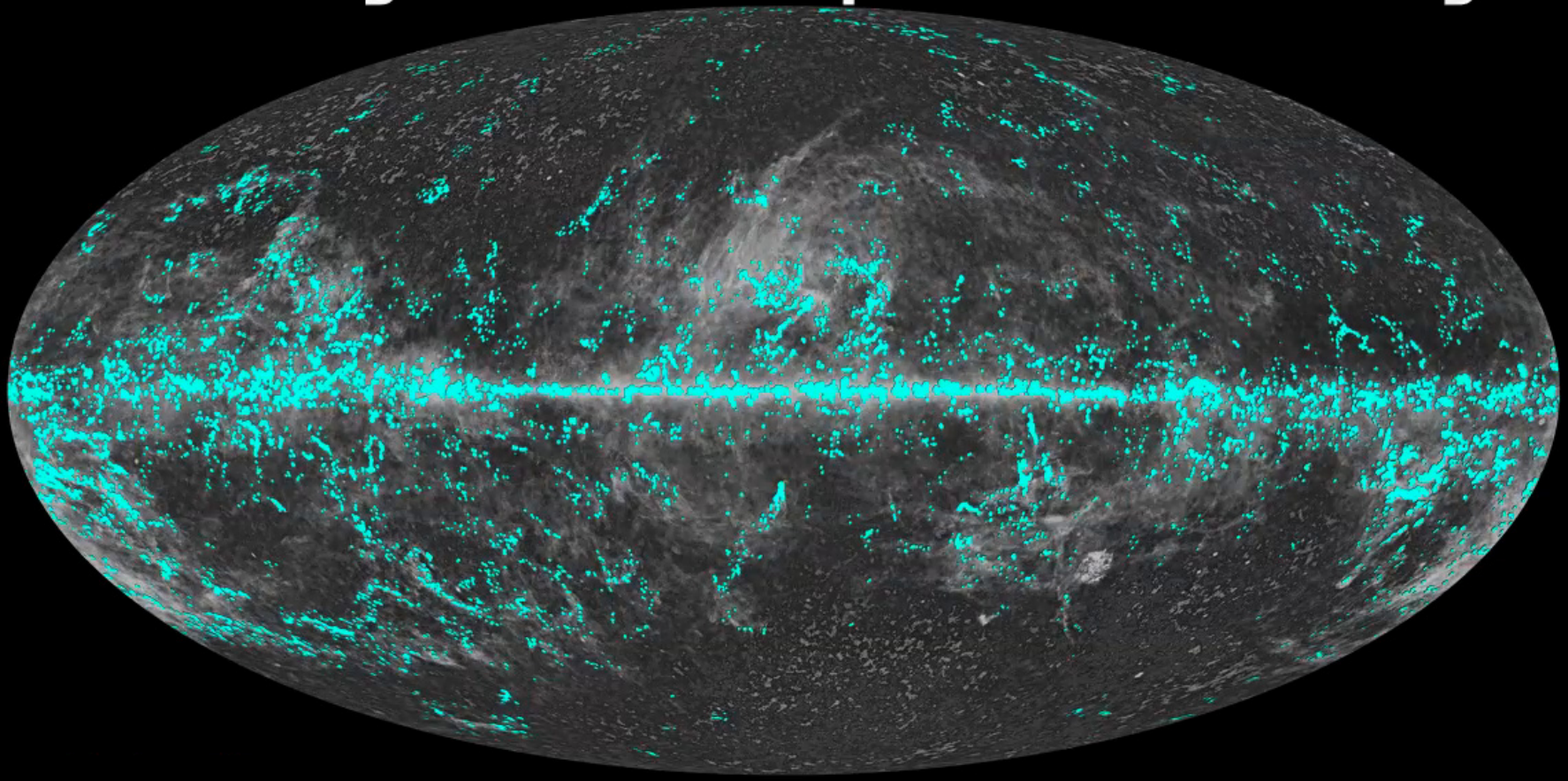

Galactic sources

Planck Early Release Compact Source Catalogue

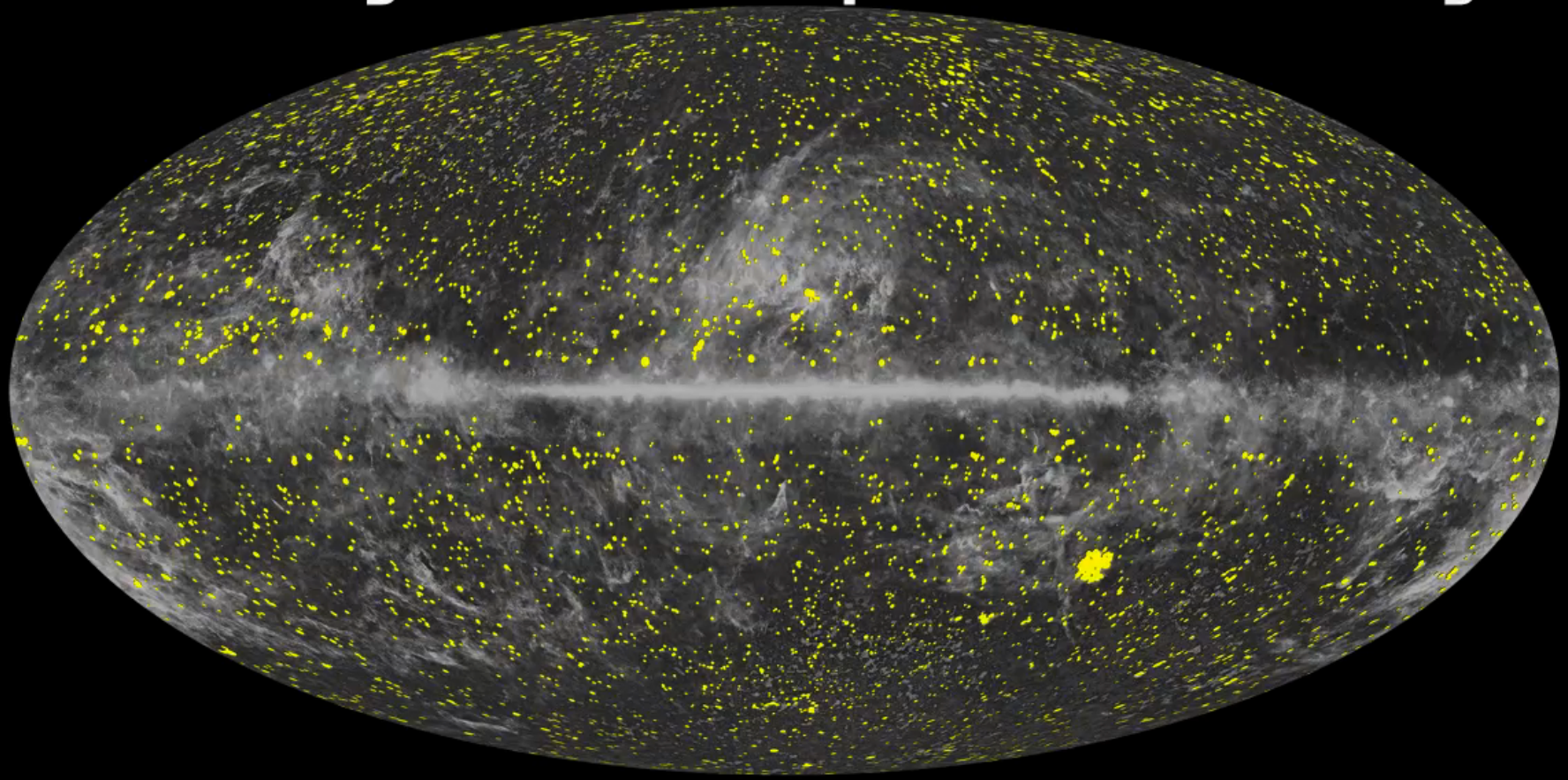

Extragalactic sources

Planck Early Release Compact Source Catalogue

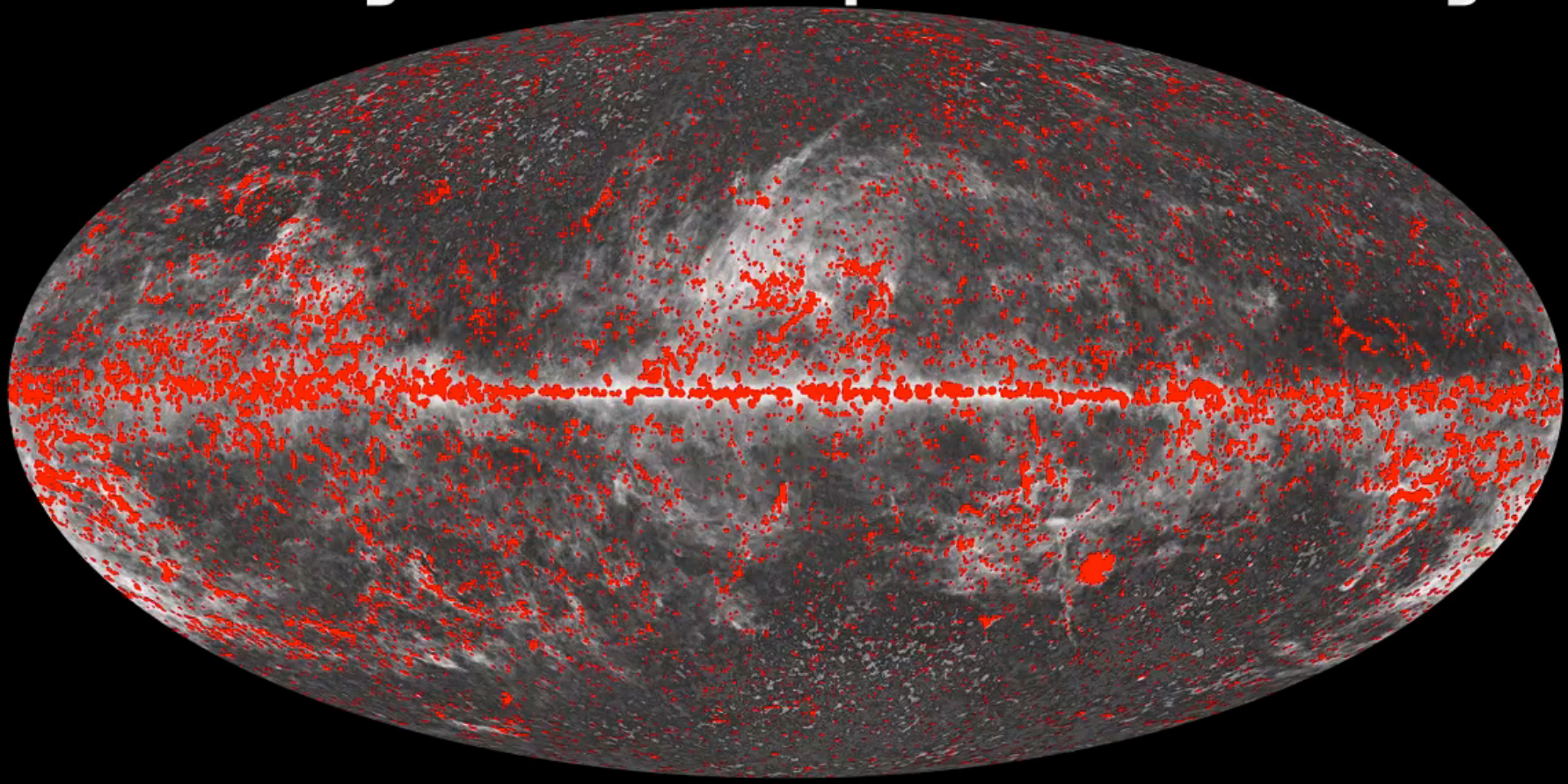

All compact sources

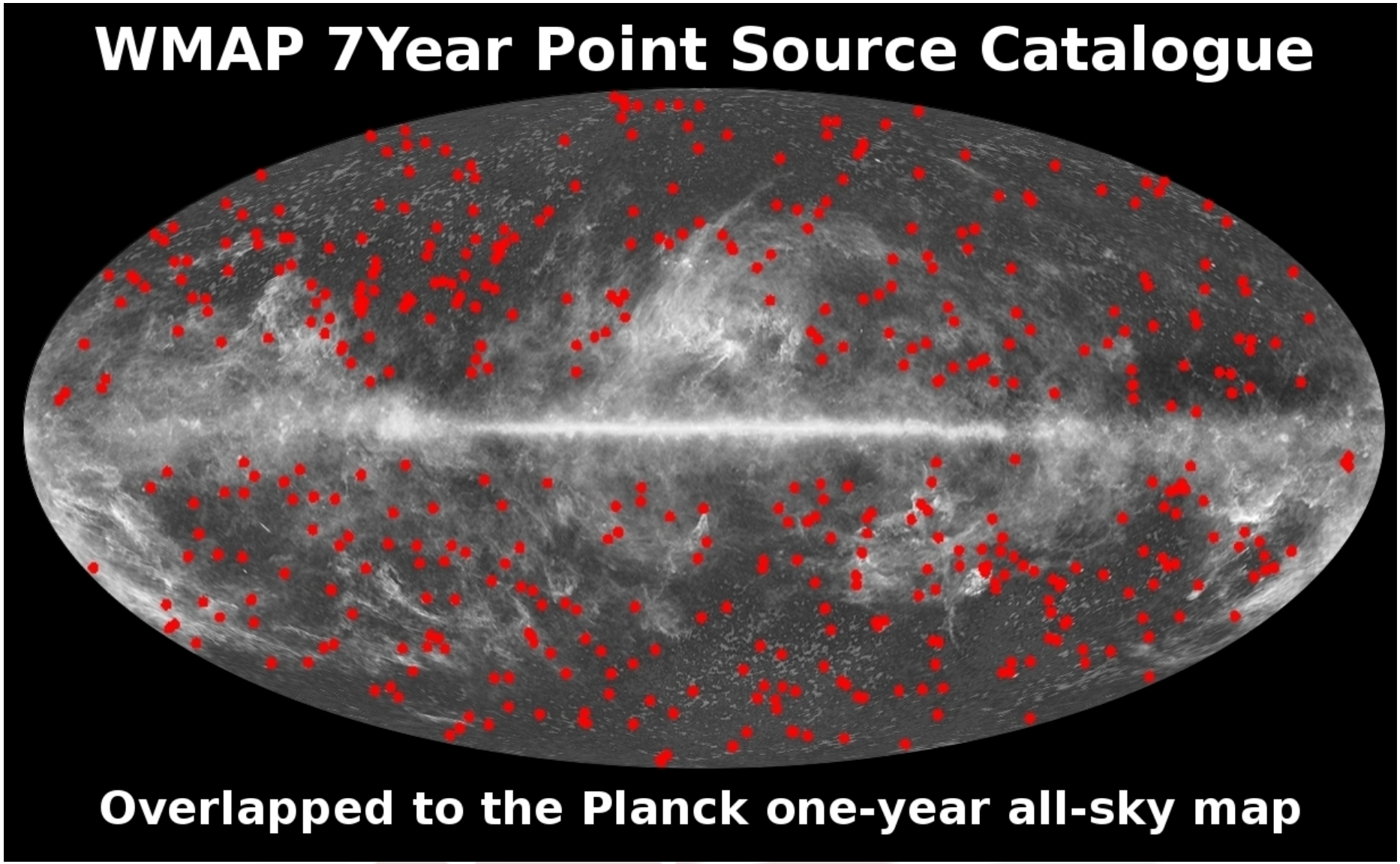
WMAP 7Year Point Source Catalogue
Overlapped to the Planck one-year all-sky map

WG5
Clusters

(see also A. Lasenby & J. Dunkley lectures)

WG5 arXiv papers

- Planck early results: Statistical analysis of Sunyaev-Zeldovich scaling relations for X-ray galaxy clusters 1101.2043
- Planck early results: Cluster Sunyaev-Zeldovich optical scaling relations 1101.2027
- Planck Early Results: Calibration of the local galaxy cluster Sunyaev-Zeldovich scaling relations 1101.2026
- Planck early results: XMM-Newton follow-up for validation of Planck cluster candidates 1101.2025
- Planck Early Results: The all-sky early Sunyaev-Zeldovich cluster sample 1101.2024
- Planck Early Results XXVI: Detection with Planck and confirmation by XMM-Newton of PLCK G266.6−27.3, an exceptionally X-ray luminous and massive galaxy cluster at z ~ 1 1106.1376

Sunyaev-Zeldovich effect: basics

It is a secondary anisotropy predicted in 1972 due to inverse Compton Scattering between CMB photons (~0.3 meV) and free electrons (~ few KeV) of the hot Intra-Cluster Medium. CMB photons acquire energy!

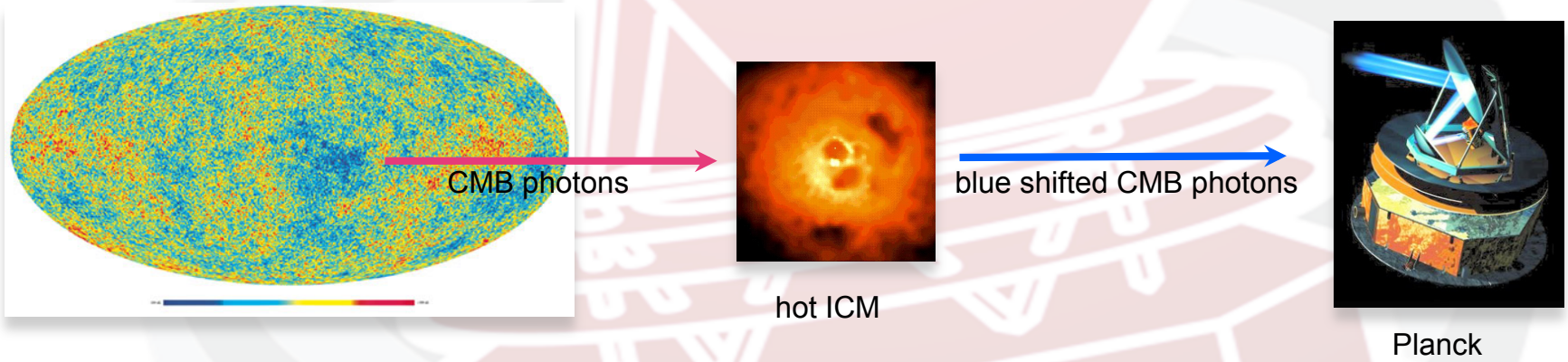

- Thermal SZ : CMB photons are scattered by random motion of thermal electrons
- Kinetic SZ : CMB photons are scattered by bulk motion of electrons

Sunyaev-Zeldovich effect: properties

$$\frac{\Delta T_{SZ}}{T_{CMB}} = f(x)\, y$$

$$y = \int_{los} n_e \sigma_T \frac{kT_e}{m_e c^2} d\ell$$ y-Compton parameter

$f(x)$ provides the frequency dependence $x = \frac{h\nu}{kT_{CMB}}$

$$Y = \int_{cluster} y\, d\Omega \qquad Y\, D_A^2 = \frac{\sigma_T}{m_e c^2} \int P\, dV$$

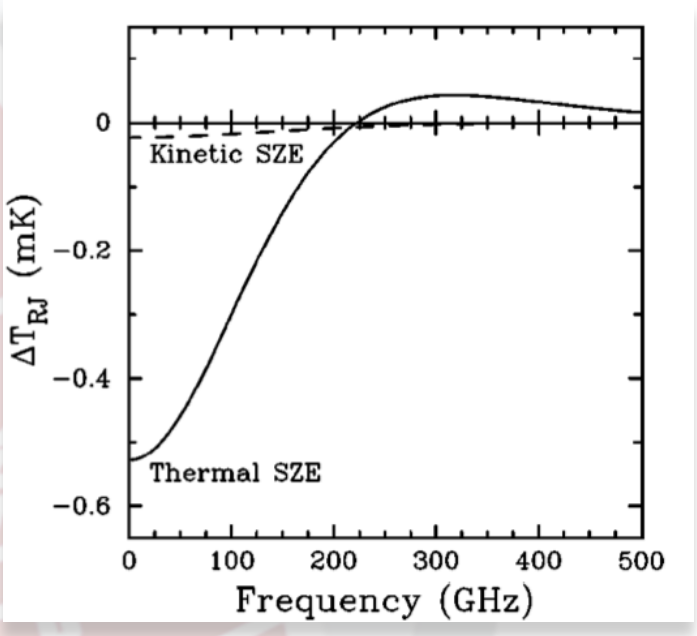

Carlstrom, Holder and Reese 2002

- SZ effect does not depend on z;
- y-Compton gives the amplitude of the effect (~ 1 mK)
- SZ vanishes for ~217 GHz (signature of the effect; one of the Planck channels is centered @ 217 GHz specifically to identify the zero transition of TSZ);
- Y is the integrated Compton that is proportional to the temperature-weighted mass of the cluster divided by the angular diameter distance D_A which is the only term depending on z (weakly). This is an useful relation for extracting cosmological information (that are in D_A) when combined with other observations (X-ray typically).

The Early SZ (ESZ) cluster sample from Planck

ESZ is made of 189 SZ clusters or candidates detected over the whole sky during the first ten months of CMB temperature observation.

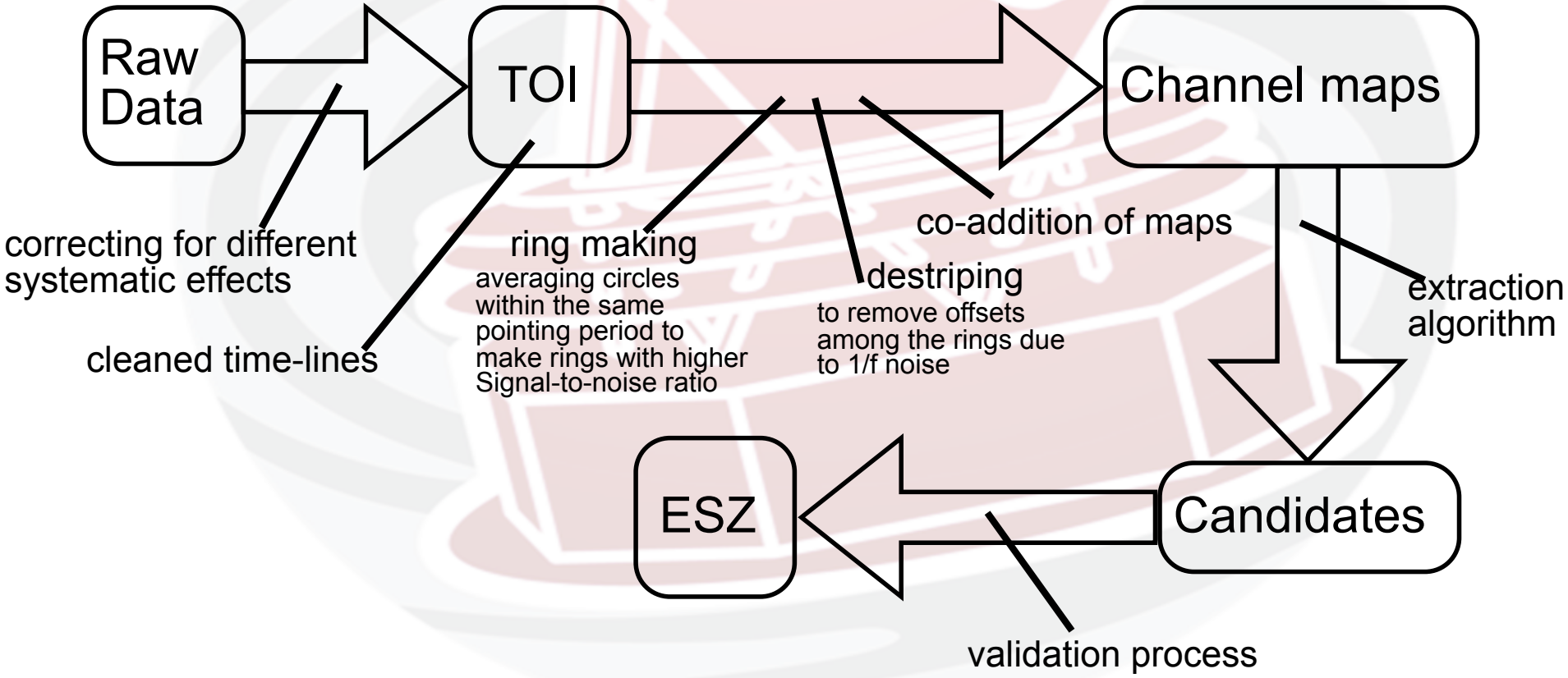

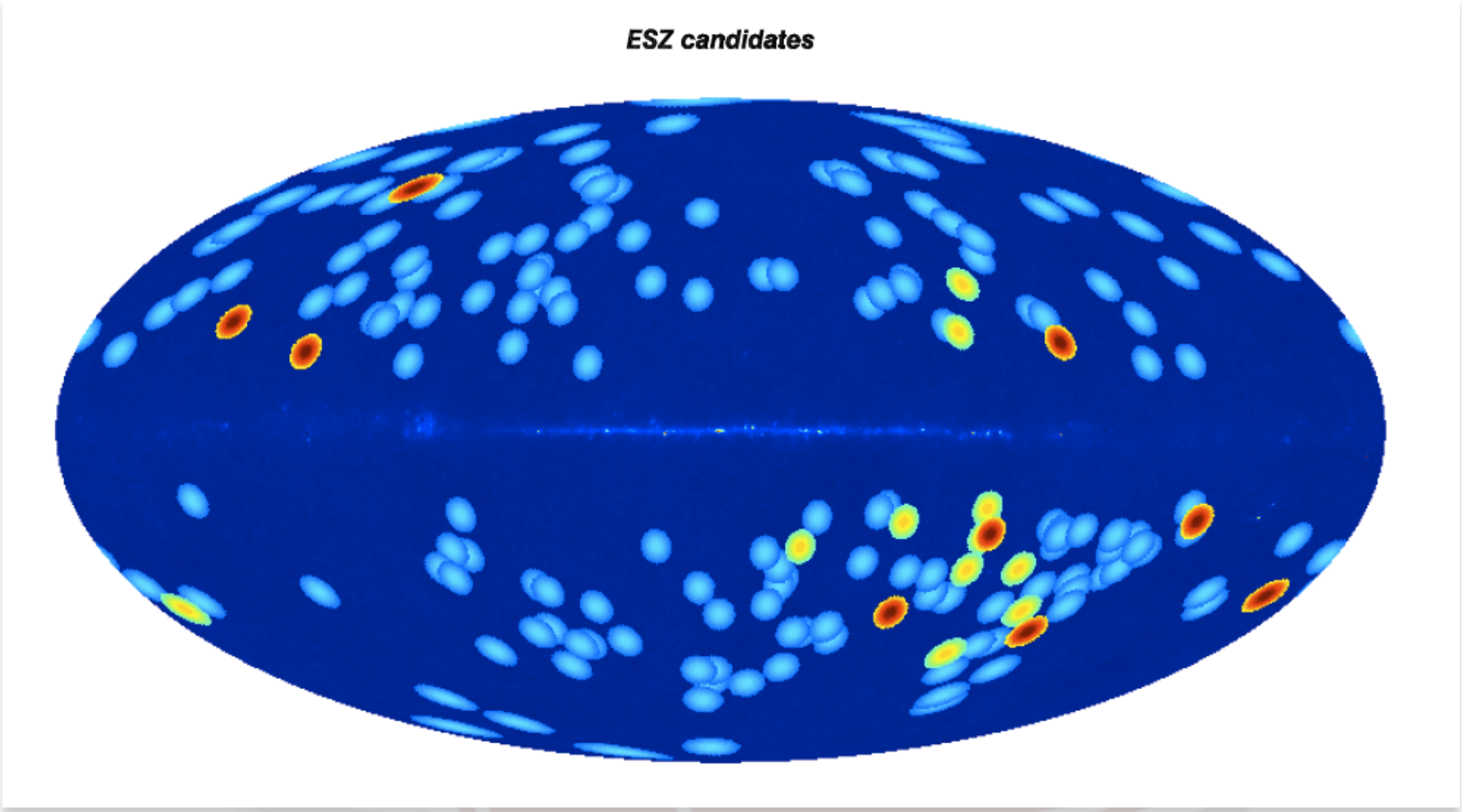

189 clusters detected (ESZ sample)
169 are known
20 are new Planck clusters
12 have been confirmed (11 by XMM and 1 by AMI)
8 are candidate new clusters

The Early SZ (ESZ) cluster sample from Planck

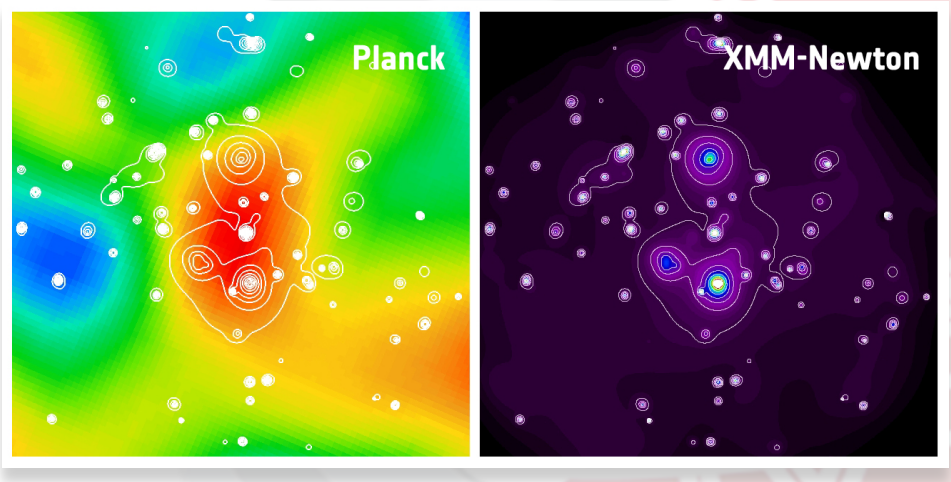

newly discovered supercluster, PLCK G214.6+37,
Planck (left) and XMM-Newton (right panel)

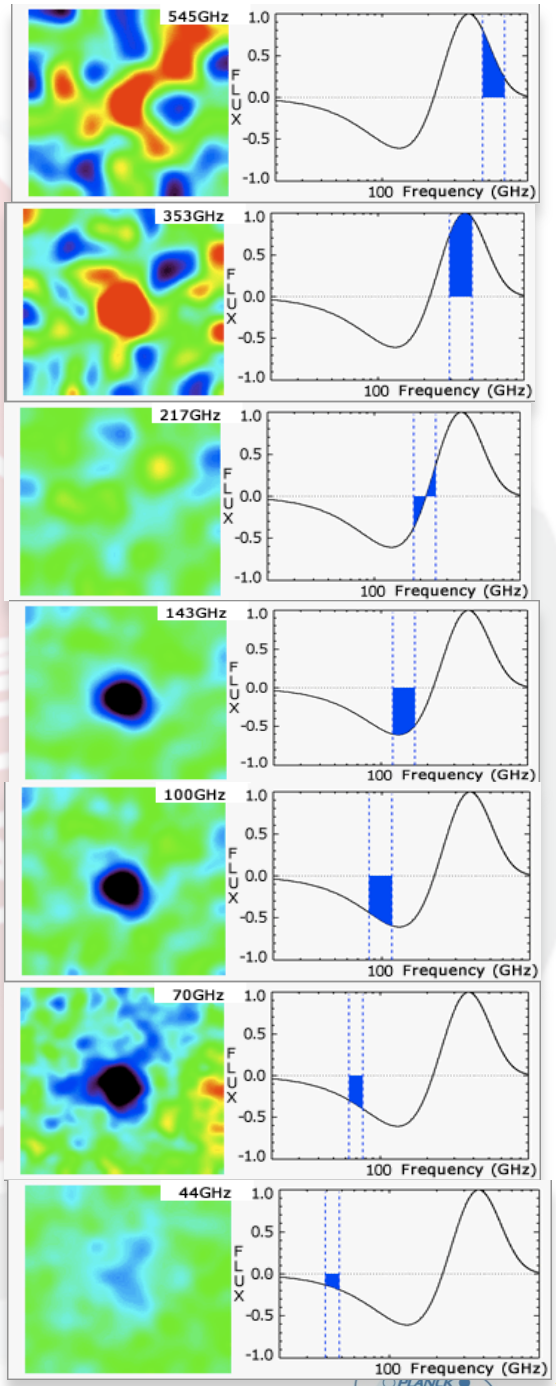

Abell 2319

At the end of the mission it will be delivered the Planck SZ cluster catalogue containing many hundreds of clusters at z~1.

The previous all-sky catalogue is RASS (Rosat All Sky Survey) but at much lower depth (i.e. z~0.1)

PLANCK DATA : target selection

A2147/2152

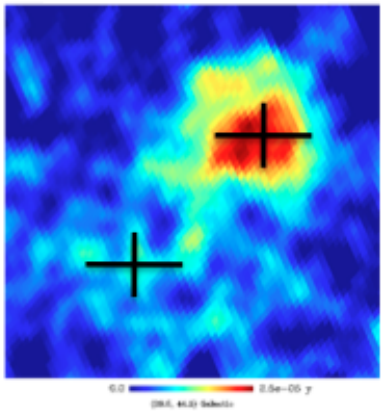

A399/A401

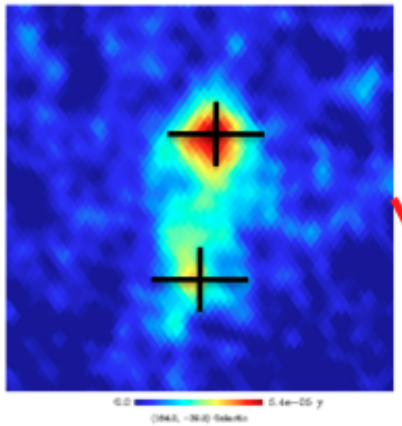

A2029/A2033

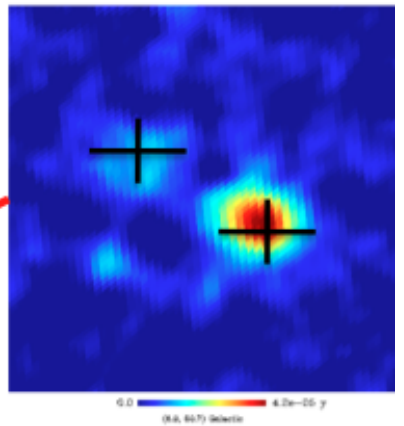

TSZ All Sky map

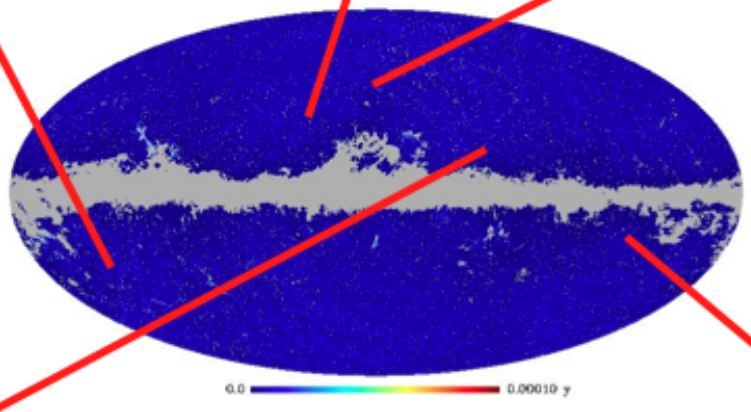

Shapley supercluster

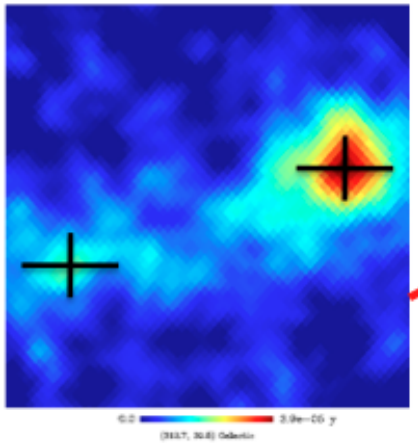

A3395/A3391

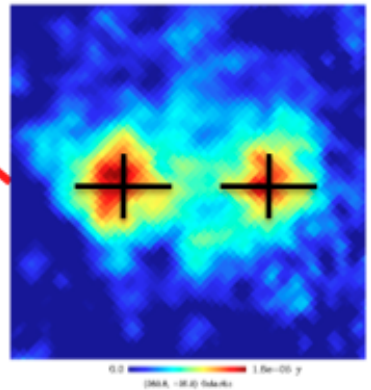

TSZ reconstructed maps

1.7 by 1.7 degrees patches

The Early SZ (ESZ) cluster sample from Planck

- Error budget on the cluster parameters

  1. Position cluster reconstruction: average error ~ 2arcmin (based on sims)

  2. Cluster size-flux degeneracy depends on signal-to-noise ratio. This is important for Planck since the vast majority of Planck detections are close to the lower threshold. This effect doubles the error bars for Y. This problem has been addressed re-estimating Y for all the ESZ candidates considering prior information on the size of the cluster derived from X-ray observations

  3. Systematic effect (uncertainties on the recovered beams is ~1-7%: this implies a 10% error on Y; uncertainties on calibration impacts Y at ~2% level; bandpass errors affects Y less than 3%; astrophysical contaminations ~3%)

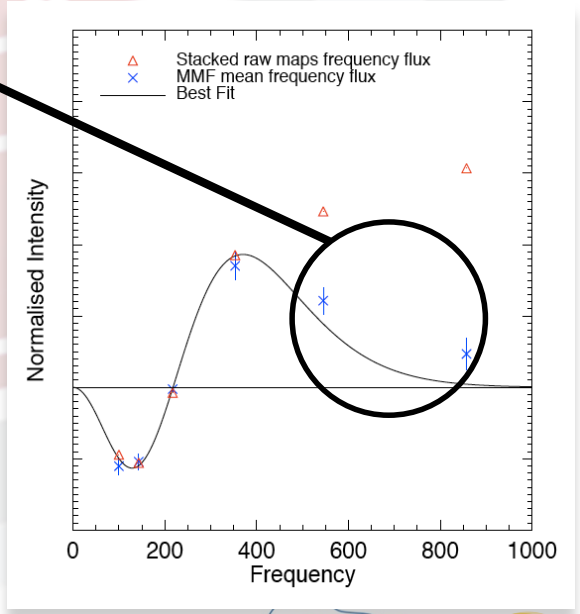

- Purity and completeness

  1. A significant fraction of the clusters and candidate clusters of ESZ lies near the selection cut. This implies problems of selection bias (the properties of the catalogued clusters are not representative of the true underlying cluster population). A careful analysis shows that Y is upward biased (on average) for M smaller than 4 10^14 M_sun.

The Early SZ (ESZ) cluster sample from Planck

- Validation consistency check: Integrated Compton parameters of ESZ are used to extract the Hubble parameter

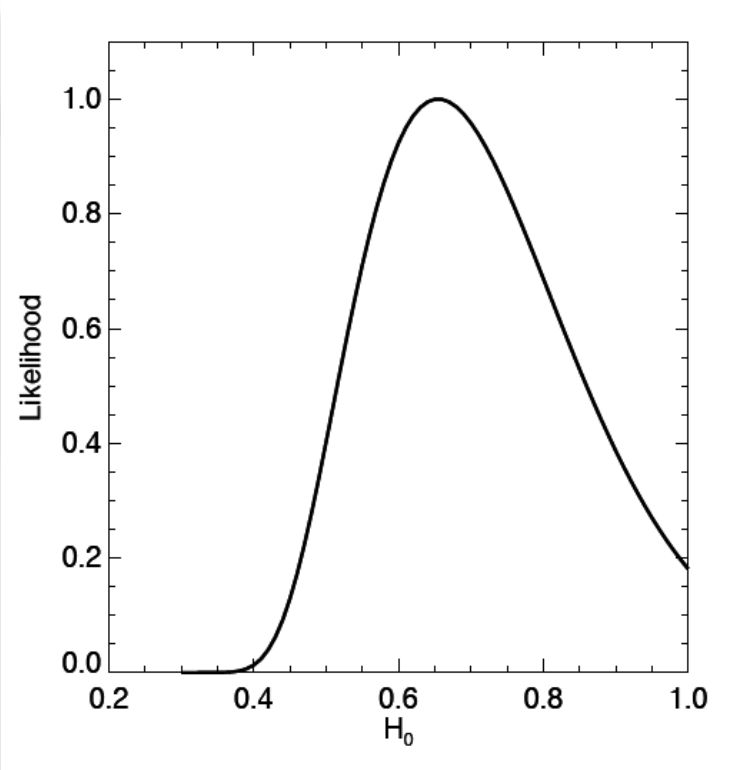

- reference used h = 0.7
- recovered parameter h = 0.71

XMM-Newton follow-up for validation of Planck discovered clusters

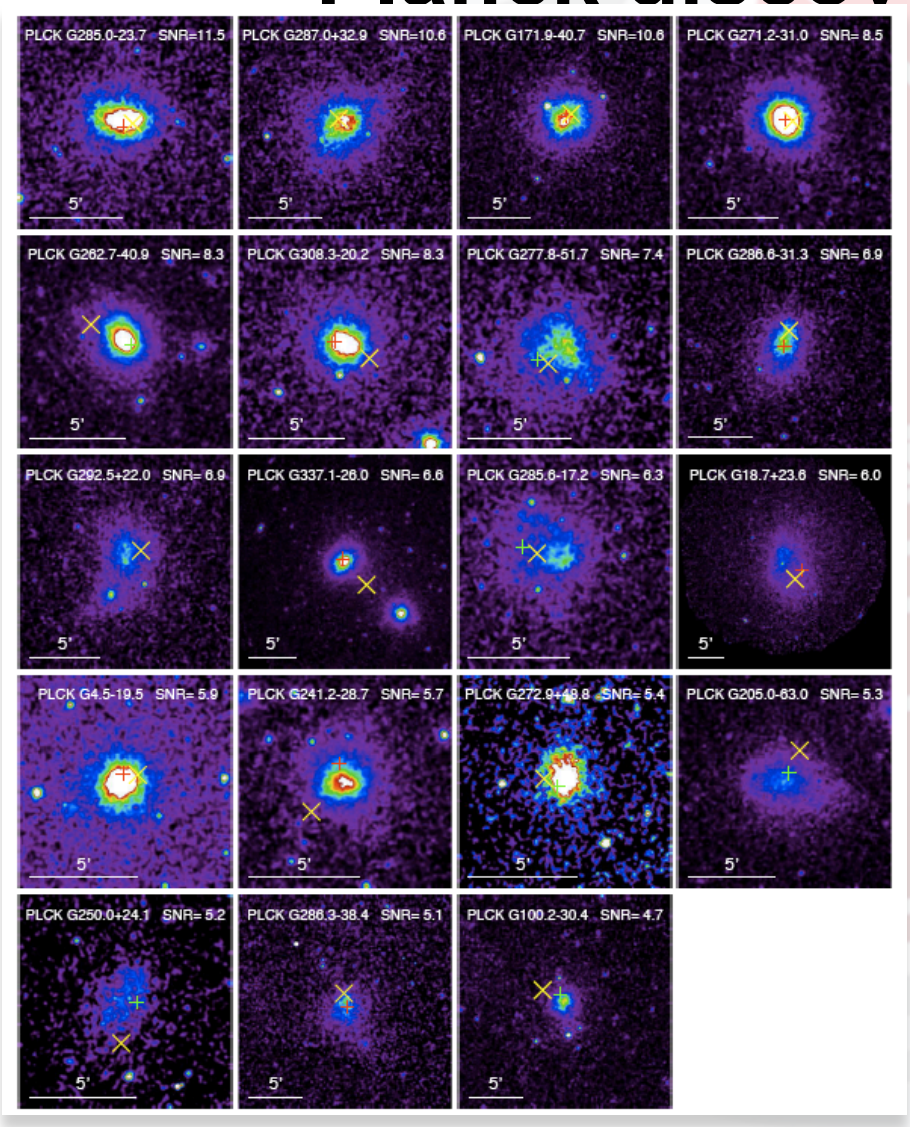

- 25 Planck candidates analyzed
- 21 are confirmed
- 17 are single clusters
- 4 are double or triple systems

XMM-Newton images (0.3-2 KeV) of the confirmed cluster candidates, except for two triple systems

WG6
External galaxies & Far-IR background

C. Burigana, Paris, 20-22/7/2011

WG6 arXiv papers

- Planck Early Results: Spectral energy distributions and radio continuum spectra of northern extragalactic radio sources 1101.2047
- Planck Early Results: Origin of the submm excess dust emission in the Magellanic Clouds 1101.2046
- Planck Early Results: The Planck View of Nearby Galaxies 1101.2045
- Planck Early Results: Statistical properties of extragalactic radio sources in the Planck Early Release Compact Source Catalogue 1101.2044
- Planck Early Results: The Power Spectrum Of Cosmic Infrared Background Anisotropies 1101.2028
- Planck Early Results: ERCSC Validation and Extreme RadioSources 1101.1721

Planck Early Results: Statistical properties of extragalactic radio sources in the Planck Early Release Compact Source Catalogue

First estimate of the Early Release Compact Source Catalogue at 100, 143, and 217 GHz counts of extragalactic radio sources at bright flux density levels.

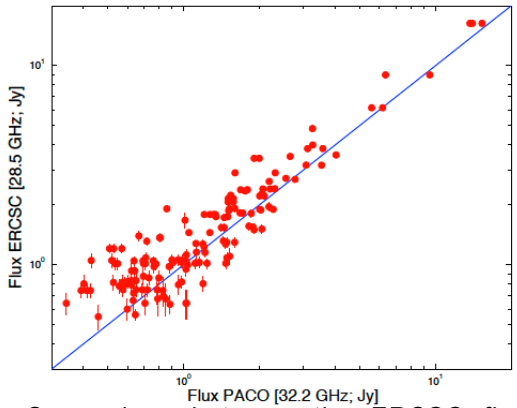

Comparison between the ERCSC flux densities at 30 GHz and at 44 GHz with the almost simultaneous ATCA measurements (PACO project) at 32.2 and 39.7 GHz, respectively. No correction for the slightly different frequencies has been applied.

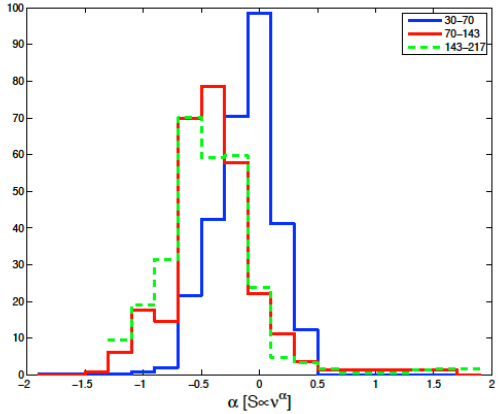

Spectral index distributions for different frequency interval calculated by taking into account all sources selected at 30 GHz with Sv > 1 Jy. There is clear evidence for a steepening above 70 GHz.

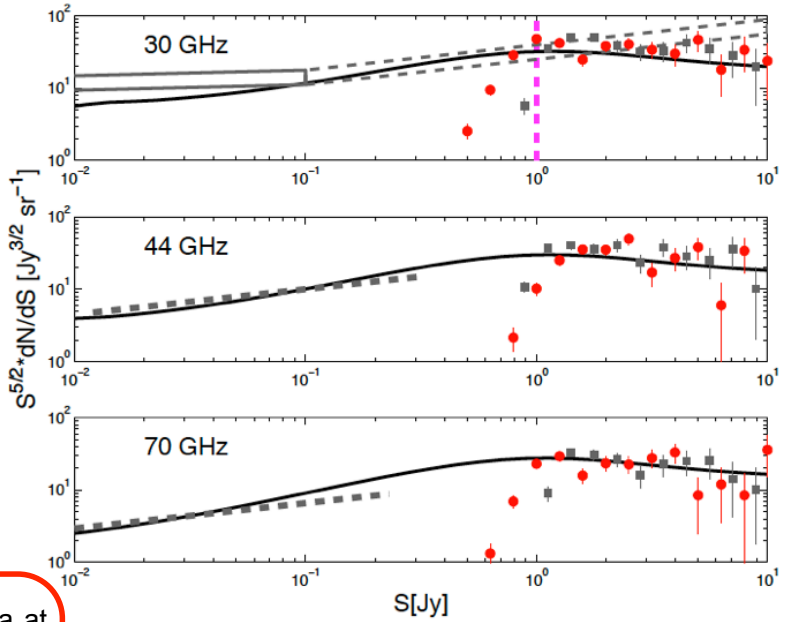

Euclidean normalized differential number counts at the LFI frequencies: red circles show the counts of sources with counterparts in our reference 30 GHz sample; solid curves show the total number counts of extragalactic radio sources predicted by the de Zotti et al. (2005) model. Also shown are: the counts at 31 GHz from DASI (grey dashed box); at 33 GHz from the VSA (grey box); counts from WMAP 5-yr survey (grey squares); counts estimated by Waldram et al. (2007) (grey dashed line); dashed magenta line in the upper panel indicates the flux completeness limit, 1.0 Jy.

- Counts at 30, 44, and 70 GHz in good agreement with those derived from WMAP data at nearby frequencies;

- The completeness limit of the ERCSC is somewhat deeper than that of WMAP at 30 and 70 GHz and somewhat shallower at 44 GHz;

- At higher frequencies the ERCSC has allowed us to obtain the first estimate of the differential number counts at bright flux density levels.

- At 30, 143 and 217 GHz, the present counts join smoothly to those from deeper surveys over small fractions of the sky.

- An analysis of source spectra finds clear evidence of a steepening of the mean spectral index above ≃ 70GHz: the contamination of the CMB power spectrum by radio sources below the detection limit is significantly lower than previously estimated.

Planck Early Results:
Validation and Extreme Radio Sources in the ERCSC

The ERCSC contains hundreds of extragalactic radio sources, many with SEDs extending to frequencies 143 GHz or higher. The Planck observations are complemented by approximately simultaneous ground-based observations at frequencies below and overlapping Planck frequency bands. The flux density scales of the ground-based and Planck observations are found to be consistent.

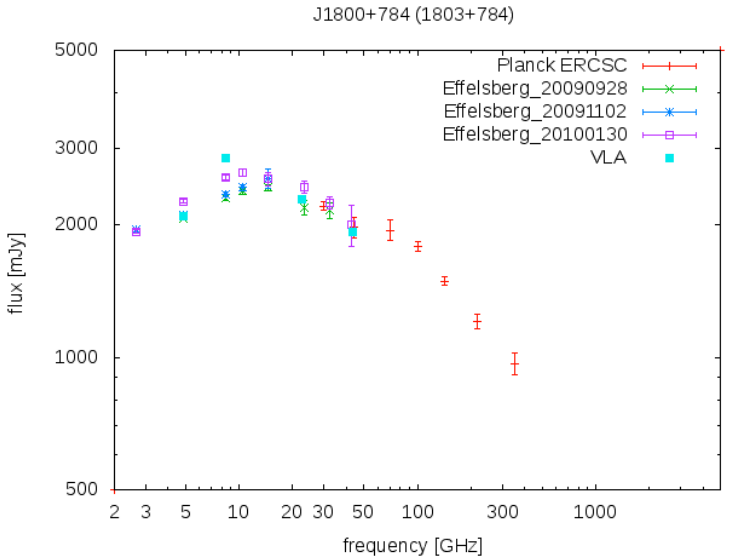

Effelsberg, VLA and Planck measurements of a true GPS quasar: J1800+784 flaring during the Planck observations

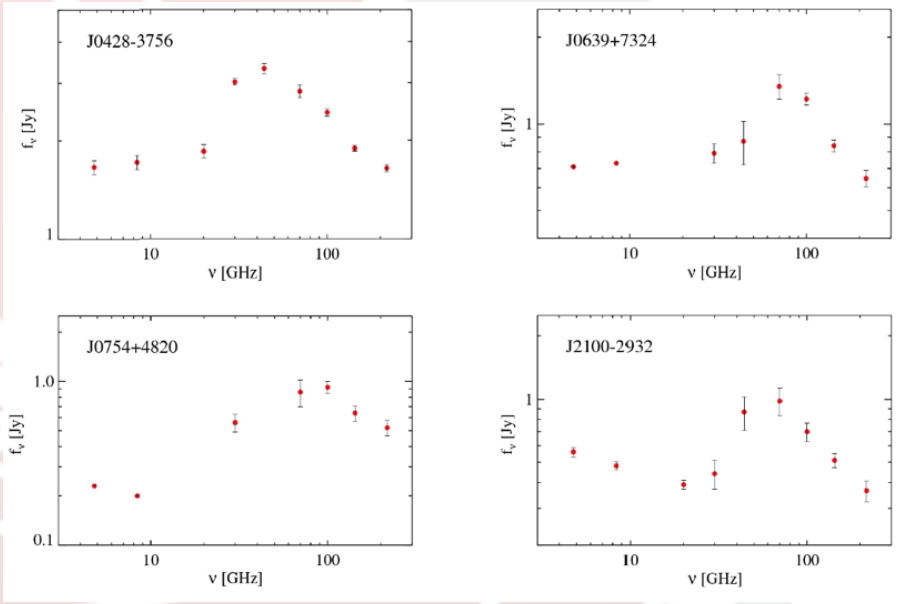

SEDs of possible new GPS candidates emerged when combining the Planck data with the low frequency archival data.

- Planck has demonstrated that the high frequency counts (at least for frequencies ≤ 143 GHz) of bright extragalactic sources are dominated at the bright end by synchrotron emitters, not dusty galaxies;

- In many cases, the spectra can reasonably be fit with a single power law, as expected for one component synchrotron emission. In some cases, such as J1800+784, the quality of the data permits us to clearly see the expected spectra break of ~ -0.5 expected from the aging of the synchrotron-producing electrons;

- In the case of some of the apparently flat spectrum sources, we find clear evidence that the nominally flat spectrum is made up of two or more peaked components.

Planck Early Results: Spectral energy distributions and radio continuum spectra of Northern extragalactic radio sources

The nine Planck frequencies, from 30 to 857 GHz, are complemented by a set of simultaneous observations ranging from radio to gamma-rays.

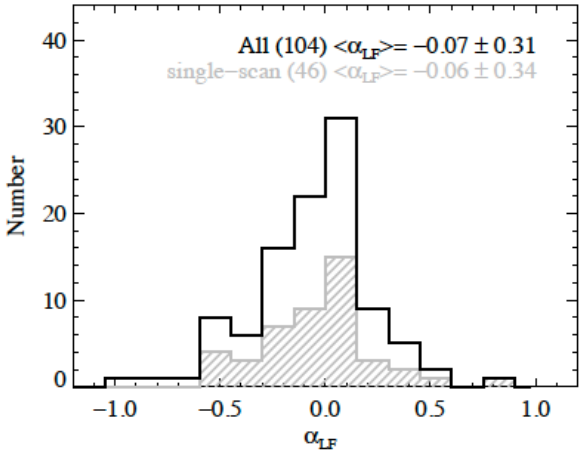

Distribution of LF spectral indices for the whole sample (104 sources).

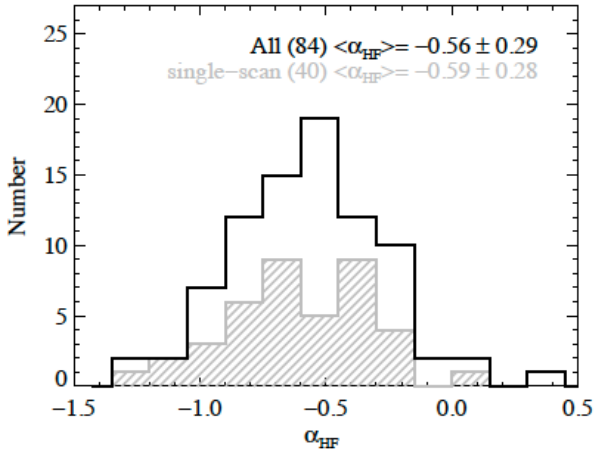

Distribution of HF spectral indices for the 84 sources that had three or more data points. The sources that have only been scanned once by Planck are shown hatched (40 sources).

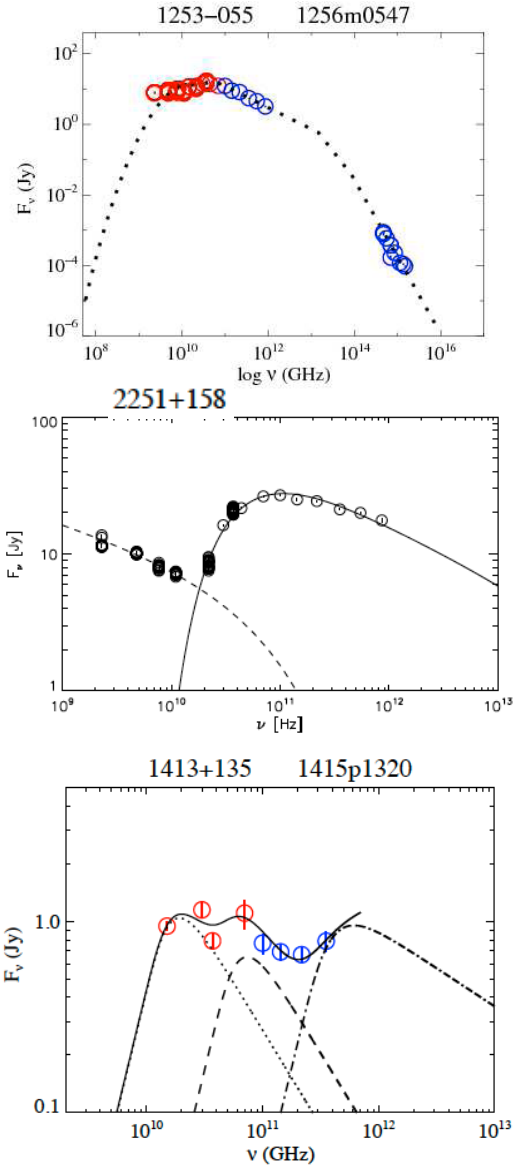

- The 104 SEDs, supplemented with archival data, demonstrate the usefulness of *Planck* data in determining the SED peak frequencies and fluxes and in modelling the spectral energy distributions in greater detail.

- The data demonstrate that the synchrotron spectrum contains contributions from several physically distinct AGN components;

- We have presented some examples of total flux density monitoring to demonstrate in how different activity stages sources have been observed during Planck scans.

SEDs and radio spectra using Planck ERCSC data

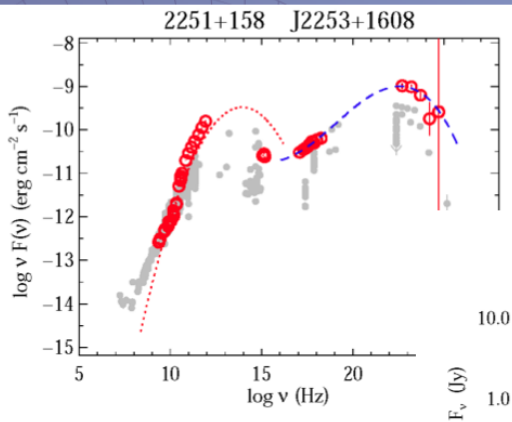

For this source, the data are from a single scan, for many others in the early paper, from averaged scans.

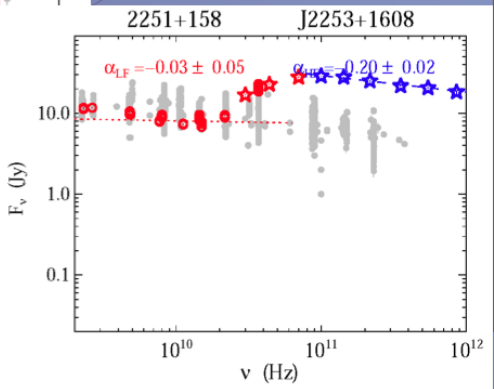

Modelling and understanding the synchrotron spectra of blazars

The physics determining SED shapes in blazars

Spectral energy distributions, SEDs

- Contemporary models fit the high-energy inverse Compton (IC) part rather nicely, but (still) almost completely ignore the synchrotron (=radio) part which most likely is the source for the high-energy emission

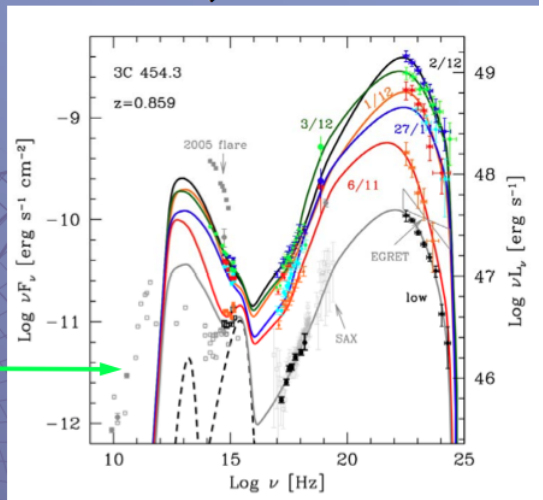

Bonnoli et al. 2010

Planck Early Results: The Planck View of Nearby Galaxies

ERCSC provides an unsurpassed survey of galaxies at sub-millimeter wavelengths, representing a major improvement in the numbers of galaxies detected, as well as the range of far-IR/submm wavelengths over which they have been observed.

ERCSC catalogue has been matched to *IRAS*-detected galaxies in the Imperial *IRAS* Faint Source Redshift Catalogue (IIFSCz)

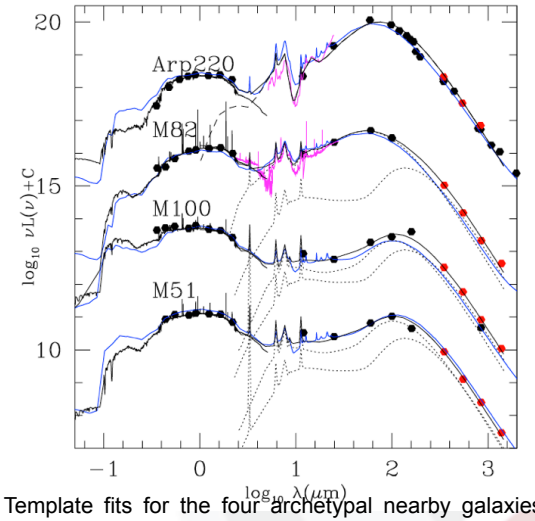

Template fits for the four archetypal nearby galaxies, M51, M100, M82 and Arp 220. Black curves: fits with Efstathiou and Rowan-Robinson templates (black dotted lines), blue curves: Silva et al. (1998) models. *Planck* ERCSC data shown as red filled hexagrams. *ISO*-SWS mid-infrared spectroscopy data are shown in magenta.

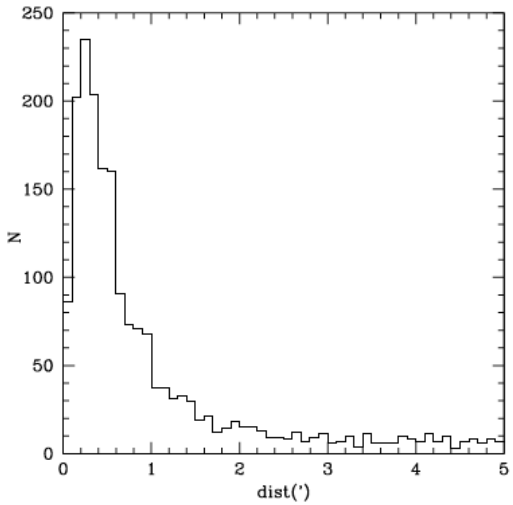

Histogram of offsets between ERCSC and IIFSCz positions.

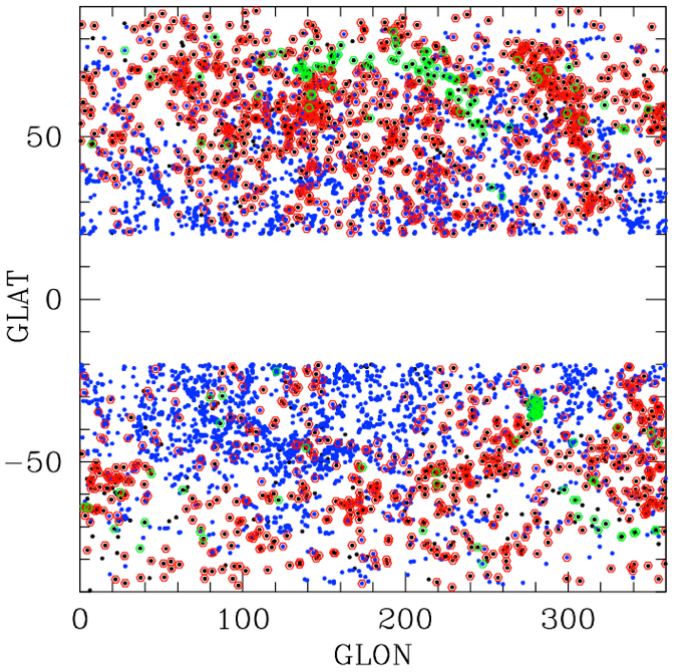

Sky plot of ERCSC sources in galactic coordinates. Black filled hexagons are ERCSC point-sources and blue filled hexagons are ERCSC sources flagged as extended. Red hexagons are sources associated with IIFSCz *IRAS* FSC galaxies, after scrutinising suspect categories with NED (and excluding some, as described in the text). Green hexagons are ERCSC sources not associated with IIFSCz, but associated with bright galaxies in NED (only for $|b| > 60^\circ$ for extended sources).

- Our studies of nearby galaxies detected by Planck have shown evidence for colder dust than has previously been found in local galaxies. This suggests that previous studies of dust in local galaxies have been biased away from such luminous cool objects;

- We also find that the dust SEDs in most galaxies are better described by parametric models containing two dust components, one warm and one cold, with the cold component reaching temperatures as low as 10K.

Planck Early Results:
Origin of the submm excess dust emission in the Magellanic Clouds

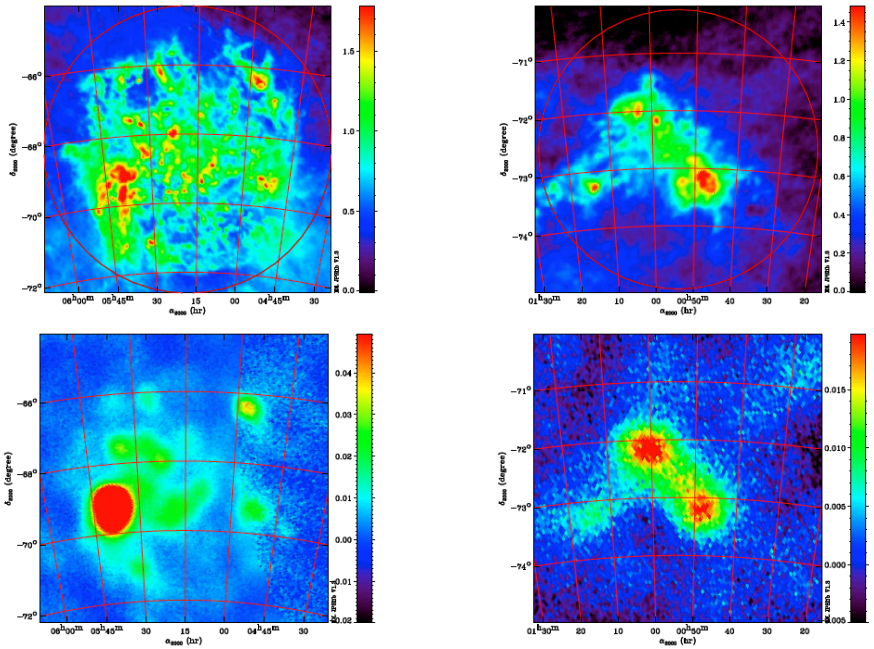

Planck Data for the LMC (Left) and SMC (right) at 857 (top) and 28.5 GHz (bottom) at full resolution. The upper panels are shown in log scale. The circle shows the region used to extract average SEDs.

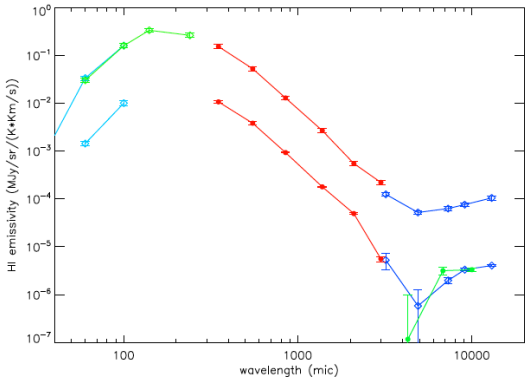

Average foreground SED toward the LMC and SMC including DIRBE , IRAS-IRIS , Planck-HFI , Planck-LFI and WMAP (lower curve) compared to the SED of the high latitude low column-density SED, scaled up by a factor of 10 for clarity (upper curve).

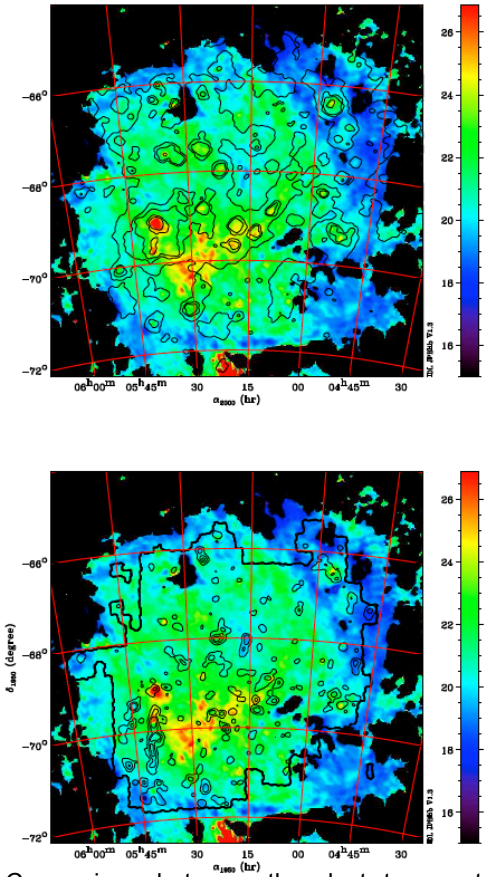

Comparison between the dust temperature map of the LMC with H_alfa (Top) and CO emission (Bottom). The CO contours are at 0.5, 2., 4 and 10 Kkm/s. H_alfa contours are at 1, 10, 50, 100, 500 and 1000 Rayleigh. The thick line shows the edge of the available CO surveys.

- We assessed the existence and investigated origin of millimeter excess emission in the LMC and the SMC using the Planck data.

- The LMC temperature map shows the presence of a warm inner arm already found with the Spitzer data, but also shows the existence of a previously unidentified cold outer arm.

- We show that the excess previously reported in the LMC can be fully explained by CMB fluctuations.

- Possible interpretation of the SMC excess employs the Two-Level-System (TLS) model developed by Meny et al. (2007) combined with spinning dust.

C. Burigana, Paris, 20-22/7/2011

The University of Manchester
Jodrell Bank Observatory

MANCHESTER 1824

Morphology

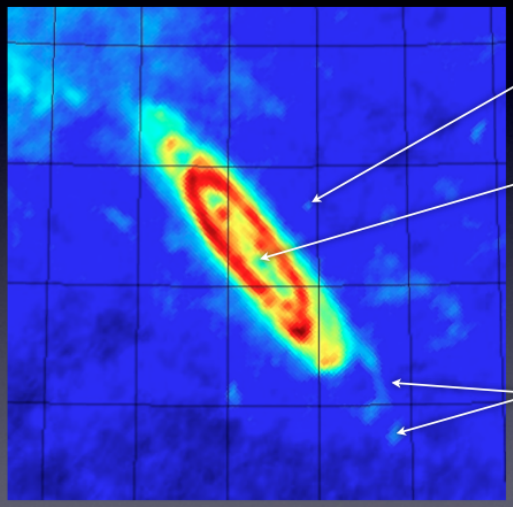

NGC 205

No central bulge

New arm?

Planck 857GHz (log), DX5

The University of Manchester
Jodrell Bank Observatory

MANCHESTER 1824

Herschel (HELGA)

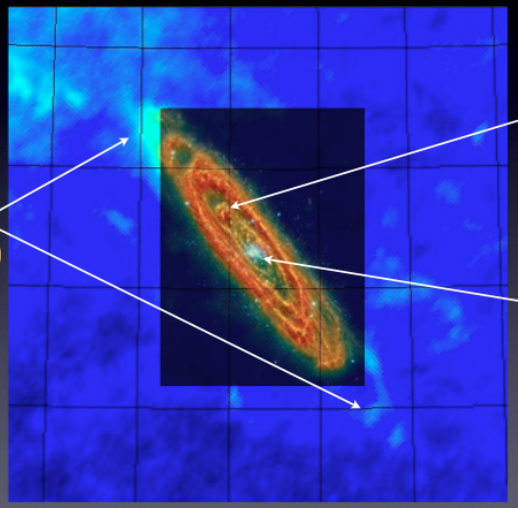

Misses outskirts(?)

NB: using press release image Includes XMM

Data will become public later this year

Cold dust spot

No sign of central emission

Planck 857GHz (log), DX5

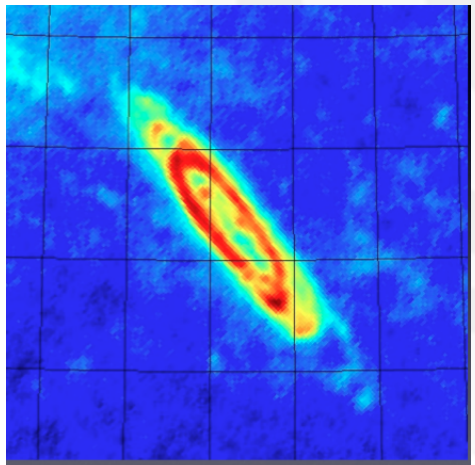

Planck 545GHz (log), DX5

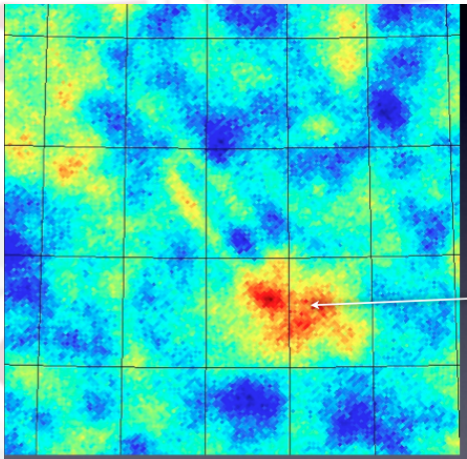

Large CMB anisotropy

Planck 143GHz, DX5

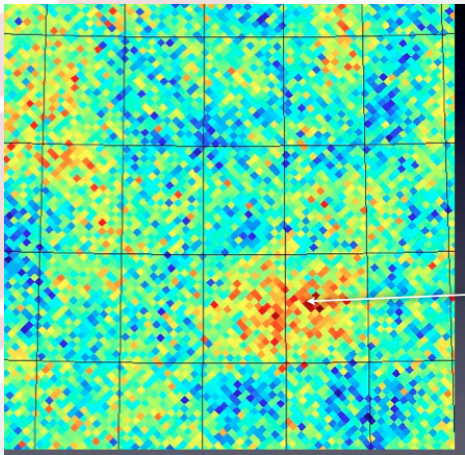

'Just' CMB?

Planck 70.3GHz, DX5

The case of NGC 205

Planck Early Results:
Power spectrum of CIB anisotropies with Planck/HFI

Cosmic Infrared Background records much of the radiant energy released by processes of structure formation that have occurred since the decoupling of matter and radiation following the Big Bang.

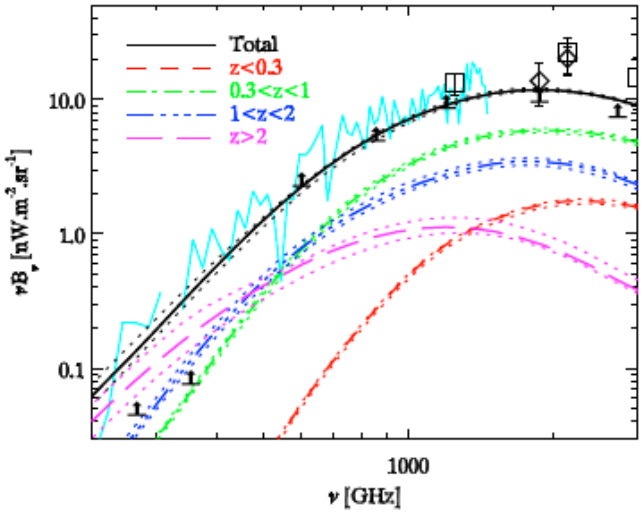

Contribution to the CIB per redshift slice, extracted from Bethermin et al. (2010b). Black solid line: CIB spectrum predicted by the model.

Due to its frequency coverage from 100 to 857 GHz, the HFI instrument onboard Planck is sensitive to the complete history of star-formation and is thus ideally suited to probe the dark matter/star-formation connection.

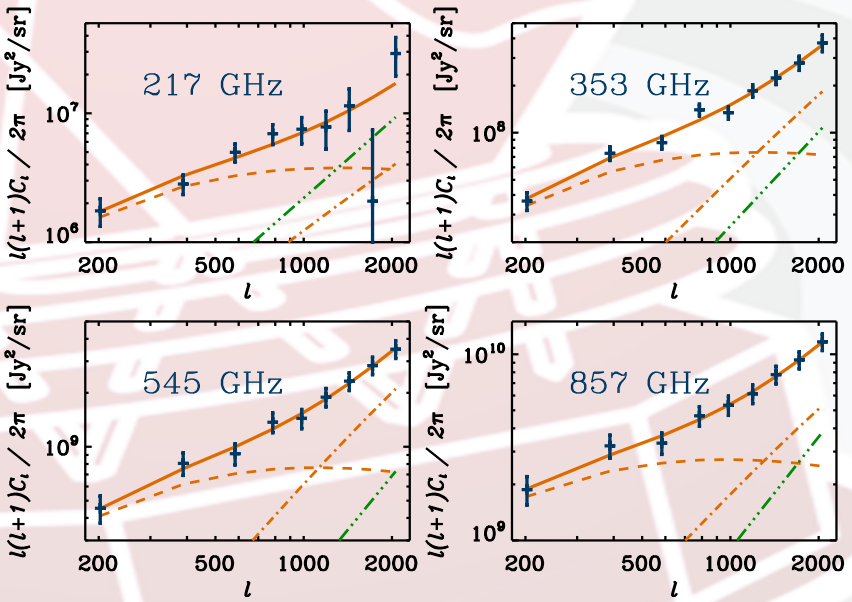

Power spectra are measured independently for the 6 fields and are then combined.

- First measurements at those wavelengths and spatial scales;

- We measure strong frequency-correlated structures consistent with the expected CIB signal. The correlation decreases with increasing frequency;

- No significant difference between the frequency spectrum of the CIB anisotropies and the CIB mean is observed;

WG7
Galactic science

WG7 arXiv papers

- Planck Early Results: Dust in the diffuse interstellar medium and the Galactic halo 1101.2036
- Planck Early Results: The Galactic Cold Core Population revealed by the first all-sky survey 1101.2035
- Planck Early Results: The submillimetre properties of a sample of Galactic cold clumps 1101.2034
- Planck Early Results: Properties of the interstellar medium in the Galactic plane 1101.2032
- Planck Early Results: New Light on Anomalous Microwave Emission from Spinning Dust Grains 1101.2031
- Planck Early Results: All sky temperature and dust optical depth from Planck and IRAS: Constraints on the “dark gas” in our Galaxy 1101.2029
- Planck Early Results: Thermal dust in Nearby Molecular Clouds 1101.2037

Galactic studies with Planck

- The Planck multifrequency view of our Galaxy allowed for the first time a detailed investigation of many interesting topics
- Early studies/papers achieved crucial results on the following aspects:
  - Dark gas in the Galaxy
  - Microwave anomalous emission
  - Interstellar medium
  - Cold cores
  - Thermal dust on nearby molecular clouds

All sky temperature and dust optical depth from Planck and IRAS: Constraints on the ”dark gas” in our galaxy

The temperature map trace the spatial variations of radiation field intensity associated to star formation in the Galaxy

Correlations between the dust optical depth and gas column density as derived from HI and CO observations

The optical depth in the intermediate column density range shows

→ an excess in all photometric channels considered in this study

We interpret the excess as dust emission associated to Dark-Gas, most likely in the molecular phase where H2 survives photodissociation, while the CO molecule does not

The derived mass of the dark molecular gas, assuming the same dust emissivity

as in the HI phase is found to correspond to

≃ 28% of the atomic mass and ≃ 115% of the molecular gas mass

→

All-sky maps of thermal dust temperature

optical depth

column density

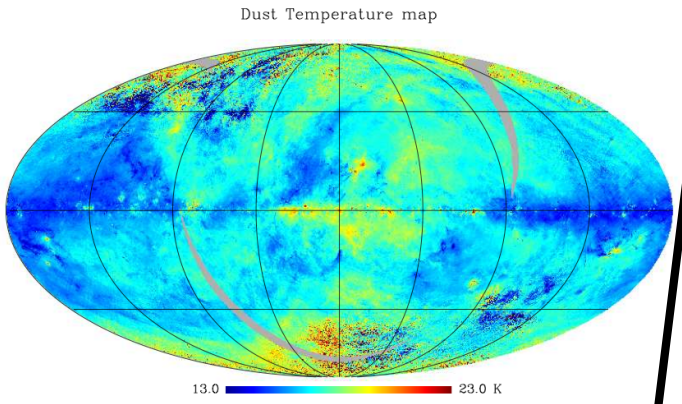

Fig. 3. All-sky map of the dust temperature in K. The temperature is derived from modeling the IRIS 100 μm and the *Planck-HFI* mission at 857and 550. The map is shown in galactic coordinates with the galactic center at the center of the image.

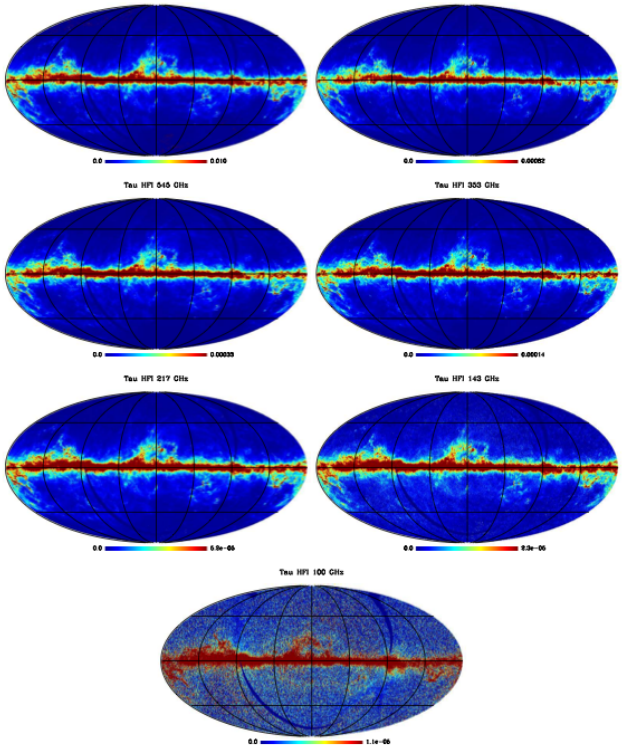

Fig. 5. Maps of the dust optical depths in the *IRAS* 100 μm and *Planck-HFI* bands. All maps are shown in galactic coordinates with the galactic center at the center of the image. The upper bound of the color scale is set as $\tau_{max} = 0.01 * (\lambda/100\,\mu\mathrm{m})^{-2}$.

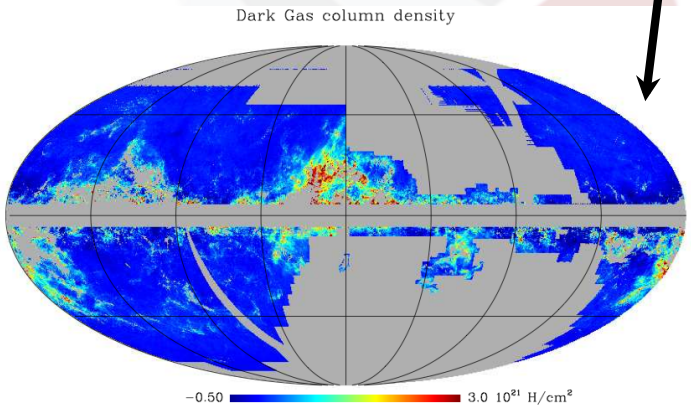

Fig. 8. Map of the excess column density derived from the 857 GHz Data. The maps is shown in galactic coordinates with the galactic center at the center of the image. The grey regions corresponds to those removed in the calculation of the dark-gas mass fraction ($W_{CO} > 1\,Km/s$ or $|b| < 5°$.)

The comparison of this value with the recent calculations for molecular clouds more massive than the ones present in the solar neighborhood indicates a

dark gas fraction about 3 times larger in the solar neighborhood.

The threshold for the onset of the Dark-Gas transition is found to be ≃ 0.37mag and

appears compatible to, although slightly larger than the ones predicted by this model

New Light on Anomalous Microwave Emission from Spinning Dust Grains

Planck, combined with ancillary radio and FIR data, has provided a unique opportunity to establish a comprehensive spectrum of AME: **present observations strongly favour the spinning dust (electro-dipole radiation) mechanism** which provides a good fit to the microwave (10 − 100 GHz) part of their spectra which peaks at ≈ 30 GHz

The two best-studied AME sources that have extensive ancillary data are in

Perseus and ρ Ophiuchus molecular clouds

Using parameters constrained at smaller angular scales, the 20 − 40 GHz AME peak in Perseus is well explained with spinning dust emission arising from dense, molecular gas (nH > 200 cm^{-3}) subjected to a few times the interstellar radiation field. The contribution from low density gas appear to only play a minor role

In the case of ρ Ophiuchus, irradiated, high density molecular gas from the PDR appears to contribute in the range 50 − 100 GHz. The picture seems to be that smaller PAHs are found in PDRs (G0 > 100) as suggested by recent Spitzer observations

- Determination of the PAH size degenerate with that of nH and G0 and quantitative conclusions will be obtained from consistent modeling of the gas state, radiative transfer and spinning dust
- At this level of modelling it is not possible to constrain the electric dipole moment of PAHs
- Planck data provide a rich source of observations that can be used as a basis for developing a realistic understanding of the AME mechanism in a range of Galactic environments

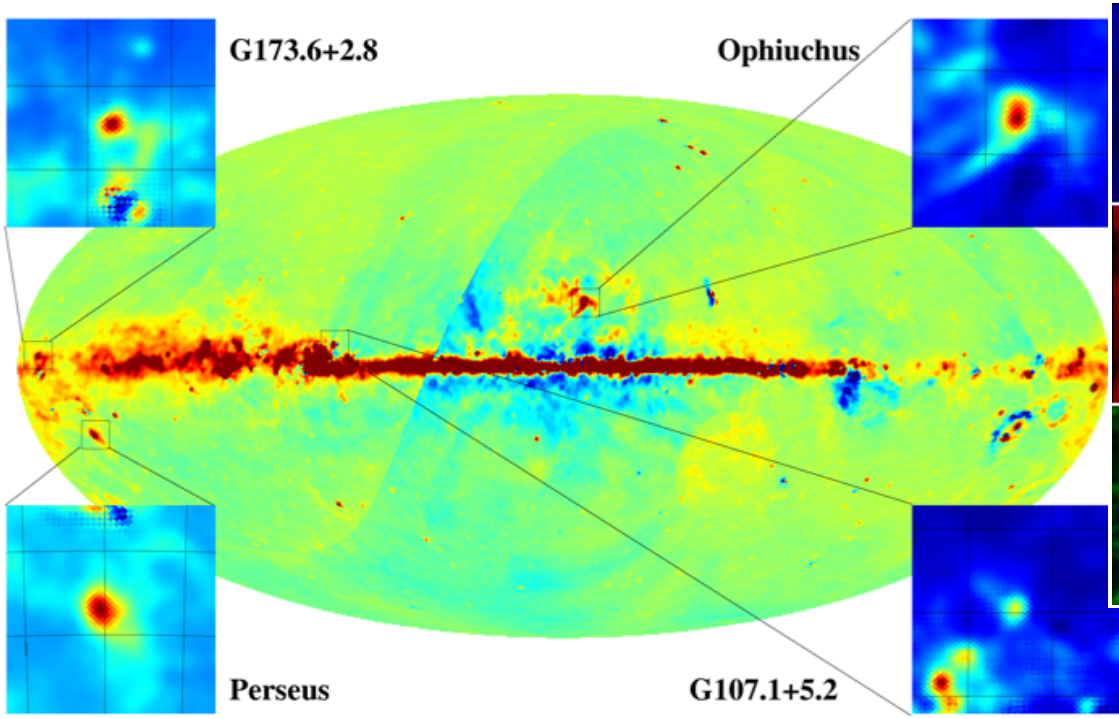

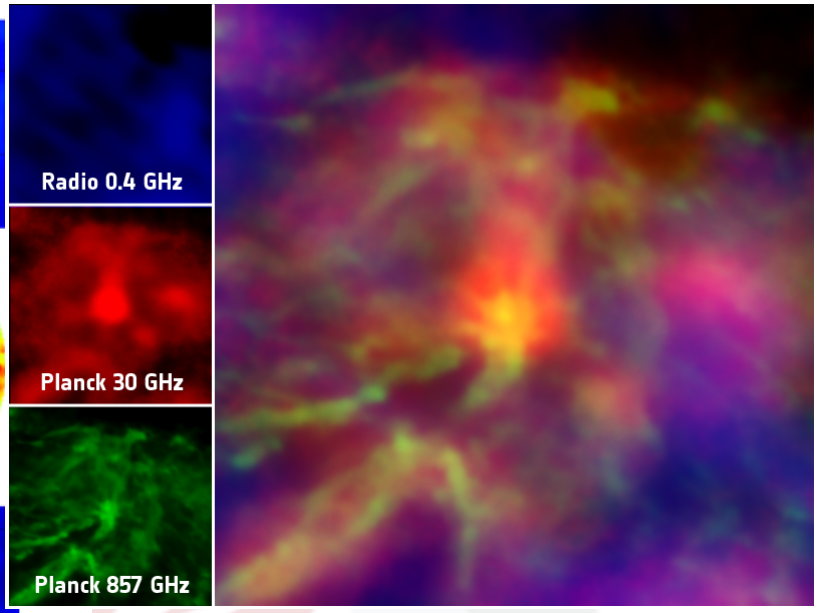

Fig. 10. Residuals in the full sky *Planck* LFI 28.5 GHz 1° smoothed map after subtraction of synchrotron, free-free and thermal dust emission (see text). 12.°5 × 12.°5 cut out maps are shown for the Perseus and ρ Ophiuchus molecular clouds, and the two new regions of AME, G107.1+5.2 and G173.6+2.8.

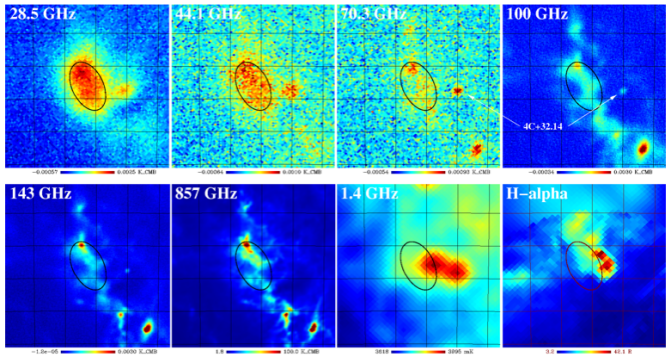

Fig. 1. Maps of the Perseus molecular cloud region at their original angular resolution. From left to right, top row: *Planck* 28.5, 44.1, 70.3 and 100 GHz, bottom row: *Planck* 143 and 857 GHz, 1.4 GHz and Hα. The maps cover 5° × 5° centred on $(l, b) = (162.°26, -18.°62)$ and have linear colour scales. The graticule has 1° spacing. The FWHM of the elliptical Gaussian model used to fit the flux density in the filtered maps (see text) is shown. The strong AME is evident at 30 – 70 GHz.

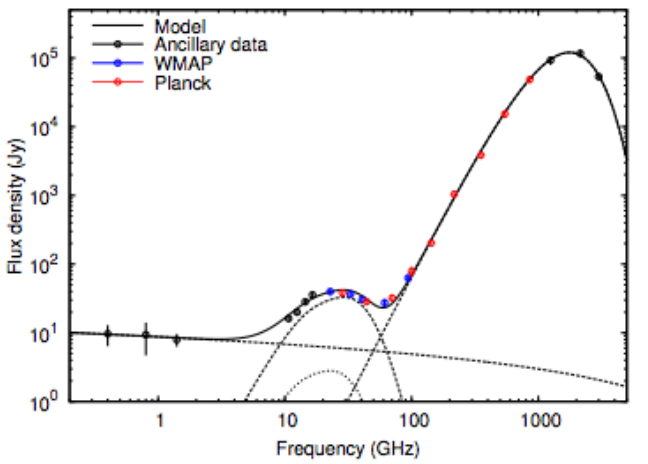

Fig. 4. Spectrum of G160.26-18.62 in the Perseus molecular cloud. The best-fitting model consisting of free-free, spinning dust (2 components), and thermal dust is shown.

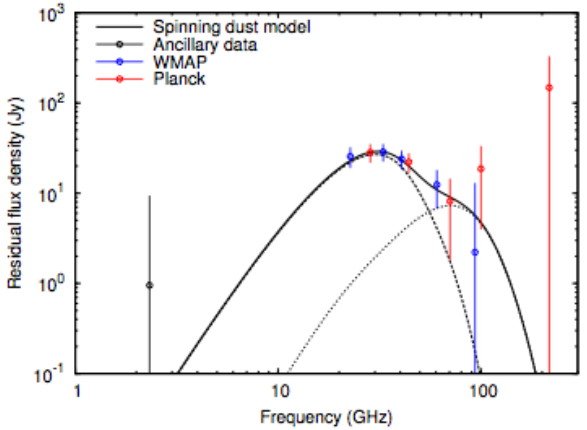

Fig. 9. Spectrum of G353.05+16.90 in the ρ Ophiuchus molecular cloud after subtracting the best fit free-free, CMB and thermal dust components. A theoretical spinning dust model consisting of two components (dark cloud and PDR; see text), is shown.

The Galactic Cold Core Population revealed by the first all-sky survey - I

- Statistical properties of **the first version of the Cold Core Catalogue of Planck Objects (C3PO)**, in terms of their **spatial distribution, temperature, distance, mass, and morphology**
- Statistics of the Early Cold Core Catalog (ECC): it is a subset of the complete catalogue that contains only the most reliable detections
- ECC is delivered as a part of the ERCSC
- CoCoCoDeT algorithm to extract **about 10 thousands cold sources**
- The method uses the **IRAS 100μm data as a warm template** that is extrapolated to the Planck bands and subtracted from the signal, leading to a detection of the cold residual emission
- **Cross-correlation with ancillary data** to increase the reliability of our sample, and to derive other key properties like distance and mass
- **Temperature and spectral index values** derived using the fluxes in the **IRAS 100 μm band** and the **three highest frequency Planck bands**

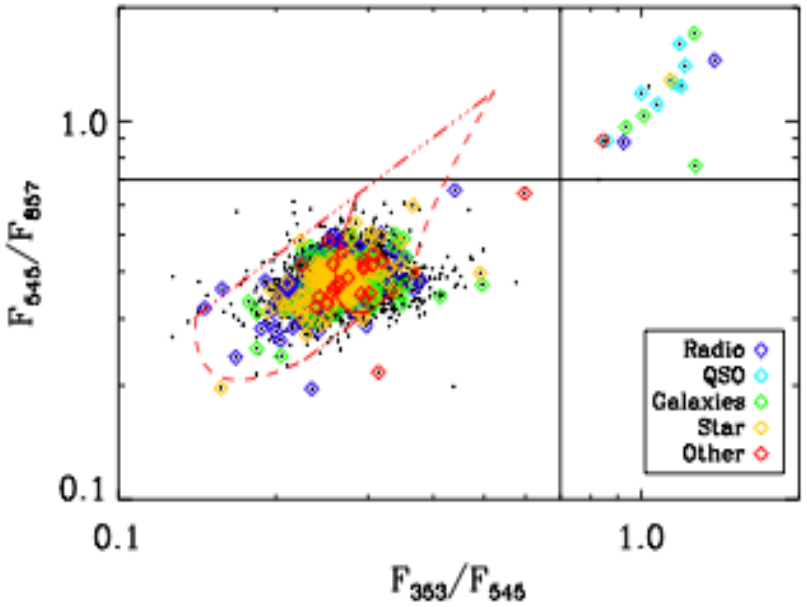

Fig. 1. Color-Color diagram of the catalogue. The over-plotted symbols stand for the positive cross-macthes with non ISM objects. The red contours give the domain of the diagram filled by Archeops cold cores assumed to follow a grey-body law, with a temperature ranging from 6 K < T < 25 K, and a spectral index β given by Désert et al. (2008).

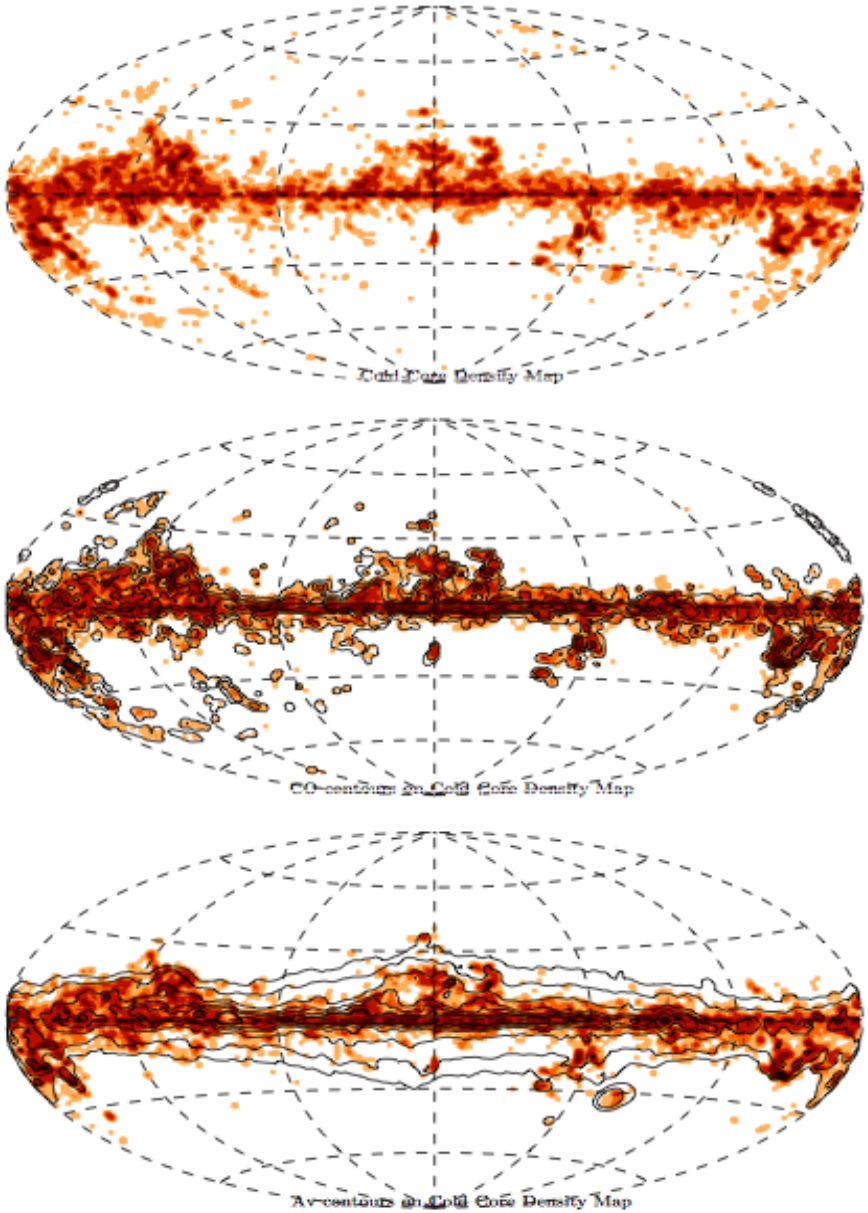

Fig. 3. Upper panel: All-sky density map of the C3PO *Planck* Cold Clumps, smoothed at 3°. Middle panel: CO contours are over-plotted on the C3PO density map which is set to 0 where CO map is not defined. Lower panel: Av contours are over-plotted on the C3PO density map which is set to 0 where Av map is lower than 0.1 Av.

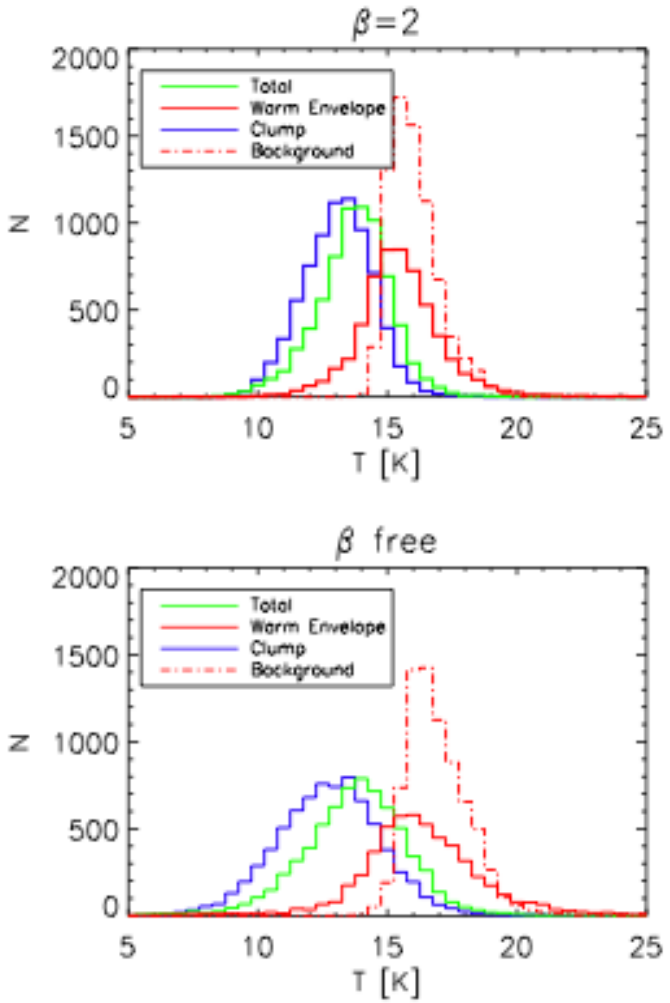

v1.0

Fig. 6. Distribution of the temperature of the cold clumps (blue), of the warm envelope (red) and of the total (green) estimated inside the elliptical gaussian of the clump itself. The averaged temperature of the local background is plotted in red dot-dash line.

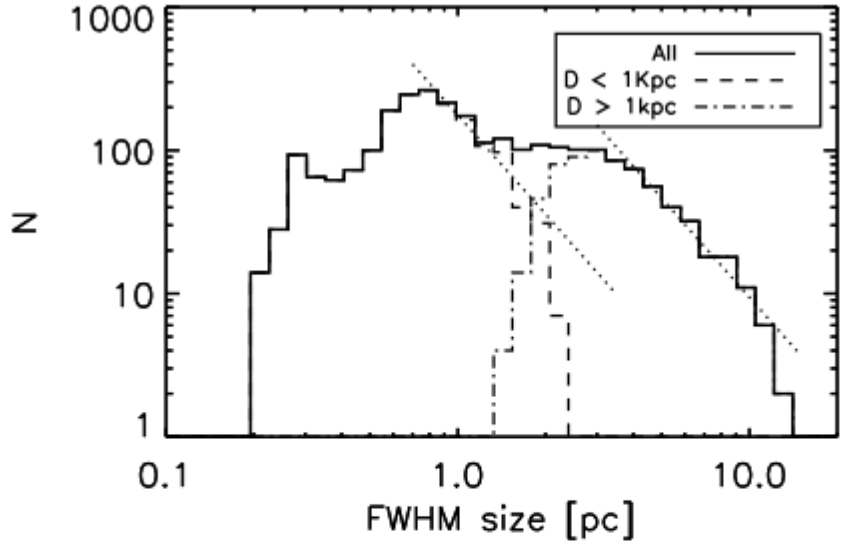

Fig. 9. Distribution of the physical size of the cold clumps in pc. The distinction is done between the local sample ($D < 1$kpc, dashed line) and the distant sample ($D > 1$kpc, dot-dash line). A power law with $\alpha = -2.3$ is overlaid in dotted line over the 2 subsets.

Next steps

- Intermediate papers will appear almost continuously during 2011, with a “burst” at February 2012 in occasion of the *Planck 2012 Conference in Bologna CNR Area* "***Astrophysics from radio to sub-millimeter wavelengths: the Planck view and other experiments***” (Feb 13-17) and then again continuously during 2012 and later.

- 2013 – delivery of Planck products & release of cosmological papers based on the first 15 months of data.

- Astrophysical papers will be roughly divided into two wide categories: those mainly based only total intensity data and those requiring well established polarization data; this (but not only of course!) will reflect into readiness/submission period.

Next steps

- All papers will be reviewed by the (*Planck* Internal) Editorial Board & the *Planck* Science Team.
- Astrophysical projects are carried out by dedicated project teams in the context of *Planck* Working Groups (5 – clusters & secondary anisotropies – 6 – extragalactic sources – 7 – Galactic & solar system science).
- Each project team will prepare one or (typically) more papers.
- We expect several tens of papers in next year.

Topics: extragalactic sources

- (a) Analysis of the statistical properties and evolution of radio and sub-mm sources, and their classification into dominant populations.
- (b) Survey of extreme radio sources, i.e. those with unusual, sharply peaked, or inverted spectra.
- (c) Construction and analysis of a catalogue of quasars and BL Lac objects, combining Planck data with data from a wide variety of other wavelengths. Specific effort is being made to detect flaring sources and follow them up quickly with ground facilities.
- (d) Construction and analysis of a catalogue of nearby galaxies, and the detailed study of a small number of resolved galaxies (LMC, SMC, M 31, M 33).
- (e) All-sky survey and analysis of bright high-redshift dusty galaxies, and possibly proto-clusters.
- (f) Extraction of the cosmic far-infrared background believed to consist of unresolved galaxies, and analysis of the angular power spectra of this component.

Topics: Galactic science

- (a) Construction of a model of the large scale ordered magnetic field in the Galaxy, based on the polarised Planck maps.
- (b) Study of the diffuse warm ionized gas in the Galaxy, based on the Planck map of free-free emission.
- (c) Reconstruction of the Galacto-centric distribution of emission of the different phases of the interstellar medium in the Galaxy (H2, HI, H), by correlation of the Planck maps to tracers of each phase.
- (d) Study of the diffuse synchrotron emission from the Galaxy, in particular its spectrum and its spatial structure.
- (e) Study of the physical characteristics of the circumstellar environment of various types of stellar objects in the final phases of their evolution.
- (f) Construction and analysis of a catalogue of compact and ultra-compact HII regions and massive young stellar objects.
- (g) Construction and analysis of a catalogue of cold pre-stellar cores in the Galaxy.

Topics: Galactic science

- (h) Study of the spectral energy distributions of Supernova Remnants across the Planck bands.
- (i) Study of the spatial and spectral distribution of thermal dust polarisation to elucidate the nature of dust in the various phases of the interstellar medium.
- (j) Establishment of the spatial and spectral properties of the anomalous emission so far attributed to spinning dust particles.
- (k) Combination of Planck maps with lower frequency large-scale ground based surveys to study the relationships between the various phases of the Galactic interstellar medium (atomic, molecular, ionized, relativistic, magnetic, etc.).
- (l) Study of the properties of dust in regions at high Galactic latitudes and in intermediate and high velocity clouds, using the Planck data in combination with other tracers such as HI, IRAS/IRIS etc.
- (m) Study of the Planck maps to determine the structure and distribution of mass in molecular clouds.
- (n) Study of the structure and intensity of the magnetic fields (ordered and tangled components) within nearby inter-stellar clouds, in relation with their density and velocity structure.

Detailed characterization of Galactic diffuse components

- 1. Synchrotron: pattern, spectral behaviour
- 2. Free-free: its relevance in particular close to the Galactic plane
- 3. Thermal dust: cold, warm components
- 4. Anomalous emission (spinning dust?)
- 5. (?) DM annihilation
- → Galactic magnetic fields (ordered vs turbolent components)
- Dust grain properties
- ISM history

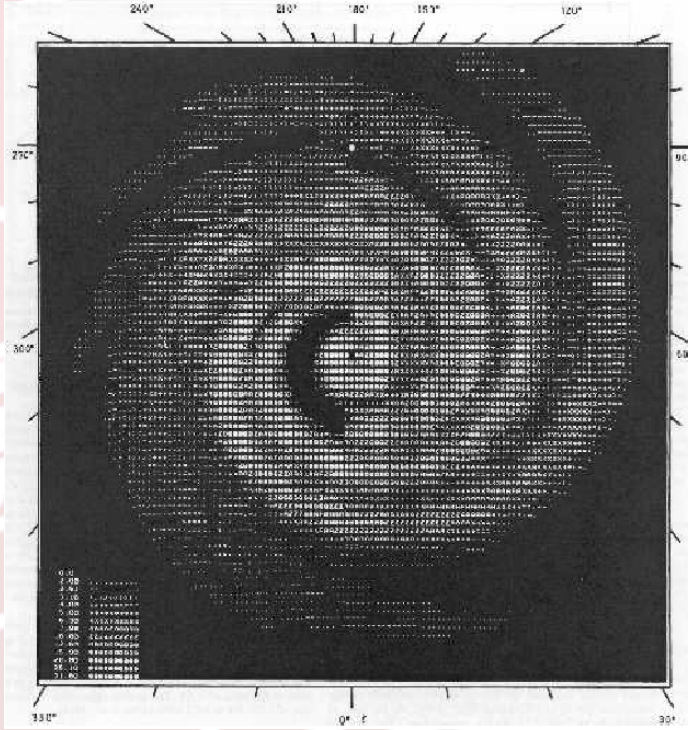

FIG 5.7.— Top view of the 3-D model of synchrotron emissivity derived from the Haslam map by Beuermann et al. (1985). The model contains assumptions on the Galactic magnetic field orientation and degree of alignment along the spiral arm, and therefore can be used to synthesize a map of synchrotron polarisation around the Sun (filled circle).

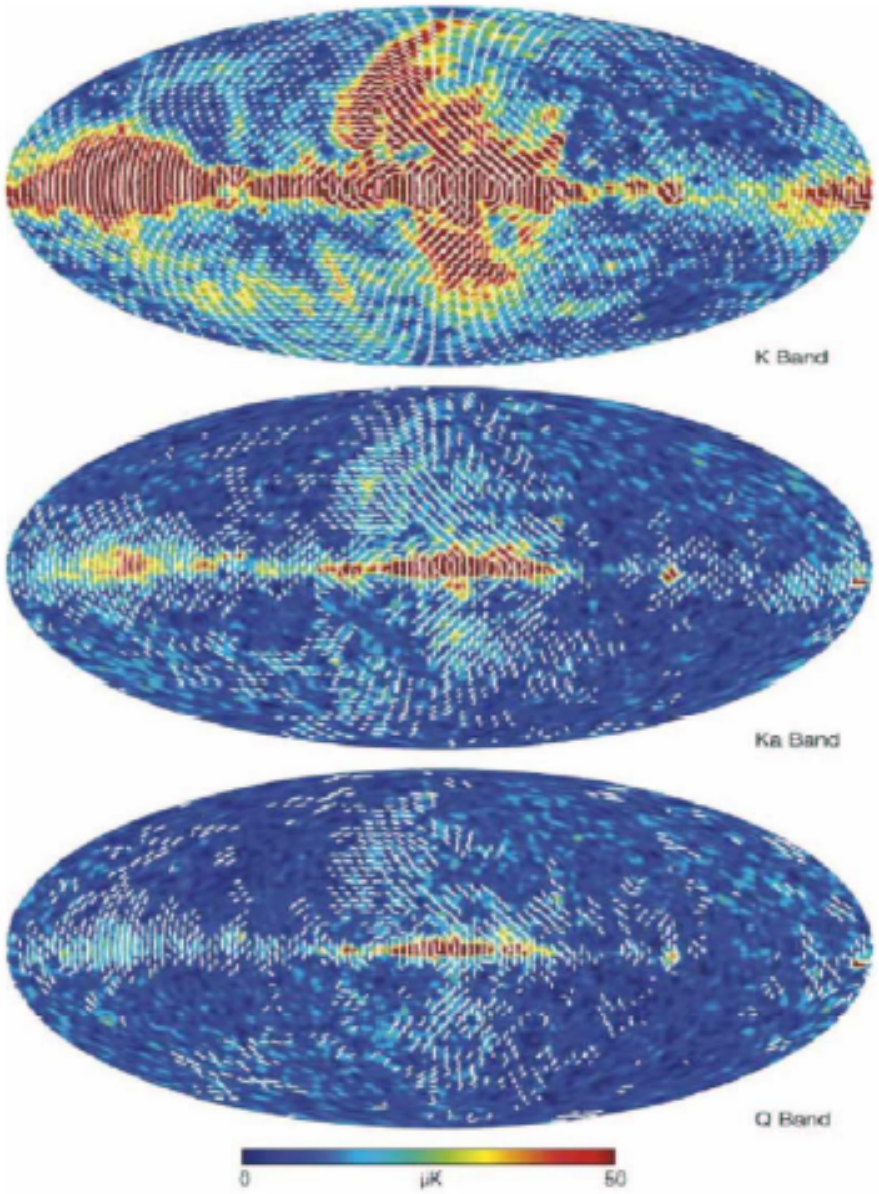

WMAP 3 yr Pol. maps and mask.

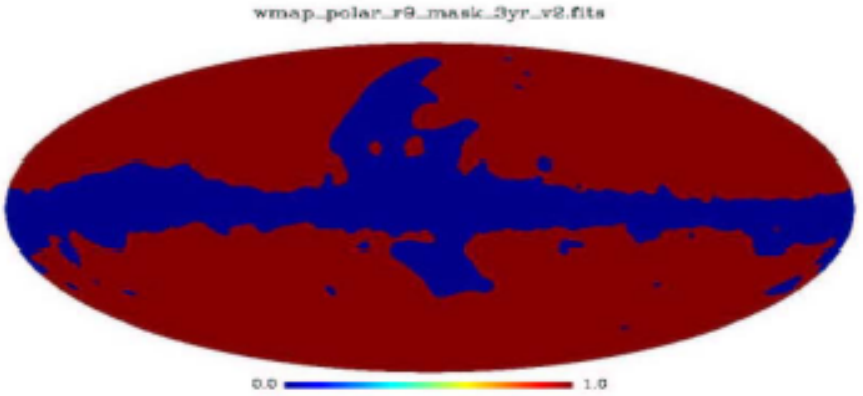

- **Synchrotron Polarization**
  - **Info from WMAP**
  - **Info from radio surveys**
  - **Relevance of Planck**

Polarization: Comparison of radio 1.4 GHz surveys with WMAP

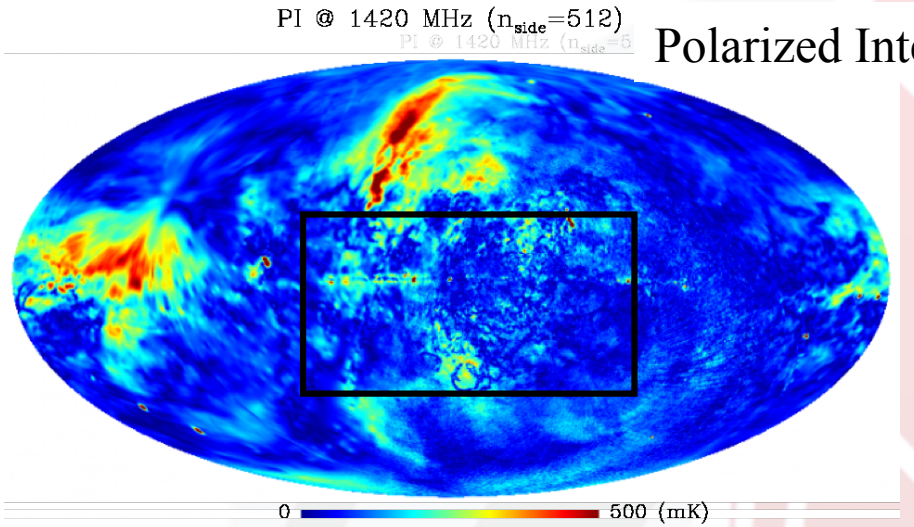

Polarized Intensity

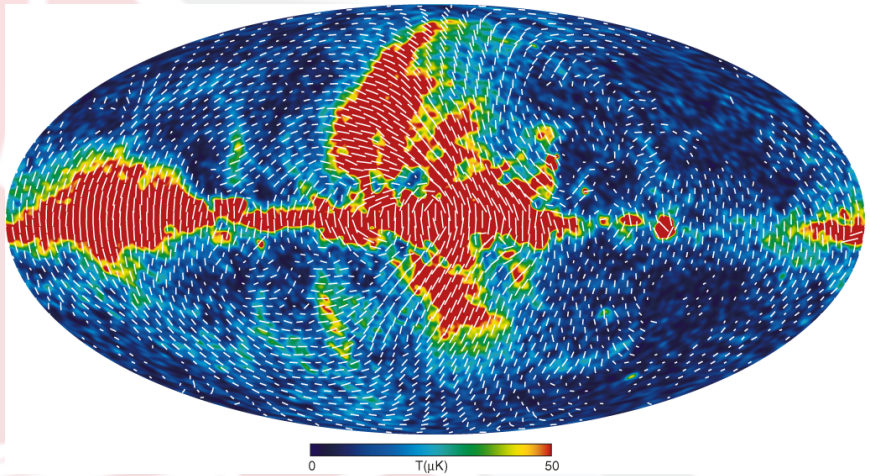

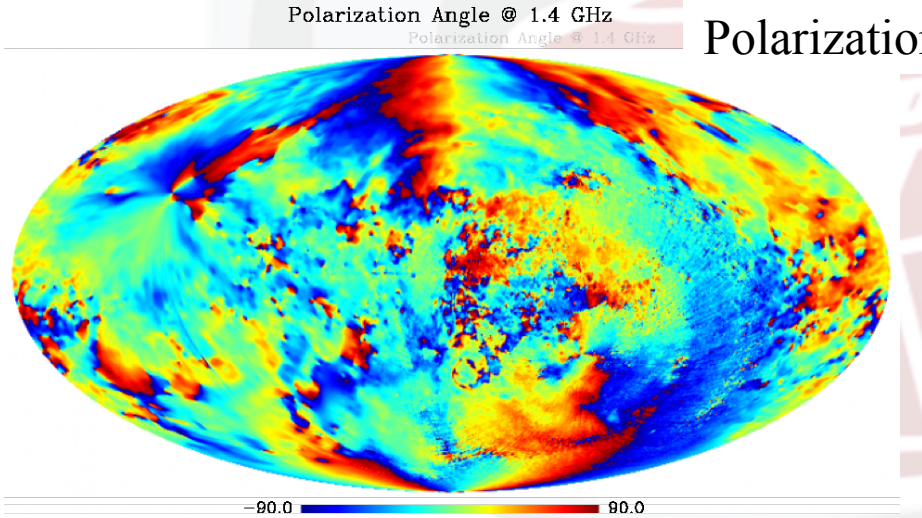

Polarization Angle

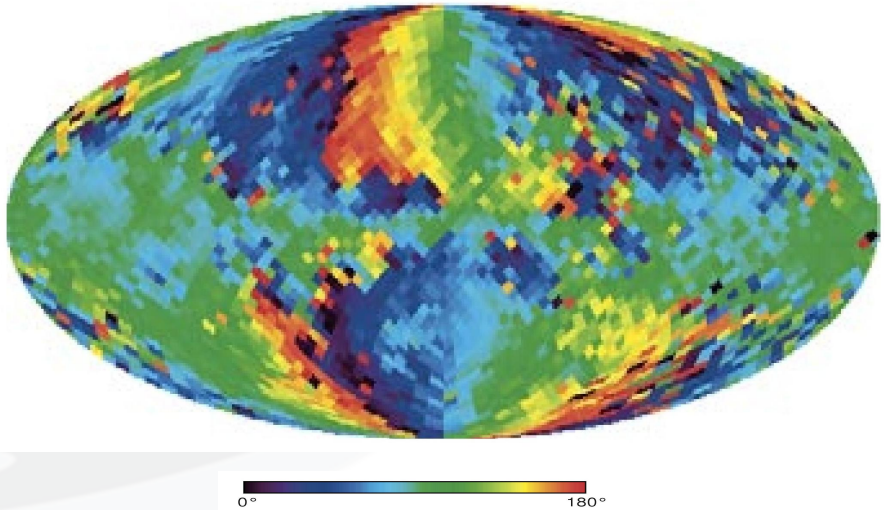

Polarization Angle + 90°

1.4 GHz *[Reich et al., in preparation]*

WMAP 23 GHz *[Page et al. 2006]*

Polarization: Comparison with WMAP

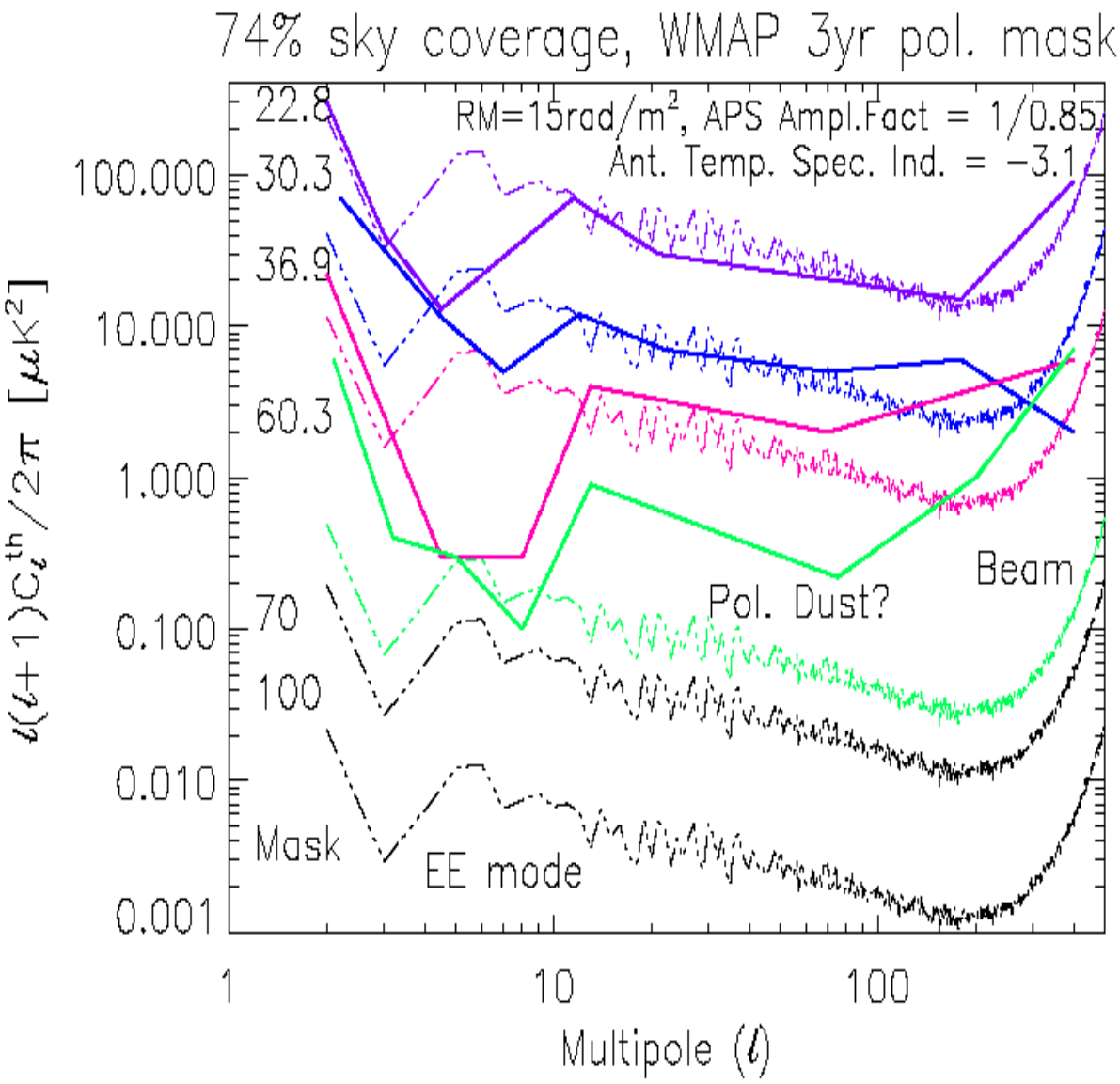

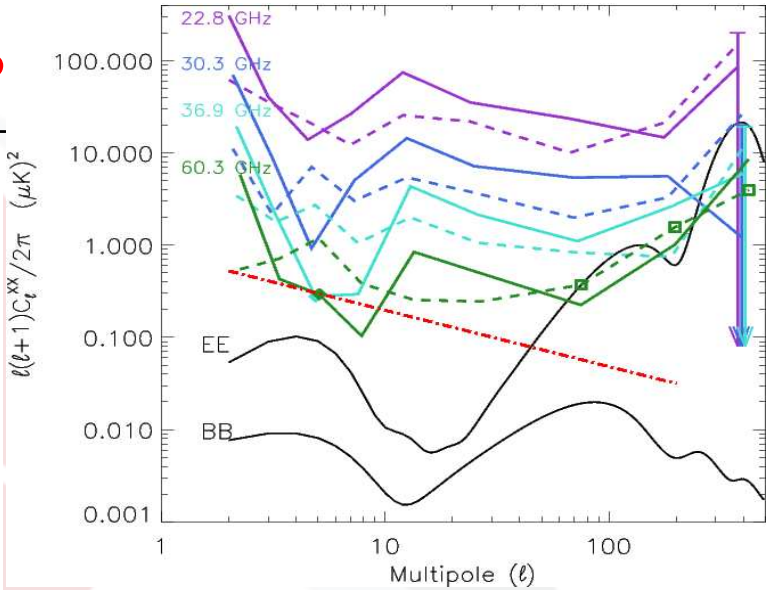

In agreement with WMAP results at intermediate ℓ (~ 10-100) within a factor ~ 2 or better, @ ν ≤ of about 40 GHz. Dust important @ higher ν

1.4 GHz new polarization maps good template of the large scale synchrotron emission

Burigana et al. 2006, PoS(CMB2006)016

Topics: solar system

- (a) Extraction and analysis of the zodiacal light emission, and constraints on dust properties and content within the solar system.

- (b) Detection and analysis of the emission from several classes of objects, such as main belt asteroids, planets, and comets.

Solar System Science

NUMBER OF DETECTABLE MAIN BELT ASTEROIDS[a]

R/d	Differential Number	Cumulative Number[b]
$1–2 \times 10^{-7}$	299	397
$2–3 \times 10^{-7}$	76	98
$3–4 \times 10^{-7}$	15	22
$4–5 \times 10^{-7}$	4	7
$R/d > 5 \times 10^{-7}$	0	3

[a] The lower threshold considered here for asteroid detection is set to a radius to distance ratio $R/d \sim 10^{-7}$, derived by assuming a typical asteroid temperature of ~ 150 K and by taking into account the *Planck* sensitivity at different channels (see Cremonese et al. 2003 for details).

[b] The cumulative number is computed at the lower limit of the range listed for the differential number.

ZLE with *Planck*

FIRAS Spectra

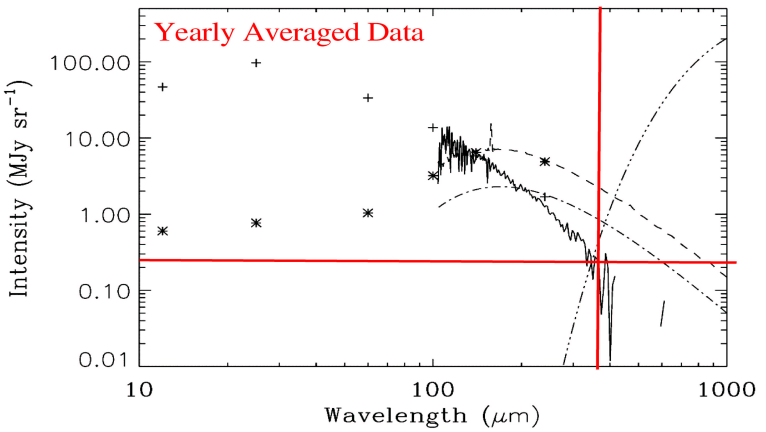

Fixsen, Dwek, 2002 ApJ, 578, 1009

ZLE COBE/DIRBE MAP

12 μm, ecliptic projection

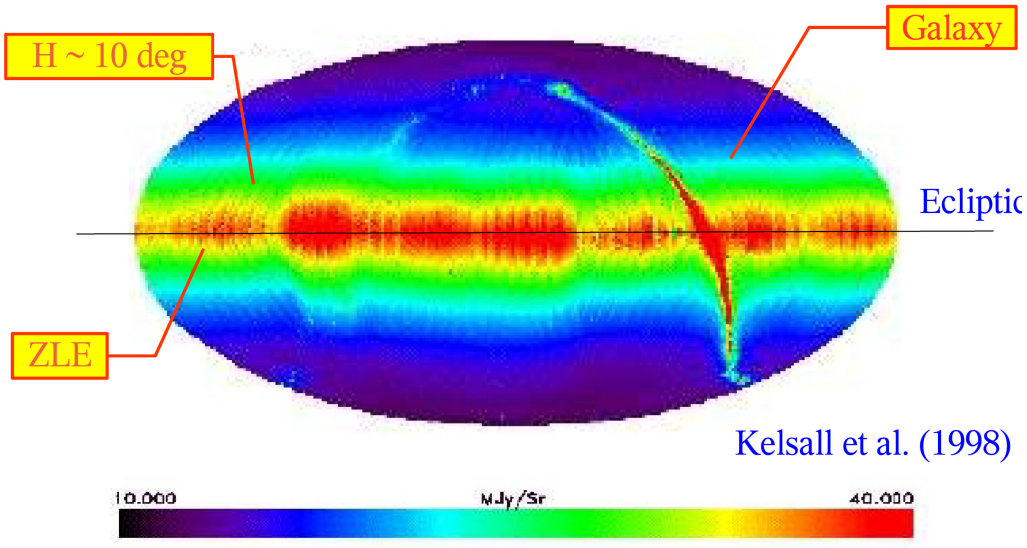

Kelsall et al. (1998)

Two Components Signal $F_f(P)$

f = Frequency (857 GHz, 550 GHz, …)

Pointing — Planck Position

$$F_f(P, R_P) = E_f Z_f(P, R_P) + G_f(P) + n$$

Emissivity Correction

Function of size distribution and grains properties

E_f(Smooth) ~ 0.5

E_f(Secondary) ~ 1±0.2

Galaxy

Spatial Pattern

Black Body emission averaged for grains spatial density

KBOE - Large Scale Traces of Solar System Cold Dust on CMB Anisotropies

M. Maris, C. Burigana, A. Gruppuso, F. Finelli. J.M. Diego - MNRAS in press

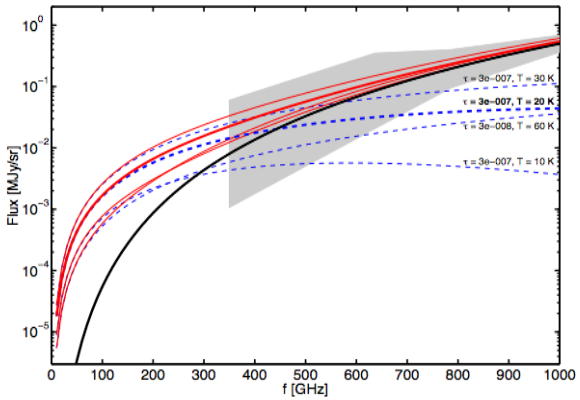

Figure 1. Comparison of ZLE fluxes compatible with COBE/FIRAS data (Fixsen & Dwek 2002) and a set of possible models of KBOE (Stern 1996). The black solid line shows the ZLE derived from the best fit model to COBE/FIRAS data and extrapolated to lower frequencies. The gray band represents a sketch of the allowed region obtained from the error bars in Fixsen & Dwek (2002). The blue dashed lines display four different models of KBOE corresponding to different values of τ and T. The resulting fluxes, sum of KBOE and ZLE, are represented by the red solid lines. Note that the classical ZLE (estimated on the basis of COBE data) is negligible in practice at WMAP frequencies, whereas KBOE might not be ignored.

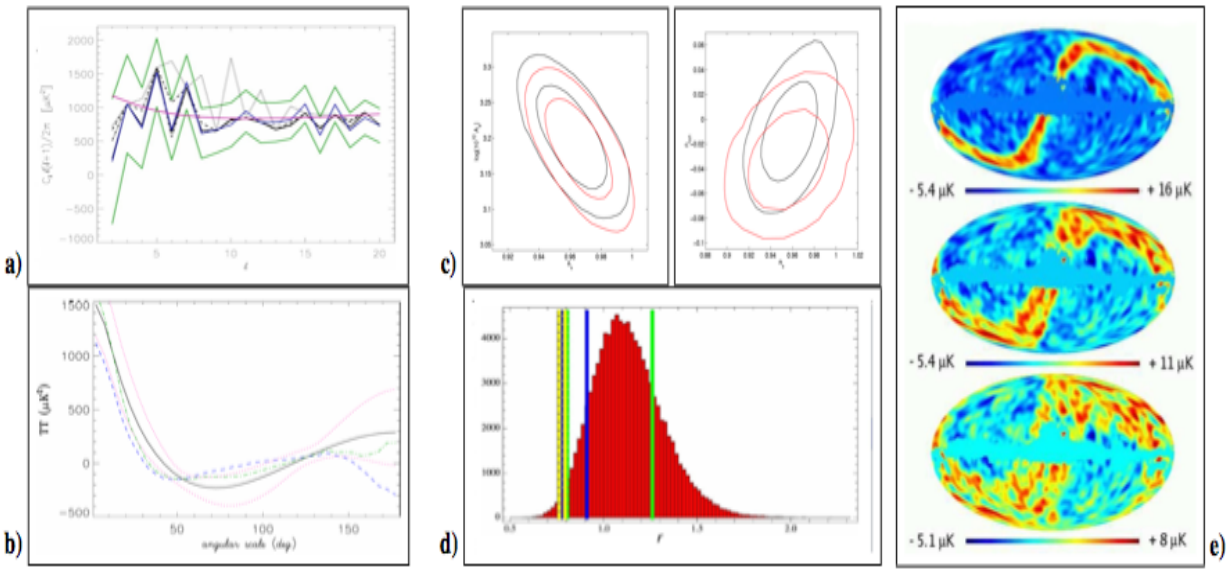

Figure 2. Panel a): APS at low multipoles as derived by the WMAP team analyzing the ILC 7 yr map (blue solid line) with its 1σ errors (green solid lines); APS of the ILC 7 yr map derived using `Anafast` (black solid line); APS of the ILC 7 yr map after the subtraction of our KBOE template with $H_{\rm KBOE} = 70°$, 35° and 17.5° (black dotted–dashed line, dashed line, and dotted line, respectively). The dust model with $\tau = 3 \times 10^{-7}$ and $T = 30$ K (CM) and the V band is here considered. The red solid line shows APS of the best fit ΛCDM model for the WMAP 7 yr map. Panel b): two-points correlation function computed for maps at HEALPix resolution $N_{\rm side} = 16$. The solid line displays the average of 10^5 MC realizations of CMB anisotropy maps extracted from the WMAP 7 yr best fit ΛCDM model APS shown in panel a). The red dotted lines show the corresponding 1σ level fluctuations of the MC simulation. The blue dashed line refers to the ILC 7 yr map. The green dotted-dashed line refers to the map derived subtracting from the ILC 7 yr map one of our KBOE model, namely that obtained for the CM with $H_{\rm KBOE} = 17.5°$. Panel c): Two dimensional marginalised probability distributions for cosmological parameters by removing (black lines) or not removing (red lines) the KBOE template for the CM with $H_{\rm KBOE} = 35°$ (curves are the 68% and 95% confidence level). To the left (right) the plot for A_s ($n_{\rm run}$) vs n_s for a standard ΛCDM model (including running of the scalar spectral index). Panel d): parity anomaly of the estimator $r = P_+/P_-$ as defined in the text with $\ell_{max} = 22$. The histogram (in red) displays the distribution of r obtained from 10^5 MC realizations. Vertical lines correspond to the maps considered in this work: the black solid line (on the left) refers to the ILC 7 yr map; colored solid lines refer to the CM; colored dashed lines refer to the WM. Green, blue, and yellow lines are for $H_{\rm KBOE} = 17.5°$, 35°, and 70°, respectively. Panel e): predicted signal in the combination $V + W - 2Q$ from the CM with $H_{KBOE} = 70°$ (bottom), $H_{KBOE} = 35°$ (middle), and $H_{KBOE} = 17°$ (top). The map units are μK and it has been smoothed with a 7° Gaussian. Compare this plot with Fig. 1 of Diego et al. (2010) based on WMAP data: the model with $H_{KBOE} = 70°$ seems to agree better with the observations.

Topics: clusters & secondary anisotropies

- (a) Production and analysis of a catalogue of Sunyaev-Zeldovich (SZ) sources detected by Planck.
- (b) Analysis of the combination of Planck SZ-selected galaxy clusters with a wide range of other observations (X-ray, optical, near-IR, sub-mm), either from existing surveys or by dedicated follow-up, to study their physicsand evolution.
- (c) Reconstruction of the ionisation history of the Universe.
- (d) Estimation of the Integrated Sachs-Wolfe effect and its constraints on cosmological parameters e.g. the dark energy equation of state.
- (e) Extraction and analysis of diffuse and kinetic Sunyaev-Zeldovich components.

Reionization

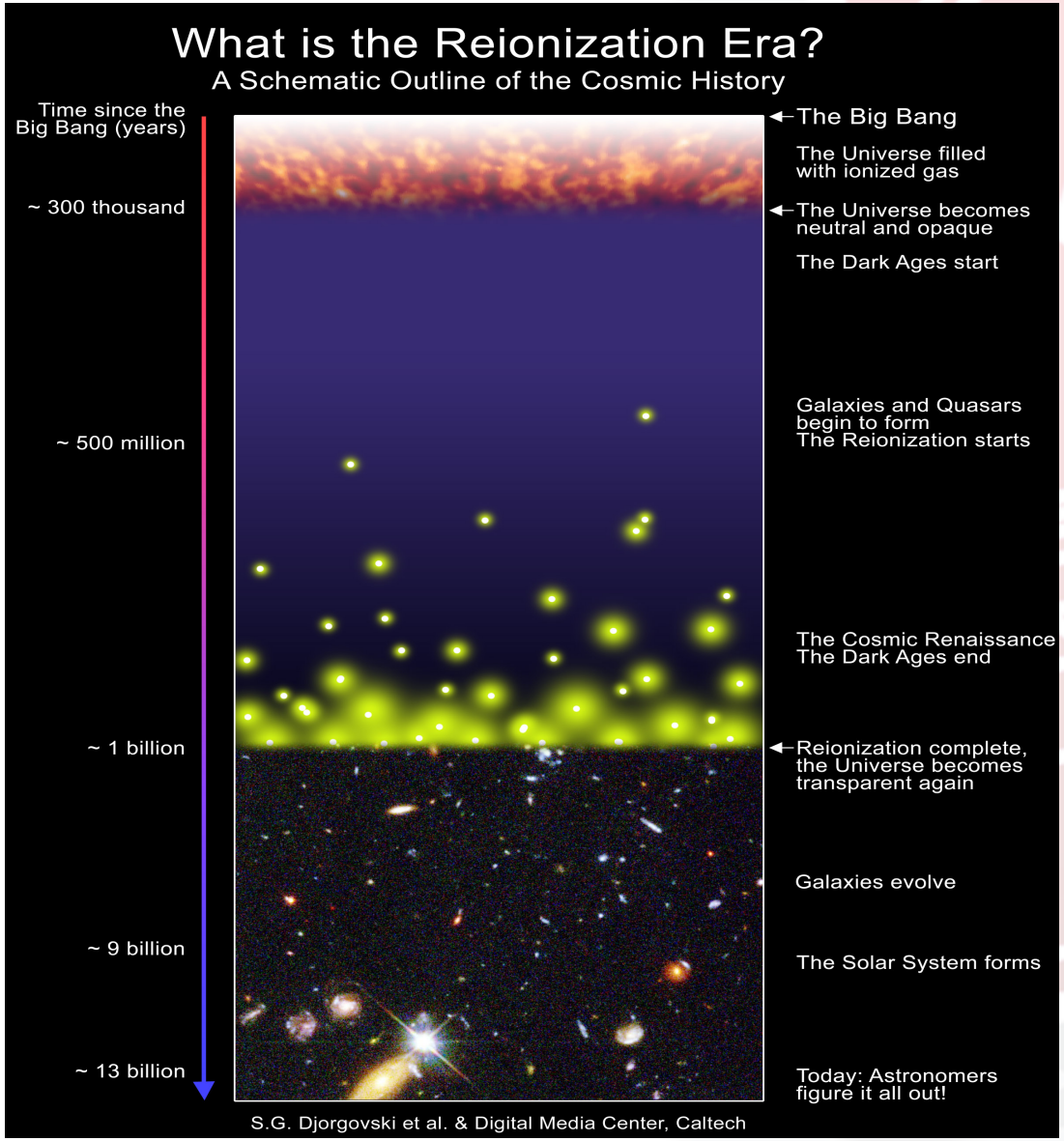

According to the seven-year WMAP analysis, the **current 68% uncertainty on τ is ≃ ±0.015**, almost independently on the specific model considered. **Under various hypotheses** (simple ΛCDM model with six parameters, inclusion of curvature and dark energy, of different kinds of isocurvature modes, of neutrino properties, of primordial helium mass fraction, or of a re-ionization width) the best fit of **τ lies in the range 0.086–0.089**. On the other hand, allowing for the **presence of primordial tensor perturbations or (and) of a running** in the power spectrum of primordial perturbations the best fit of **τ goes to 0.091–0.092 (0.096).**

Reionization history and temperatures [kinetic (CMB) & spin (21 cm)]

Reionization history

Gas temperature

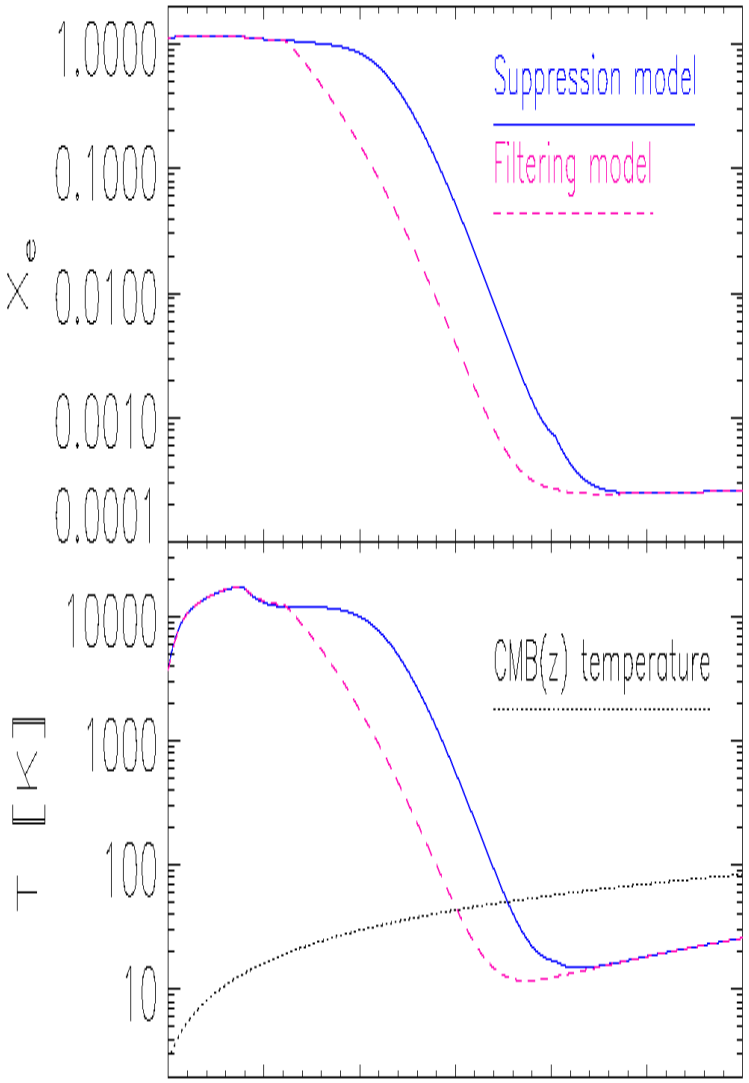

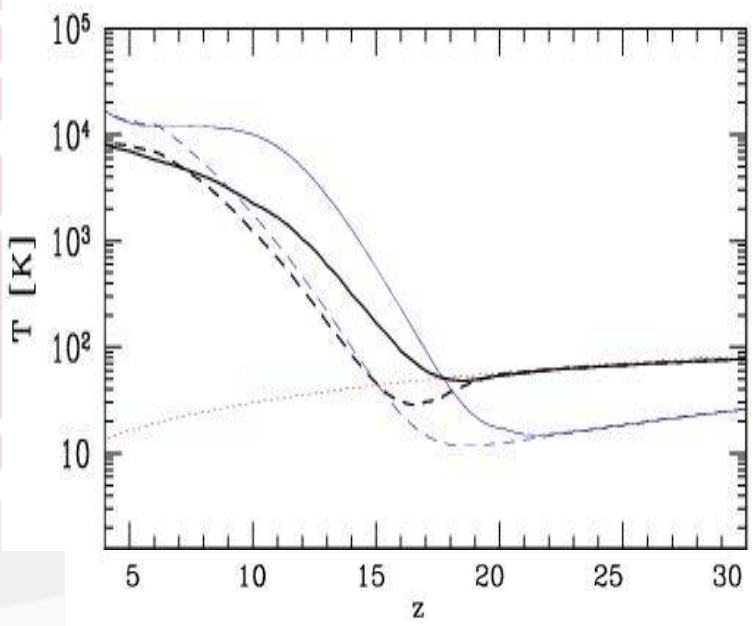

CMB anisotropy signal

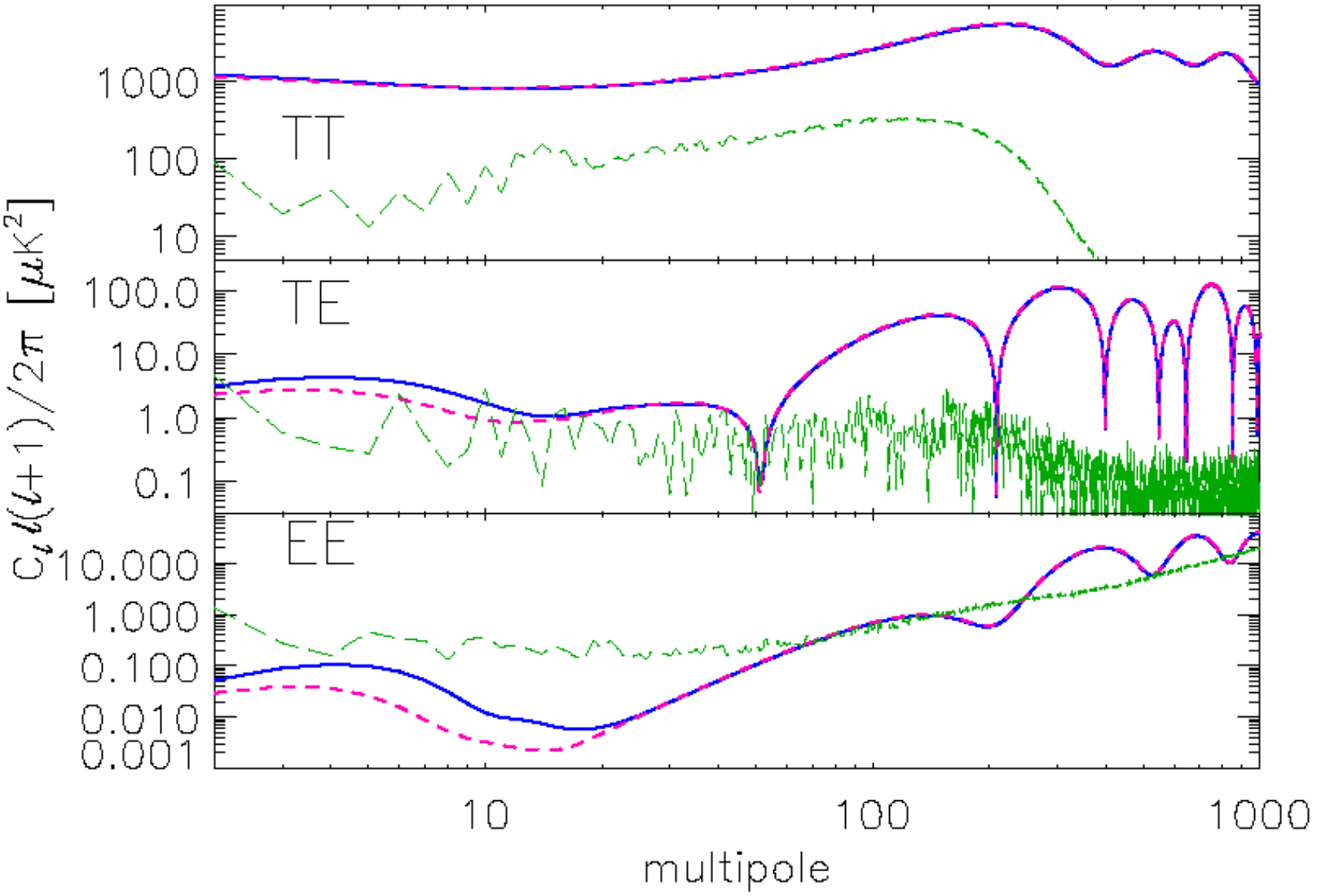

CMB signal (EE): detectability

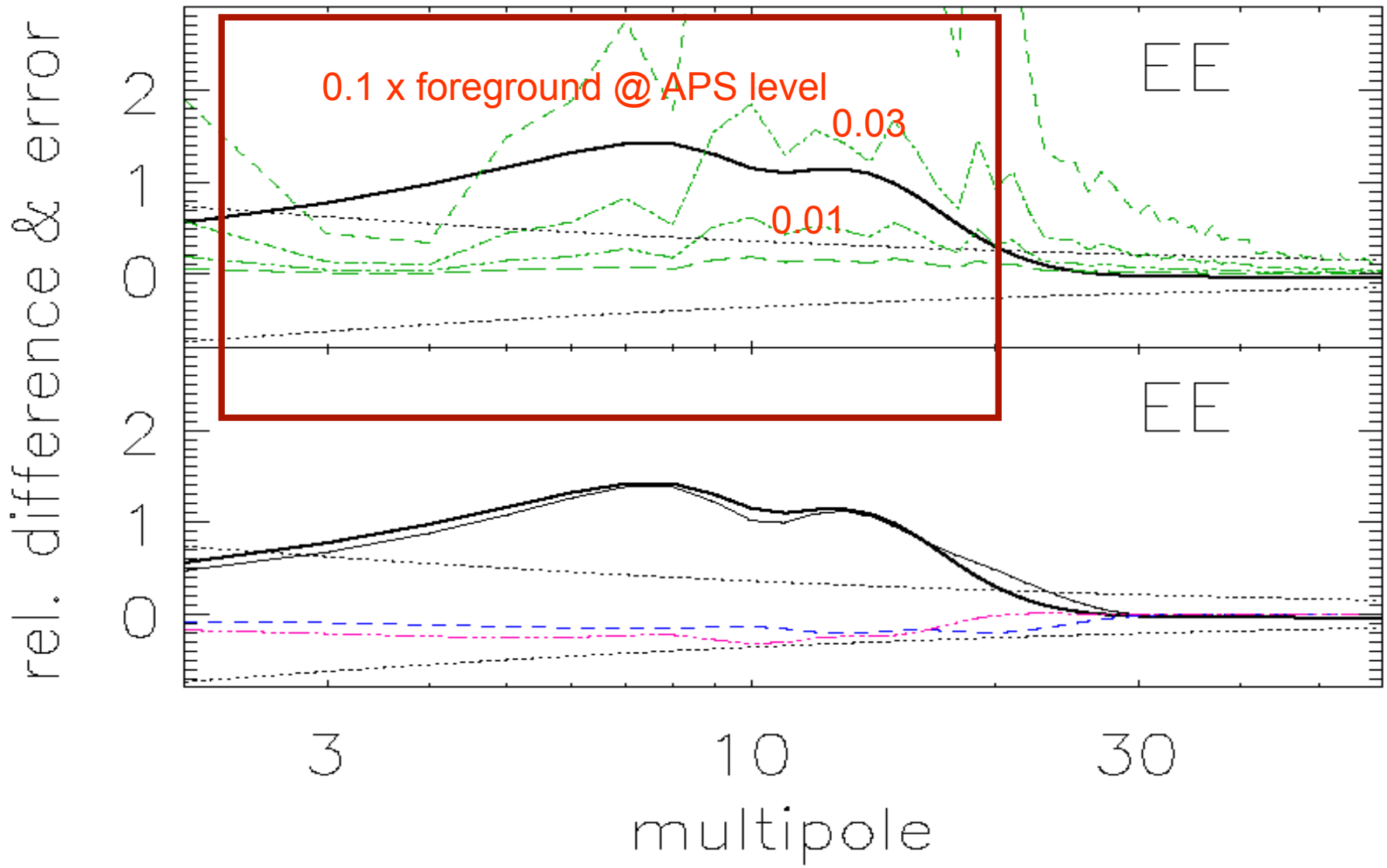

Cosmological perspectives: I. CMB-based cosmology

- **(a) Analysis of the isotropy and statistics of the CMB anisotropies, in particular by**
  - **blind application of a range of statistical tools to the CMB maps**
  - **investigation of the large-scale "anomalies" suspected in the WMAP data**
  - **investigation of large-scale "anomalies" in *Planck polarization maps***
- ***(b) Estimation of the temperature and polarisation angular power spectra and likelihood functions***
- ***(c) Estimation of cosmological parameters, based on***
  - ***Planck data alone***
  - ***Planck data and constraints from other astrophysical data. Special attention will be paid to constraints which can be put on inflationary models***
- ***(d) Search for and constraints on B-mode polarisation anisotropies***
- ***(e) Determination of the gravitational lensing signatures in the CMB caused by intervening large-scale structure***

Cosmological perspectives: II. Non-Gaussianity of the CMB

(a) Bispectrum analysis and constraints on the f_{NL} parameter for "squeezed" triangular wave vector shapes and of more general forms of non-Gaussianity

(b) Testing any measured non-Gaussianity against the predictions of specific inflationary models (e.g. multi-field inflation, curvaton perturbations, DBI inflation etc.

(c) Measuring or setting upper limits on the existence and strength of primordial magnetic fields

(d) Probing the geometry and topology of the Universe, by testing against the predictions of specific models such as Bianchi universes

(e) Testing for the presence of cosmic strings or other classes of defects

WMAP 7 CMB map

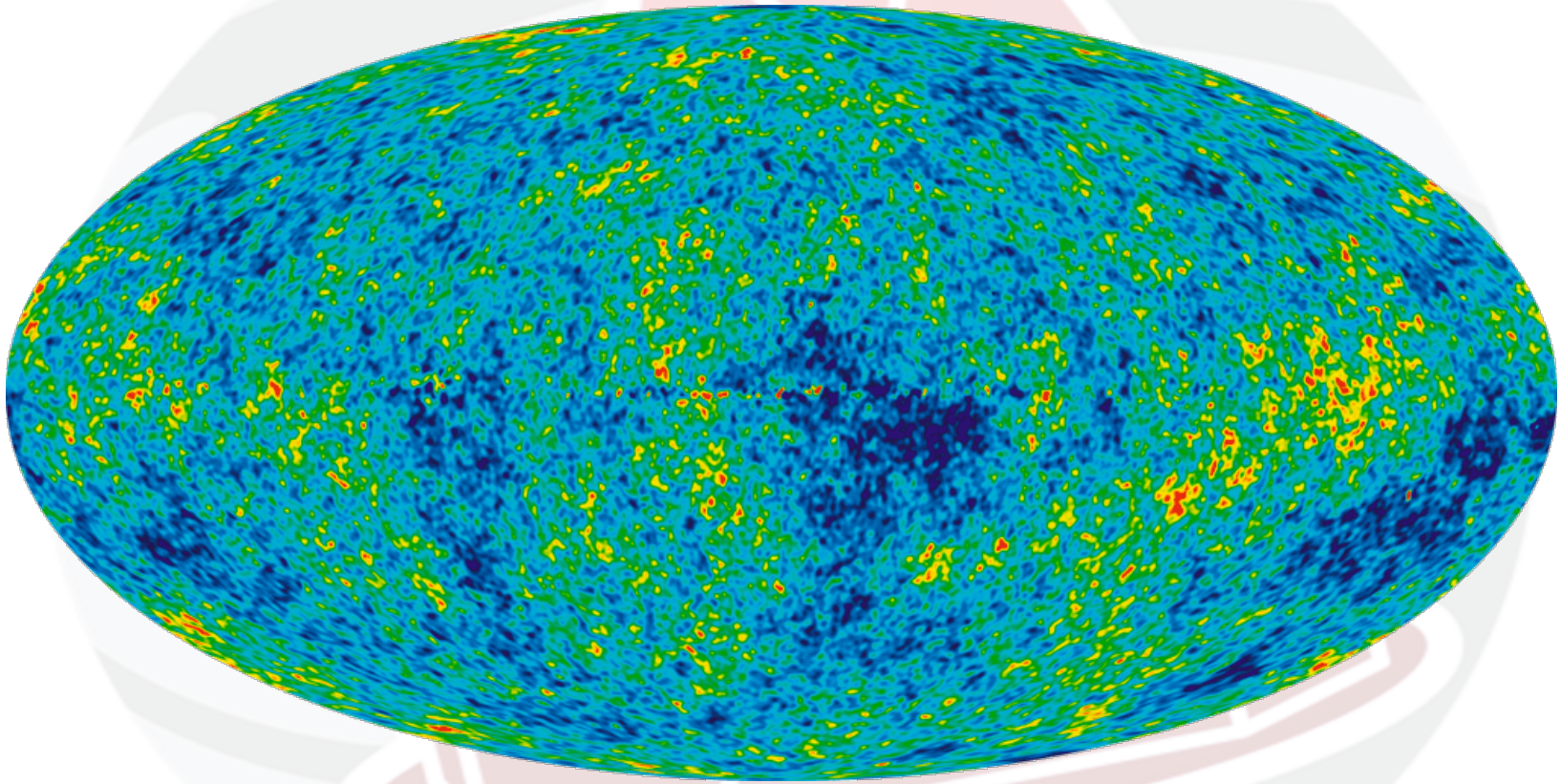

•Courtesy WMAP Science Team

Analyze the field through ***correlation functions (CF)***

$$\left\langle \frac{\Delta T}{T}(\vec{\gamma})\frac{\Delta T}{T}(\vec{\gamma}')\right\rangle$$ Two-point

$$\left\langle \frac{\Delta T}{T}(\vec{\gamma})\frac{\Delta T}{T}(\vec{\gamma}')\frac{\Delta T}{T}(\vec{\gamma}'')\right\rangle$$ Three-point

$$\left\langle \frac{\Delta T}{T}(\vec{\gamma})\frac{\Delta T}{T}(\vec{\gamma}')\frac{\Delta T}{T}(\vec{\gamma}'')\frac{\Delta T}{T}(\vec{\gamma}''')\right\rangle$$ Four-point …

For a Gaussian field (CMB is VERY Gaussian), only two-point counts

$$C(\alpha) \equiv \left\langle \frac{\Delta T}{T}(\hat{\gamma})\frac{\Delta T}{T}(\hat{\gamma}')\right\rangle$$

2-point correlation function depends only on a single angle: *statistical isotropy*

Typical model prediction for CMB anisotropy APS

$$C(\alpha) \equiv \left\langle \frac{\Delta T}{T}(\hat{\gamma}) \frac{\Delta T}{T}(\hat{\gamma}') \right\rangle \quad \Longleftrightarrow \quad \langle a_{\ell m} a^{\star}_{\ell' m'} \rangle = C_\ell \delta_{\ell \ell'} \delta_{m m'} .$$

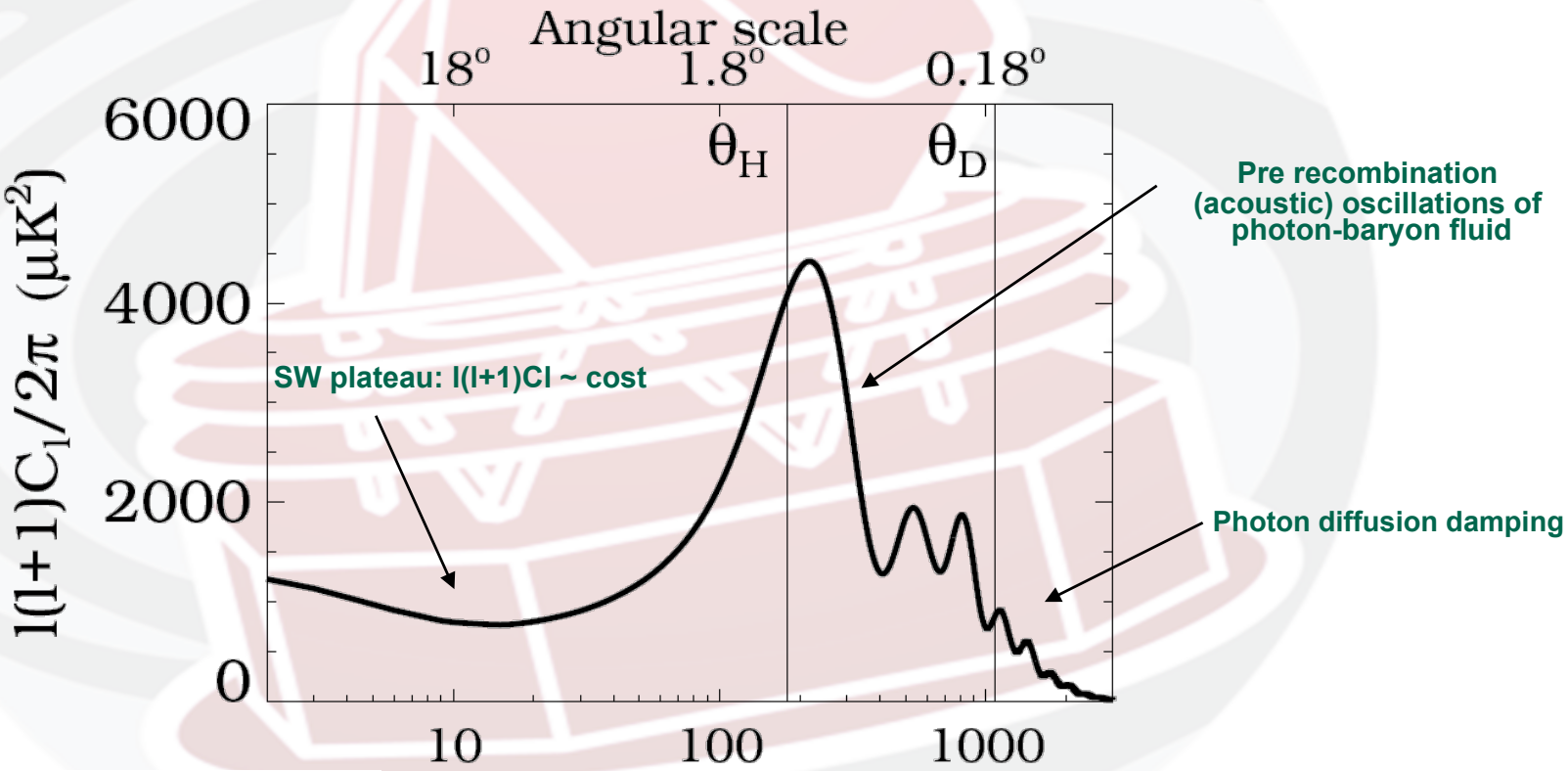

$$\frac{\Delta T}{T}(\vec{x}, \hat{\gamma}) = \sum_{\ell=0}^{\infty} \sum_{m=-\ell}^{\ell} a_{\ell m}(\vec{x}) Y_{\ell m}(\hat{\gamma}) \quad \Longleftrightarrow \quad a_{\ell m}(\vec{x}) = \int_{4\pi} Y_{\ell m}^{*}(\vec{\gamma}) \frac{\Delta T}{T}(\vec{x}, \vec{\gamma})$$

Polarization

(see also A. Lasenby & A. Kogut lectures)

2X2 SYMMETRIC TRACE-FREE POLARIZATION TENSOR $P(\hat{\mathbf{n}}) = \nabla \mathbf{E} + \nabla \times \mathbf{B}$

EXPRESSED IN TERMS OF THE STOKES PARAMETERS Q AND U, CAN BE EXPANDED IN SPIN SPH:

$$Q(\hat{\mathbf{n}}) \pm iU(\hat{\mathbf{n}}) = -\sum_{\ell m} (a^E_{\ell m} \pm i a^B_{\ell m})\ {}_{\pm 2}Y_{\ell m}(\hat{\mathbf{n}})$$

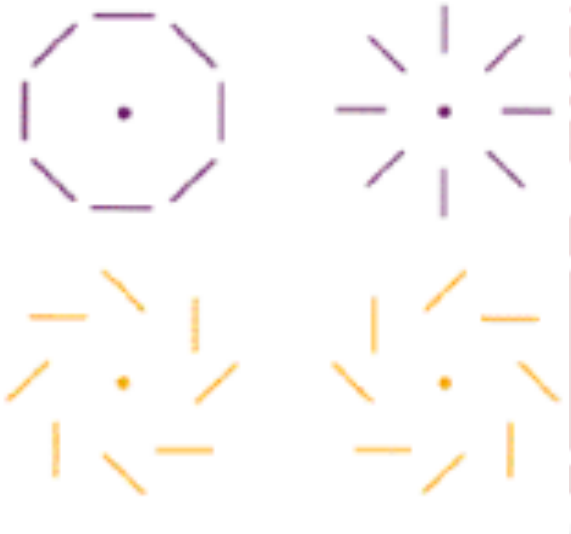

E-MODES EVEN UNDER PARITY

B-MODES ODD UNDER PARITY → CANNOT BE GENERATED BY DENSITY FLUCTUATIONS, WE NEED TENSOR PERTURBATIONS (GRAVITY WAVES)!

6 SPECTRA: $\langle a^X_{\ell m} a^{*Y}_{\ell' m'} \rangle = C^{XY}_\ell \delta_{\ell \ell'} \delta_{m m'}$ DUE TO PARITY $C^{TB}_\ell = C^{EB}_\ell = 0$

Planck: Predicted Power Spectrum

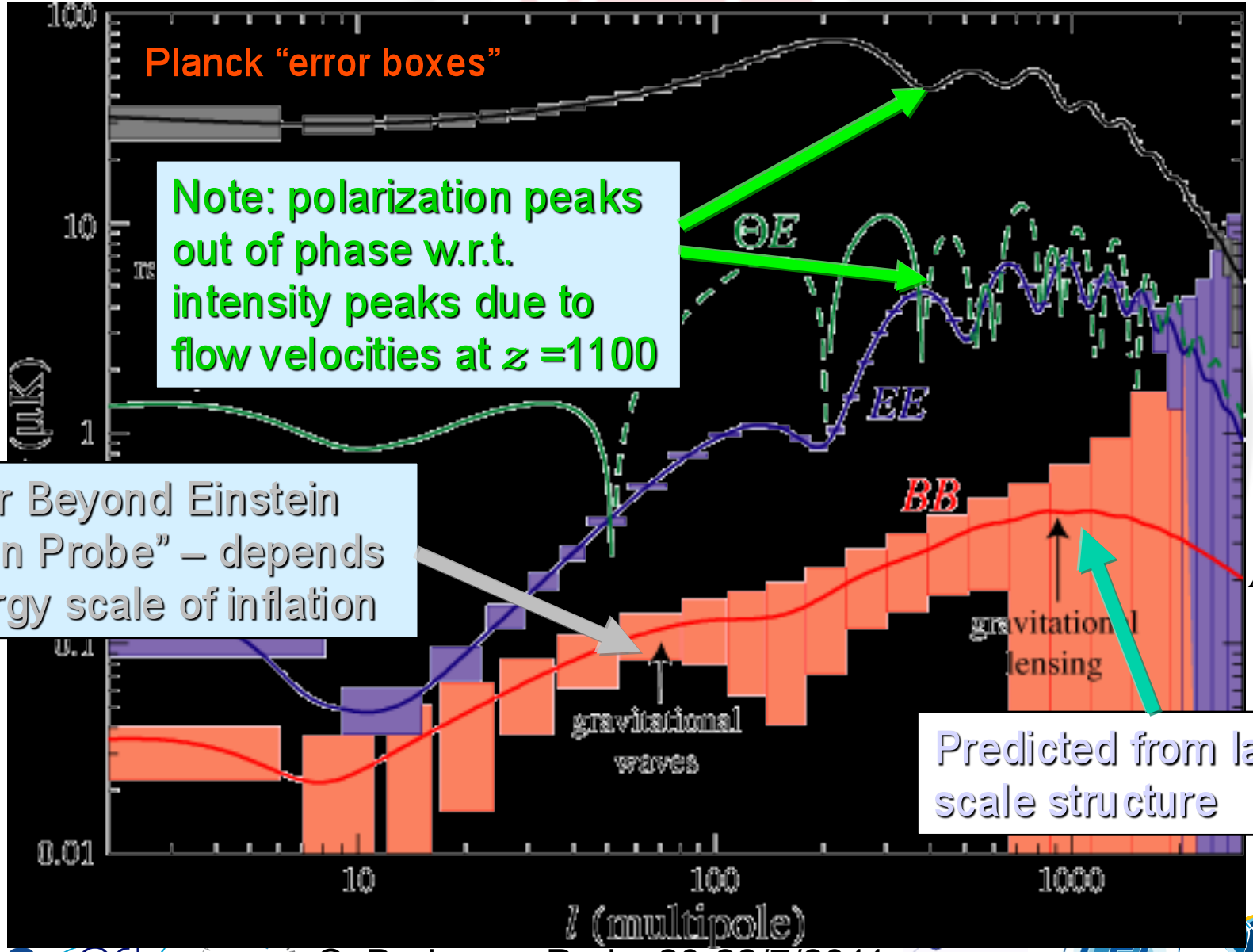

Hu & Dodelson *ARAA 2002*

CMB Angular Power Spectrum

WMAP+ 7yr TT power spectrum (Komatsu et al. 2010)

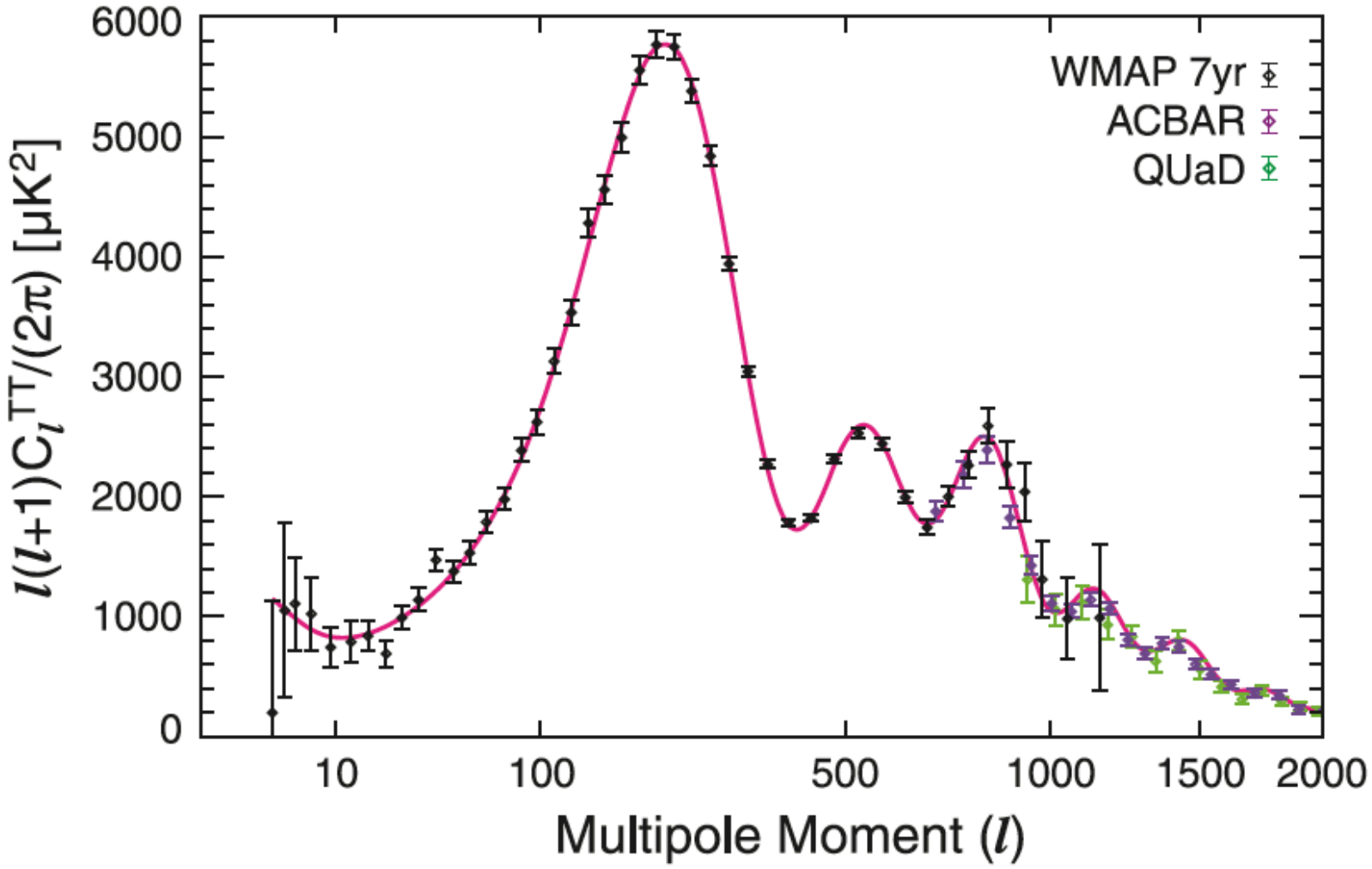

Courtesy WMAP Science Team

Table 3
Six-Parameter ΛCDM Fit [a]

Parameter	7-year Fit	5-year Fit
Fit parameters		
$10^2\Omega_b h^2$	$2.258^{+0.057}_{-0.056}$	2.273 ± 0.062
$\Omega_c h^2$	0.1109 ± 0.0056	0.1099 ± 0.0062
Ω_Λ	0.734 ± 0.029	0.742 ± 0.030
$\Delta^2_{\mathcal{R}}$	$(2.43 \pm 0.11) \times 10^{-9}$	$(2.41 \pm 0.11) \times 10^{-9}$
n_s	0.963 ± 0.014	$0.963^{+0.014}_{-0.015}$
τ	0.088 ± 0.015	0.087 ± 0.017
Derived parameters		
t_0	13.75 ± 0.13 Gyr	13.69 ± 0.13 Gyr
H_0	71.0 ± 2.5 km/s/Mpc	$71.9^{+2.6}_{-2.7}$ km/s/Mpc
σ_8	0.801 ± 0.030	0.796 ± 0.036
Ω_b	0.0449 ± 0.0028	0.0441 ± 0.0030
Ω_c	0.222 ± 0.026	0.214 ± 0.027
z_{eq}	3196^{+134}_{-133}	3176^{+151}_{-150}
z_{reion}	10.5 ± 1.2	11.0 ± 1.4

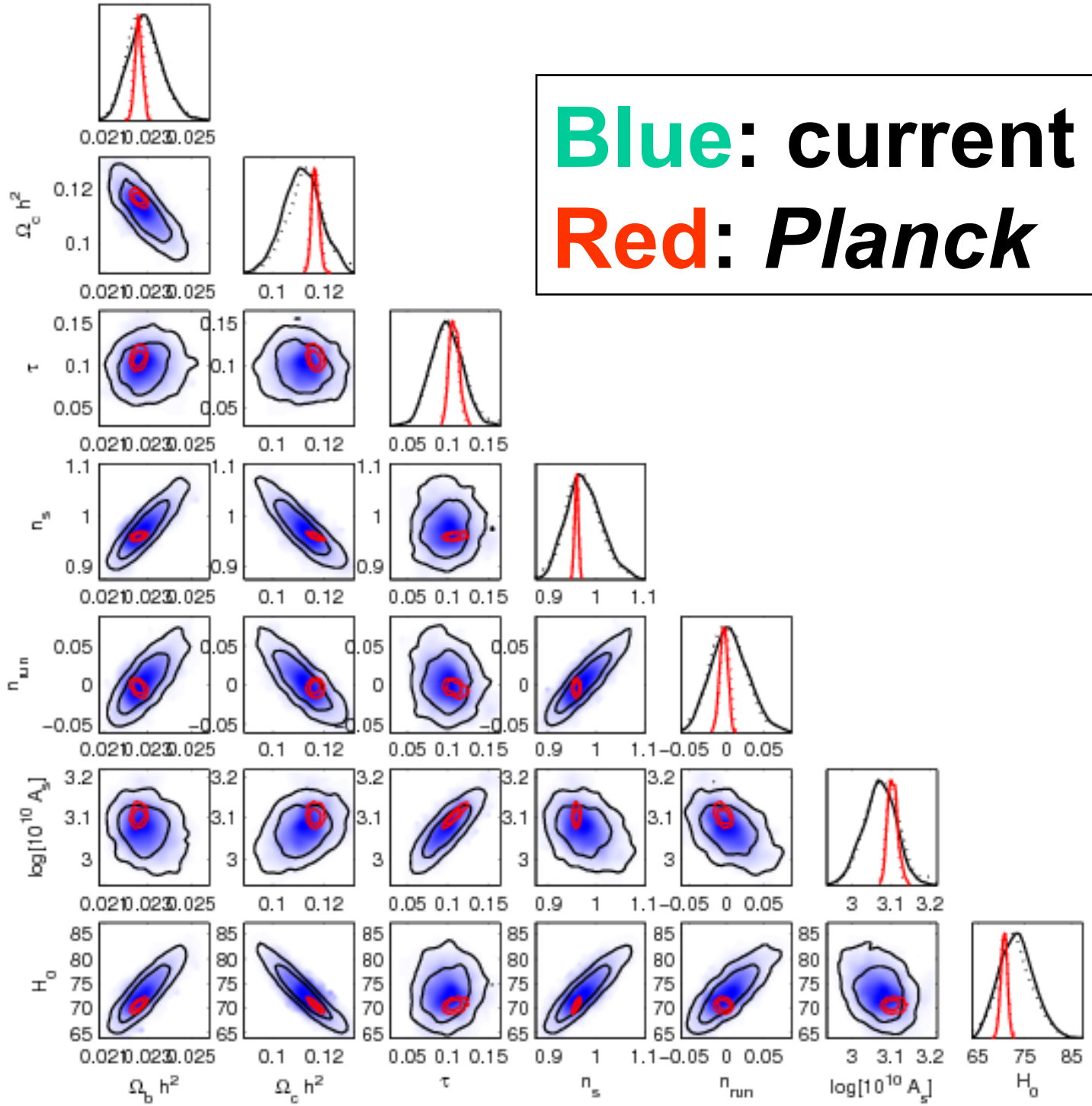

Blue: current data

Red: *Planck*

New Measurements, More Parameters !

- Neutrino masses Σm_ν
- Neutrino effective number N_ν^{eff}
- Primordial Helium Y_P

Small scale CMB can probe Helium abundance at recombination

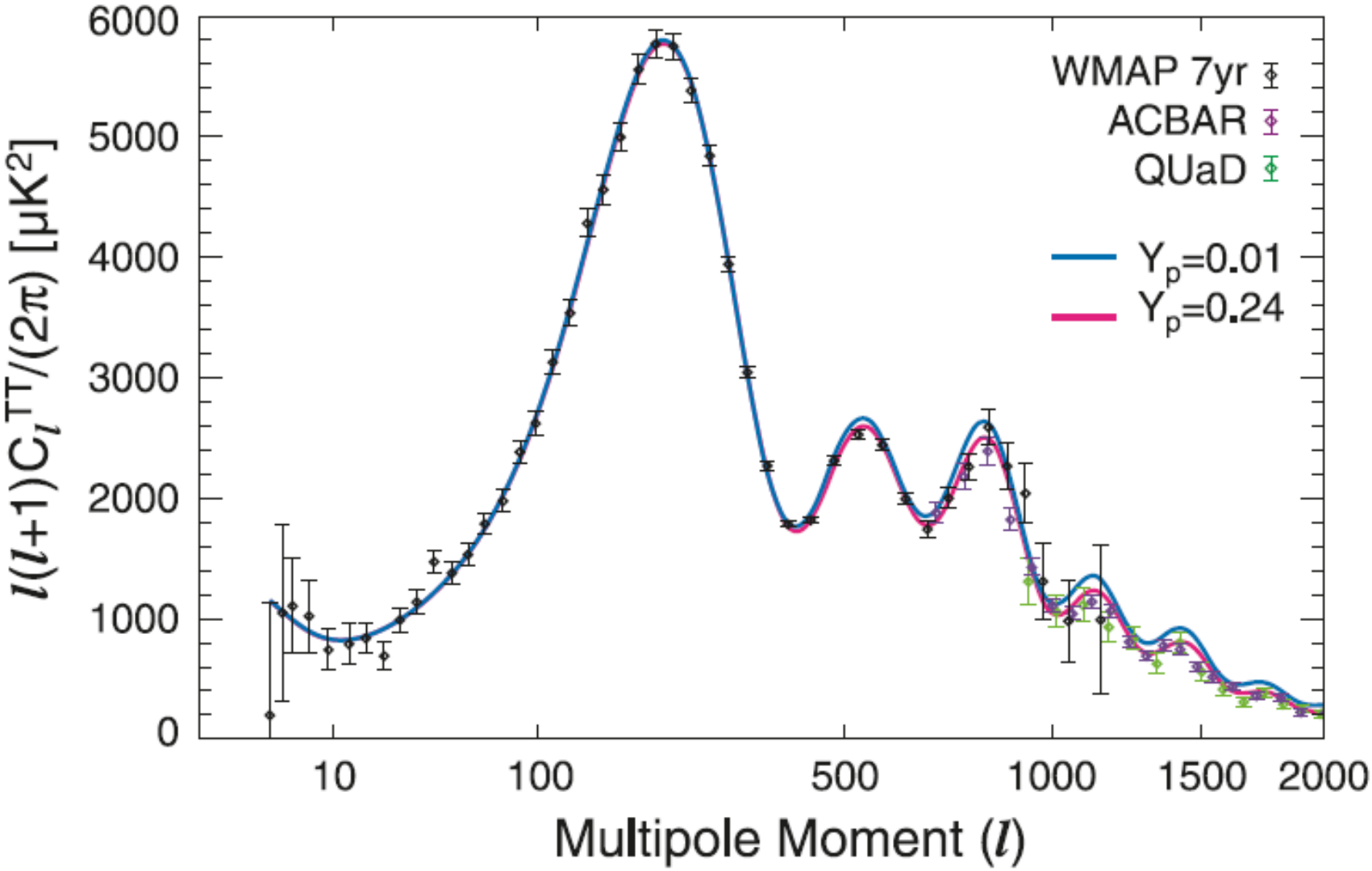

WMAP constraints

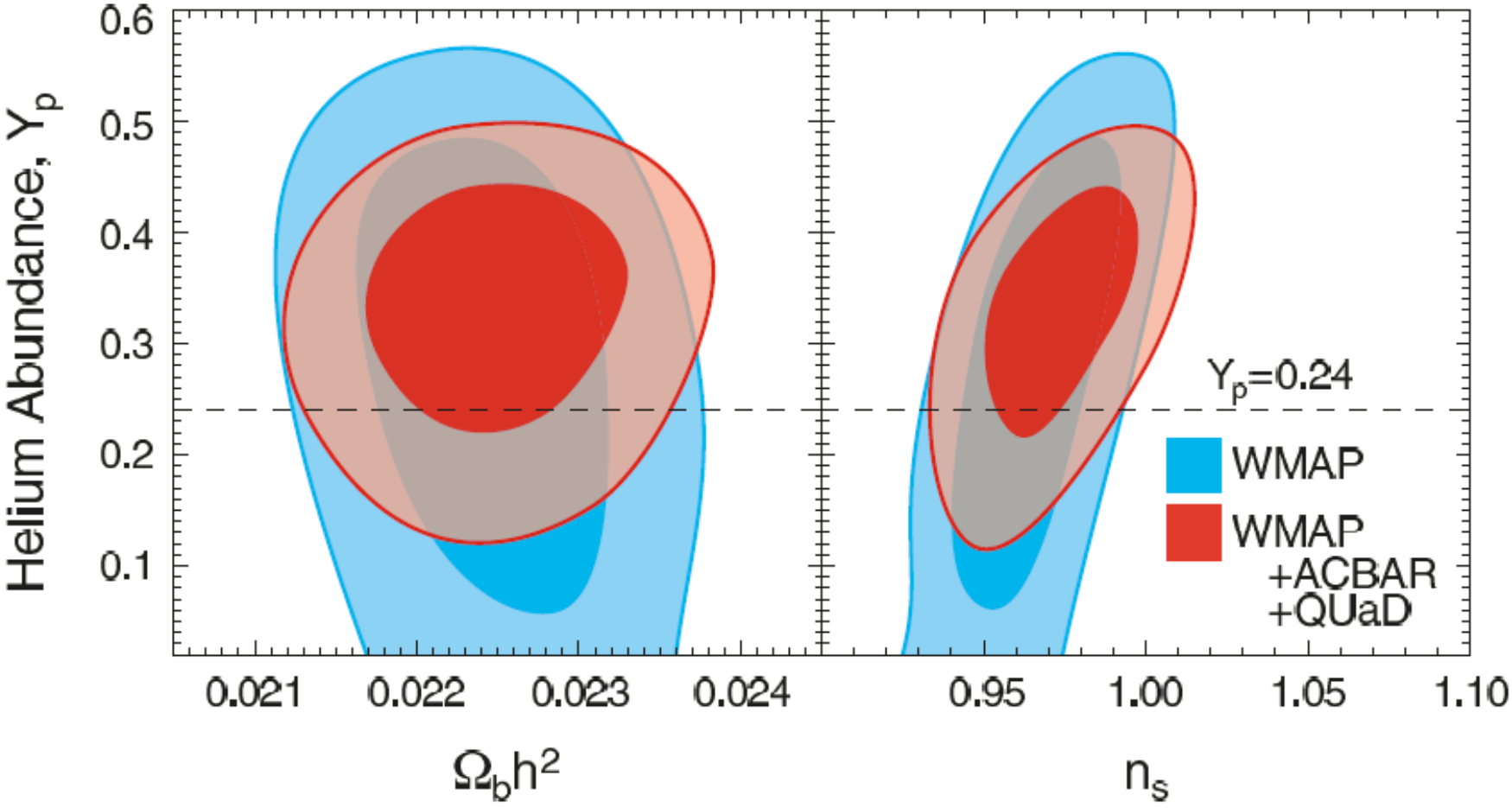

	WMAP only	*WMAP*+ACBAR+QUaD
Y_p	< 0.51 (95% CL)	$Y_p = 0.326 \pm 0.075$ (68% CL)[b]

Komatsu et al, 2010, 1001.4538

Forecasts on Helium Abundance

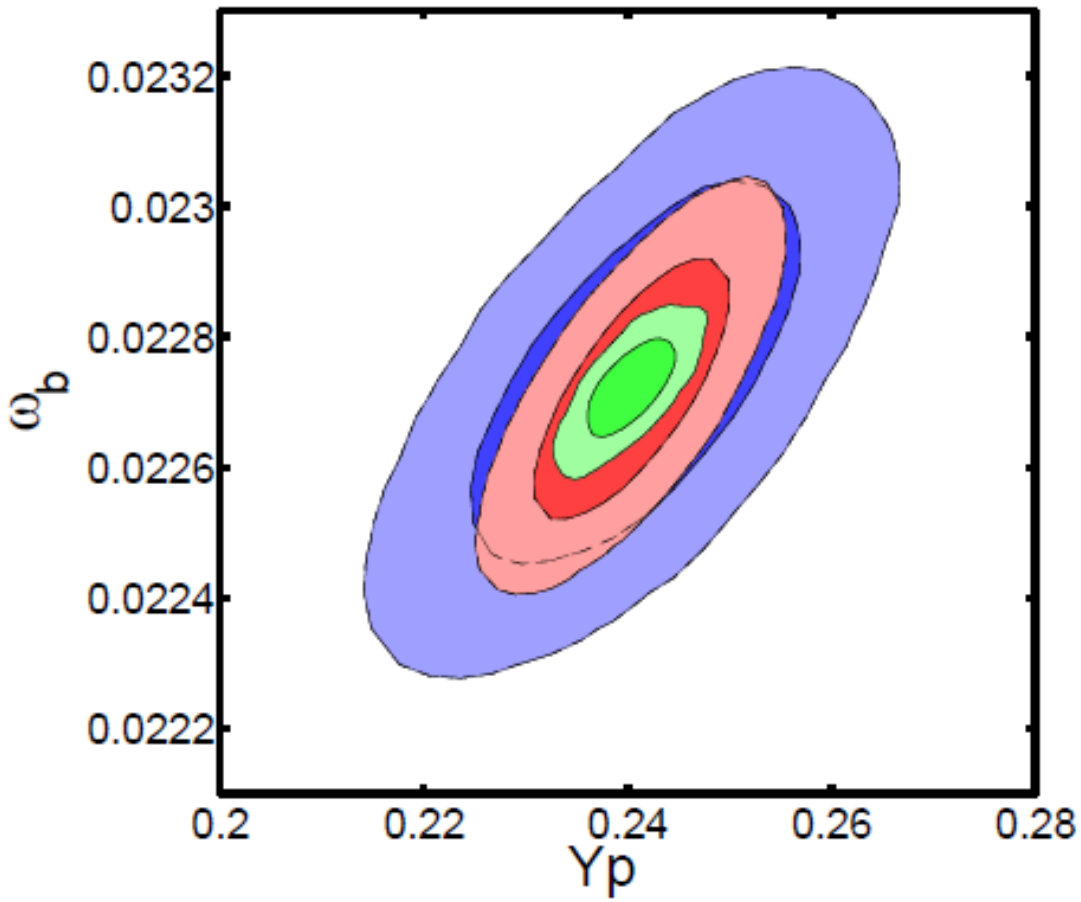

Blue: Planck
$\Delta Yp=0.01$

Red: Planck+ACTpol
$\Delta Yp=0.006$

Green: COrE
$\Delta Yp=0.003$

Galli, Martinelli, Melchiorri, Pagano, Sherwin, Spergel, PRD submitted, **arXiv:1005.3808** 2010

Current constraints on neutrino mass from Cosmology

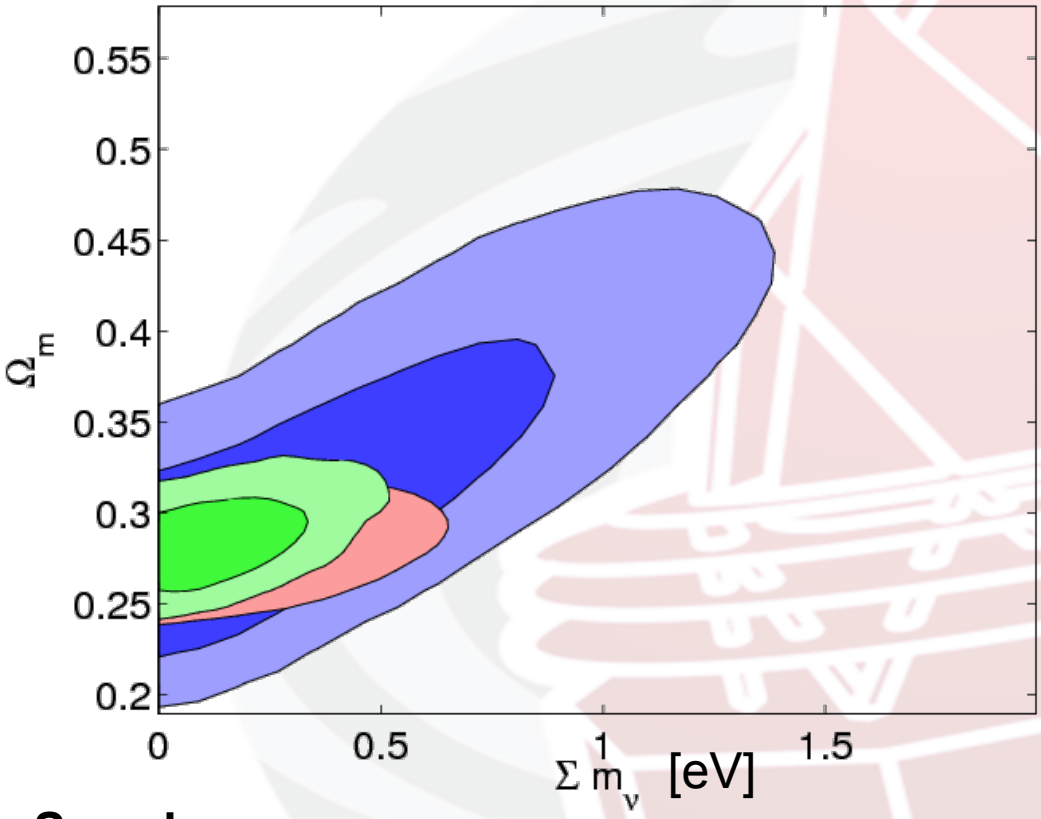

Blue: WMAP-7
Red: w7+SN+Bao+H0
Green: w7+CMBsuborb+SN+LRG+H0

Current constraints (assuming ΛCDM):

$\Sigma m_\nu < 1.2$ [eV] CMB

$\Sigma m_\nu < 0.7\text{-}0.5$ [eV] CMB+other

$\Sigma m_\nu < 0.3$ [eV] CMB+LSS (extreme)

See also:

M. C. Gonzalez-Garcia, Michele Maltoni, Jordi Salvado, arXiv:1006.3795
Toyokazu Sekiguchi, Kazuhide Ichikawa, Tomo Takahashi, Lincoln Greenhill, arXiv:0911.0976

Extreme (sub 0.3 eV limits):

F. De Bernardis et al, Phys.Rev.D78:083535,2008,
Thomas et al. Phys. Rev. Lett. 105, 031301 (2010)

Current constraints on neutrino mass from Cosmology (Fogli et al., 2010 in preparation).

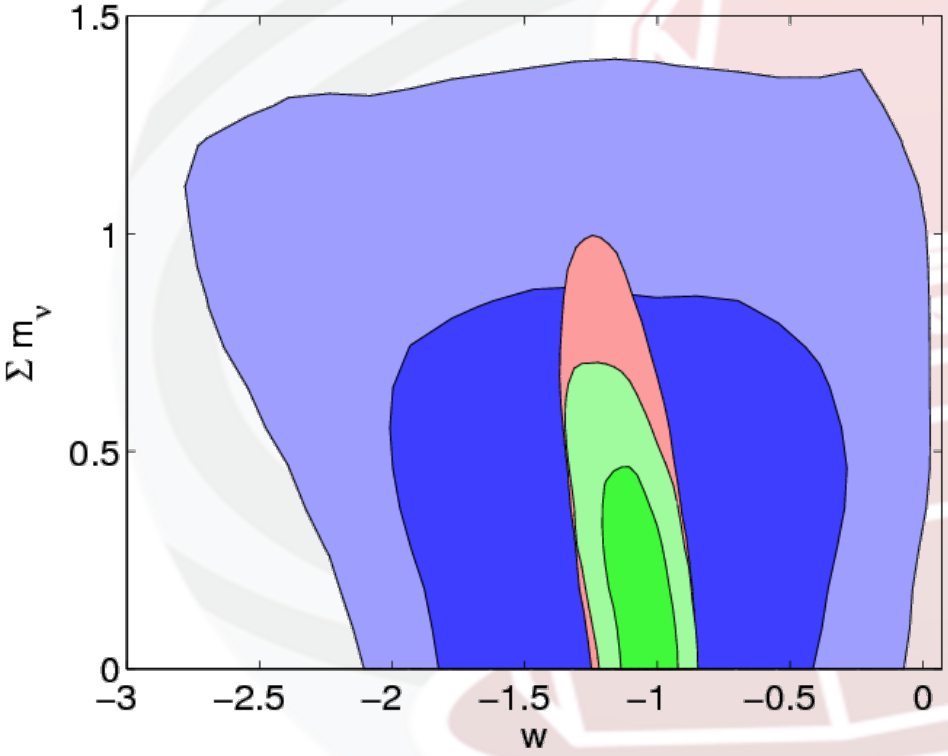

Blue: WMAP-7
Red: w7+SN+Bao+H0
Green: w7+CMBsuborb+SN+LRG+H0

Constraints weaken by 30-50% when «dark energy» is included.

Forecasts on Neutrino Number & Mass

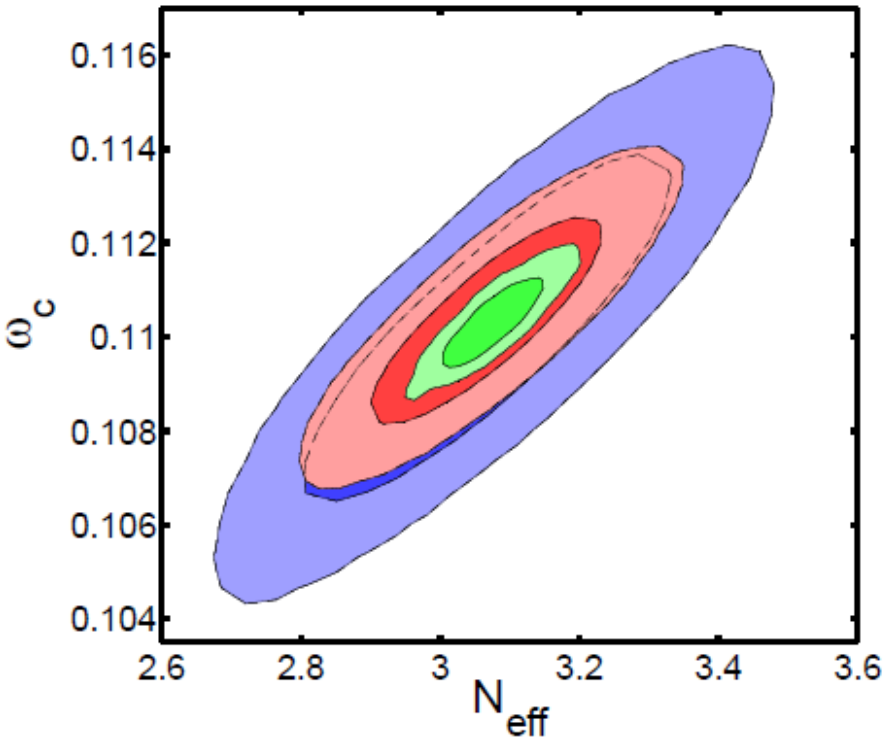

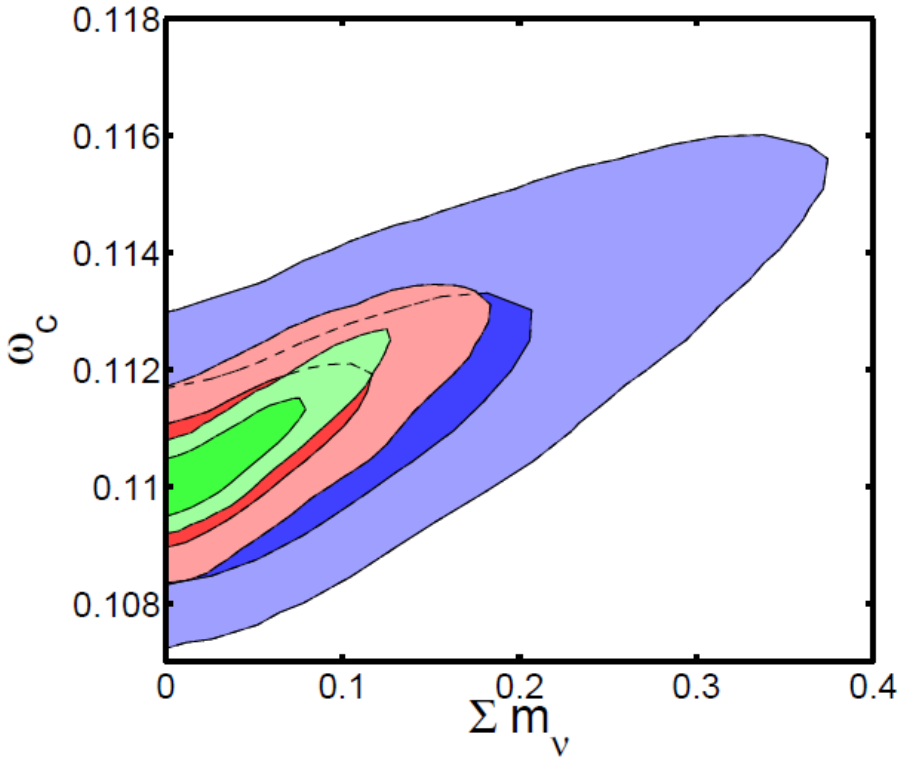

Blue: Planck $\Delta N_\nu=0.18$
Red: Planck+ACTpol $\Delta N_\nu=0.11$
Green: CMBPol $\Delta N_\nu=0.044$

Blue: Planck $\Delta\Sigma m_\nu=0.16$
Red: Planck+ACTpol $\Delta\Sigma m_\nu=0.08$
Green: CMBPol $\Delta\Sigma m_\nu=0.05$

Galli, Martinelli, Melchiorri, Pagano, Sherwin, Spergel,
PRD submitted, **arXiv:1005.3808** 2010

What is the Parity Transformation?

It is the transformation that is applied when we look at the world in a mirror.
In math it is the flip of sign of one spatial coordinate.
In three dimensions it is equivalent to the flips of all the 3 spatial dimensions (note that the flip of signs of 2 axes in 3 dimensions is equivalent to a rotation).
The determinant of a Parity transformation is -1 (whereas a Rotation has determinant =1)

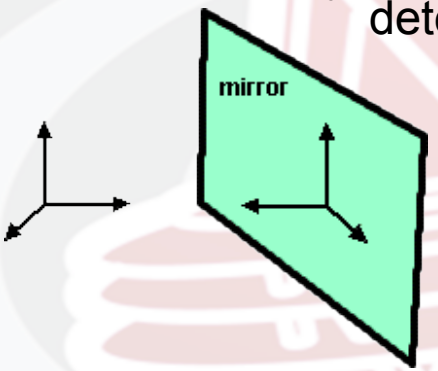

$$\begin{cases} x \rightarrow -x \\ y \rightarrow -y \\ z \rightarrow -z \end{cases}$$

If Physics equations are invariant under Parity then we say that Parity is conserved.

Specifically **Parity is conserved in electromagnetic interactions** (as well as in gravity and strong interactions) whereas is broken in weak interactions.

CMB physics is purely electromagnetic. Therefore through CMB anisotropies we can study whether the Lagrangian of the photon is Parity conserved as we expect. This analysis might help in constraining Parity-violating terms that can be introduced.

Algebraic Properties for Testing Parity in CMB Temperature Map

spherical harmonics expansion for **T anisotropies**

$$a_{T,\ell m} = \int d\Omega\, Y^{\star}_{\ell m}(\hat{n})\, T(\hat{n})$$

Parity

$$\hat{n} \rightarrow -\hat{n}$$

Property

$$a_{T,\ell m} \rightarrow (-1)^{\ell}\, a_{T,\ell m}$$

behavior of T coefficients of spherical harmonics under parity symmetry (i.e. even multipoles are invariant under parity whereas odd multipoles acquire a “-1”)

CMB physics does not distinguish between even and odd multipoles. For example at low ell the TT power spectrum is given by the so called Sachs - Wolfe plateau that reads:

$$\ell(\ell+1)C_{\ell}^{TT} \sim const$$

Therefore it is possible to divide each T map in two subsets corresponding to even and odd multipoles, satisfying two different transformation under P symmetry. Considering the angular power spectrum contained in the two subsets it is possible to study the consistency with P symmetry

Algebraic Properties for Testing Parity in CMB Polarization Maps

spherical harmonics expansion for **PoI anisotropies**

$$a_{\pm 2,\ell m} = \int d\Omega\, Y^{\star}_{\pm 2,\ell m}(\hat{n})(Q(\hat{n}) \pm iU(\hat{n}))$$

Parity

$\hat{n} \rightarrow -\hat{n}$

Property

$$a_{E,\ell m} = (-1)^{\ell} a_{E,\ell m}$$
$$a_{B,\ell m} = (-1)^{\ell+1} a_{B,\ell m}$$

$$a_{E,\ell m} = -(a_{2,\ell m} + a_{-2,\ell m})/2$$
$$a_{B,\ell m} = -(a_{2,\ell m} - a_{-2,\ell m})/2i$$

Similar consideration previously expressed for T can be applied to the E mode and (potentially) to the B mode

Moreover the opposite behavior of B w.r.t. T or E, forces the cross-correlations <T B> and <E B> to be vanishing in order to be consistent with Parity symmetry!

Testing parity (P) symmetry: definition of estimators

For X = TT, TE, EE and BB:

$$R^X = C_+^X / C_-^X$$

$$D^X = C_+^X - C_-^X$$

$$C_{+/-}^X \equiv \frac{1}{(\ell_{max}-1)} \sum_{\ell=2,\ell_{max}}^{+/-} \frac{\ell(\ell+1)}{2\pi} \hat{C}_\ell^X$$

(Kim & Naselsky, 2010)

For X = TB and EB:

$$C^X \equiv \frac{1}{(\ell_{max}-1)} \sum_{\ell=2,\ell_{max}} \frac{\ell(\ell+1)}{2\pi} \hat{C}_\ell^X$$

these estimators have been computed at large angular scale considering an optimal APS estimator. A MC of 10000 realizations with realistic noise (both for WMAP 7 and Planck) has been performed

(Gruppuso et al., MNRAS, 2010)

TT results (WMAP 7)

$\delta\ell = [2, 22]$ $\delta\ell = [2, 33]$

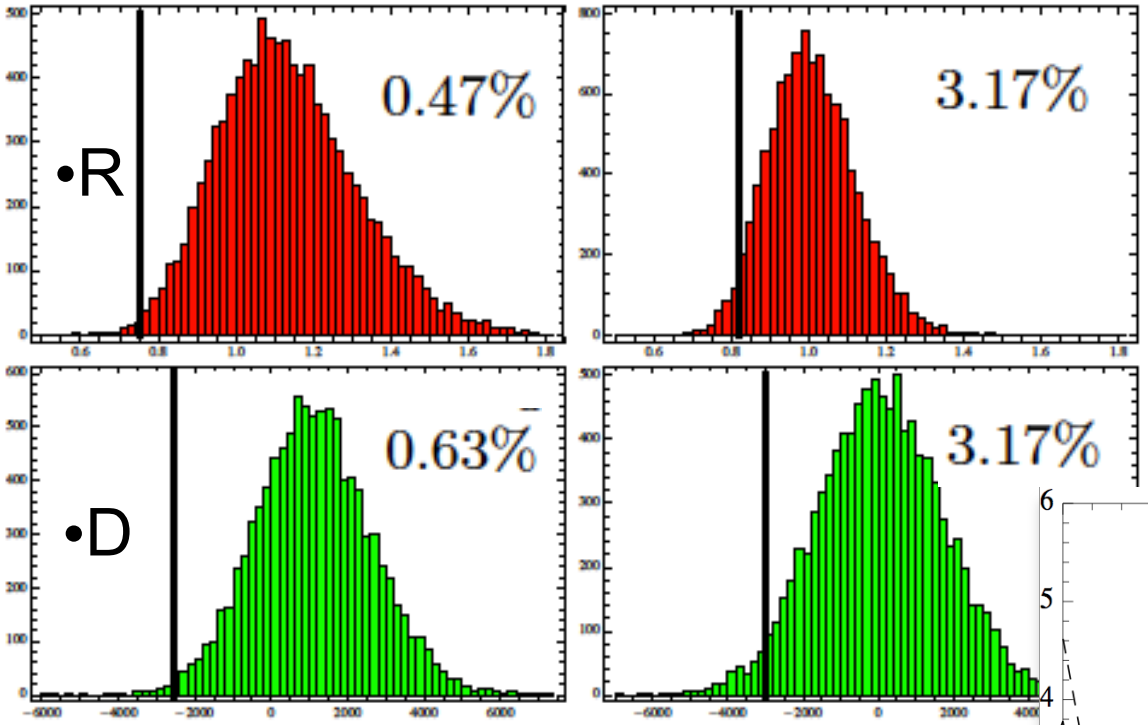

Percentage vs angular scale

solid line: R estimator

dashed line: D estimator

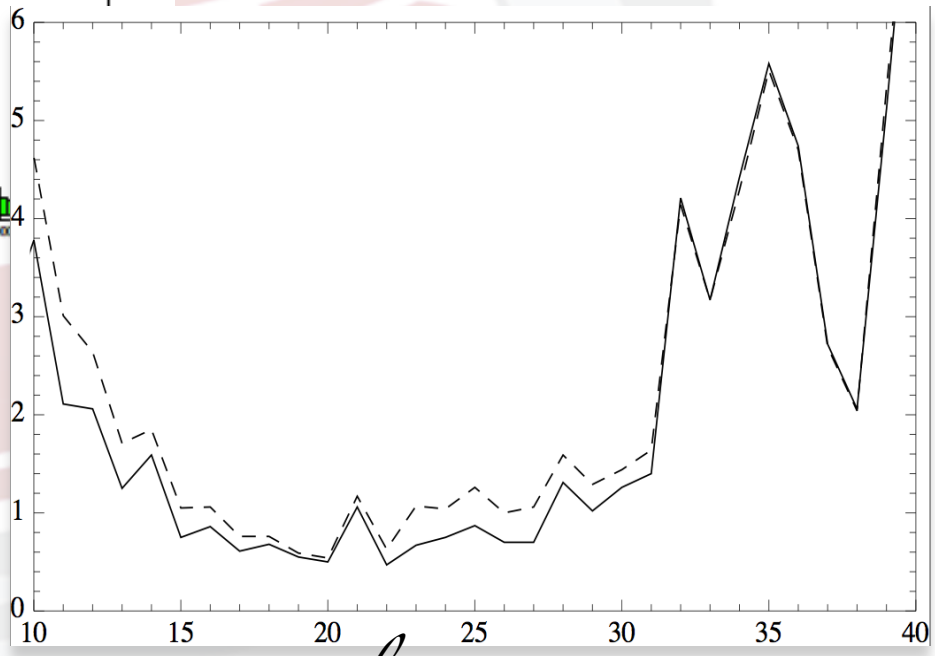

This plot suggests the existence of a characteristic scale lying in the range between 15 and 24 for which the estimators might be considered “anomalous” (<1%)

Considerations on this Parity analysis

TT anomaly detected @ large angular scale with a confidence level of 99.5% in the WMAP 7 data.

1. matter of taste if such percentage is to be considered anomalous
2. It is still unknown whether such a result comes from fundamental physics or if it is due to some not perfectly removed astrophysical foreground or systematic effect

Polarization analysis of the WMAP 7 data does not show any deviation from Parity symmetry but:

1. This might be due to the large WMAP 7 noise level that make the signal sinking
2. If ell_max is too large the considered estimators are testing the Parity of the WMAP noise

Planck data are awaited with great interest in this respect because:

1. Planck is observing the sky with a totally different scanning strategy wrt WMAP (benefit from the point of view of systematic effects analysis)
2. Confirm TT anomaly and extend the Polarization analysis

Planck forecasts (e.g. 143 GHz channel)

- Standard deviations for D

σ_D	WMAP 7 year	Planck
TT	1517.17	1509.21
TE	20.19	9.08
EE	0.65	0.10
BB	0.69	0.04

- Standard deviations for C

σ_C	WMAP 7 year	Planck
TB	0.95	0.19
EB	0.023	0.001

Planck is much more sensitive to polarization estimators

- R on EE

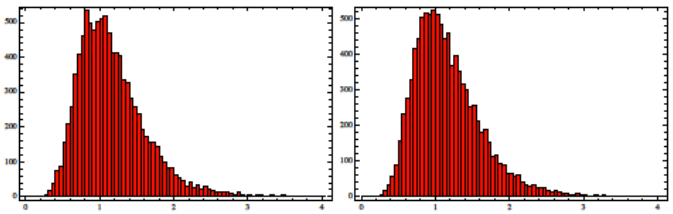

$\delta\ell = [2, 22]$ $\delta\ell = [2, 16]$

Testing CPT Symmetry

If terms like Chern-Simons have to be added to the standard electrodynamic Lagrangian, than Lorentz, P and CPT symmetries will be violated. This will induce a rotation of the polarization direction of each photon as it propagates from the LSS to us. This effect is called "Cosmic Birefringence"

$$C_\ell^{\mathrm{TE,obs}} = C_\ell^{\mathrm{TE}} \cos(2\Delta\alpha),$$

$$C_\ell^{\mathrm{TB,obs}} = C_\ell^{\mathrm{TE}} \sin(2\Delta\alpha),$$

$$C_\ell^{\mathrm{EE,obs}} = C_\ell^{\mathrm{EE}} \cos^2(2\Delta\alpha),$$

$$C_\ell^{\mathrm{BB,obs}} = C_\ell^{\mathrm{EE}} \sin^2(2\Delta\alpha),$$

$$C_\ell^{\mathrm{EB,obs}} = \tfrac{1}{2}(C_\ell^{\mathrm{EE}}) \sin(4\Delta\alpha).$$

alpha = Birefringence angle

From these equations it is possible to build estimators for alpha
(as long as it is zero these violating terms are excluded)

Current constraints

- WMAP 7 (Komatsu et al. 2010, in press in ApJS)

$$\Delta\alpha = -0.9^\circ \pm 1.4^\circ \qquad 23 < \ell < 800$$
$$\Delta\alpha = -3.8^\circ \pm 5.2^\circ \qquad 2 \leq \ell \leq 23$$

- QUAD (Wu et al. 2010, PRL)

$$\Delta\alpha = 0.83^\circ \pm 0.94^\circ \pm 0.5^\circ \quad 200 < \ell < 2000$$

Planck and CMBPol forecast

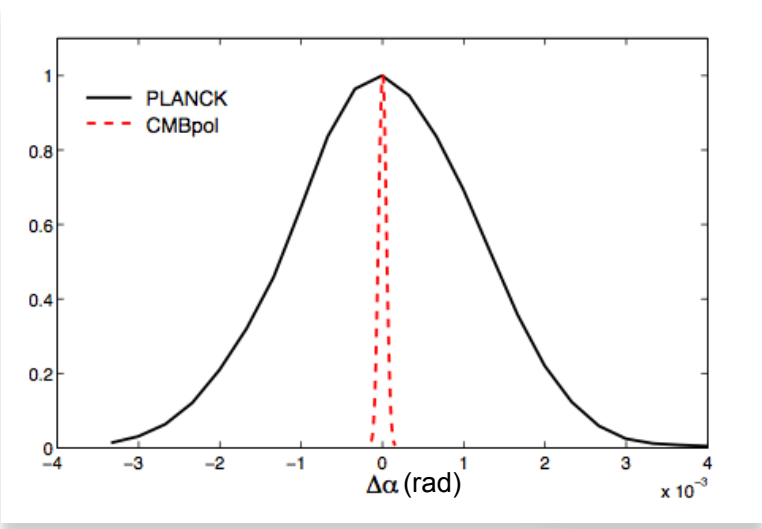

Xia et al. (2009), IJMPD

$\sigma = 0.057^\circ$ Planck

$\sigma = 2.57^\circ \times 10^{-3}$ CMBPol

Planck & B-modes

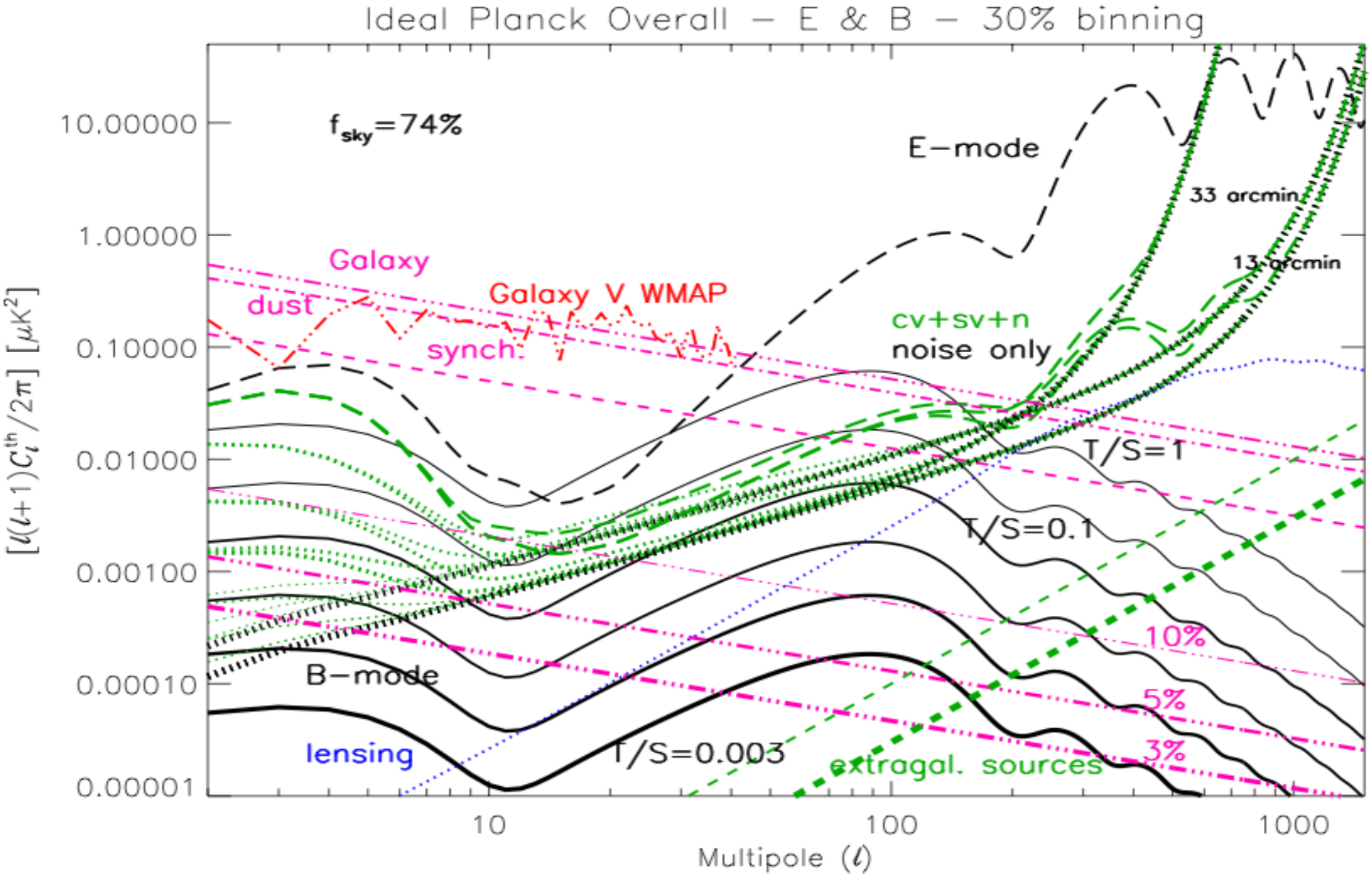

A remarkable example

A specific class of theoretical models - A toy model for foreground residuals

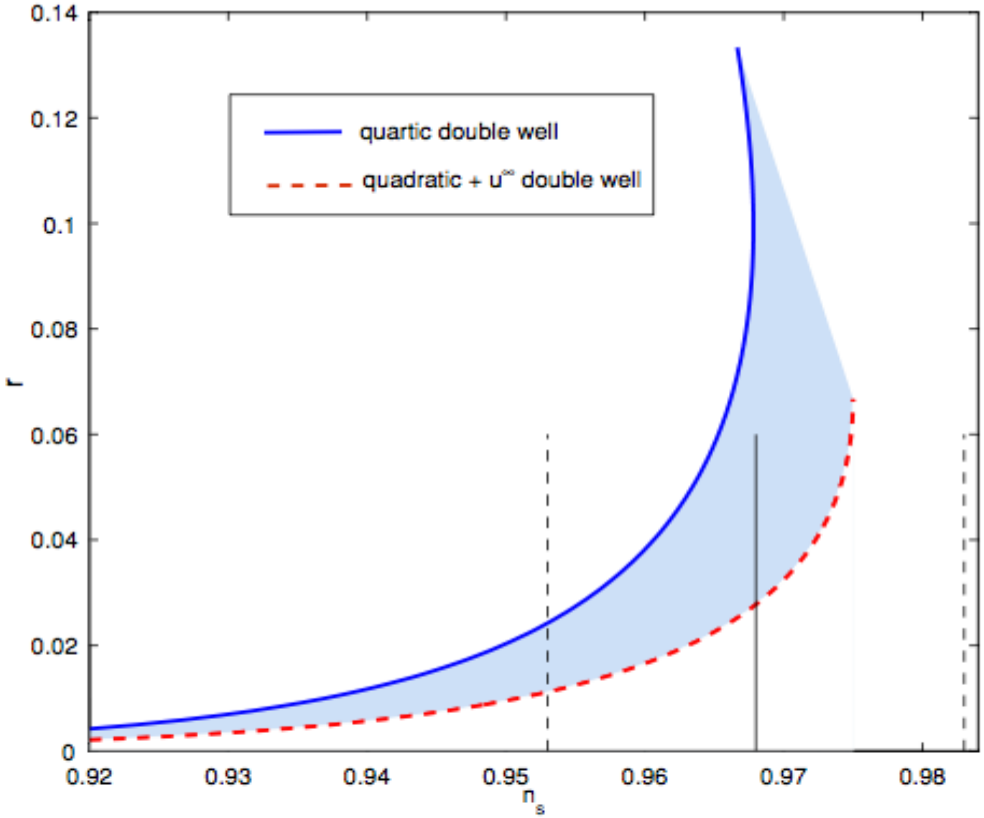

Figure 1. Universal banana region $\mathcal{B}$ in the (n_s, r)-plane setting $N = 60$. The upper border of the region $\mathcal{B}$ corresponds to the fourth-order double-well potential expressed by Equation (1). The lower border is described by the potential $V(\varphi) = \frac{1}{2}m^2(\frac{m^2}{\lambda} - \varphi^2)$ for $\varphi^2 < m^2/\lambda$ and $V(\varphi) = \infty$ for $\varphi^2 > m^2/\lambda$ (Destri et al. 2009). We display in the vertical full line the ΛCDM*r* value $n_s = 0.968 \pm 0.015$ using the *WMAP*+BAO+SN data set. The broken vertical lines delimit the $\pm 1\,\sigma$ region.

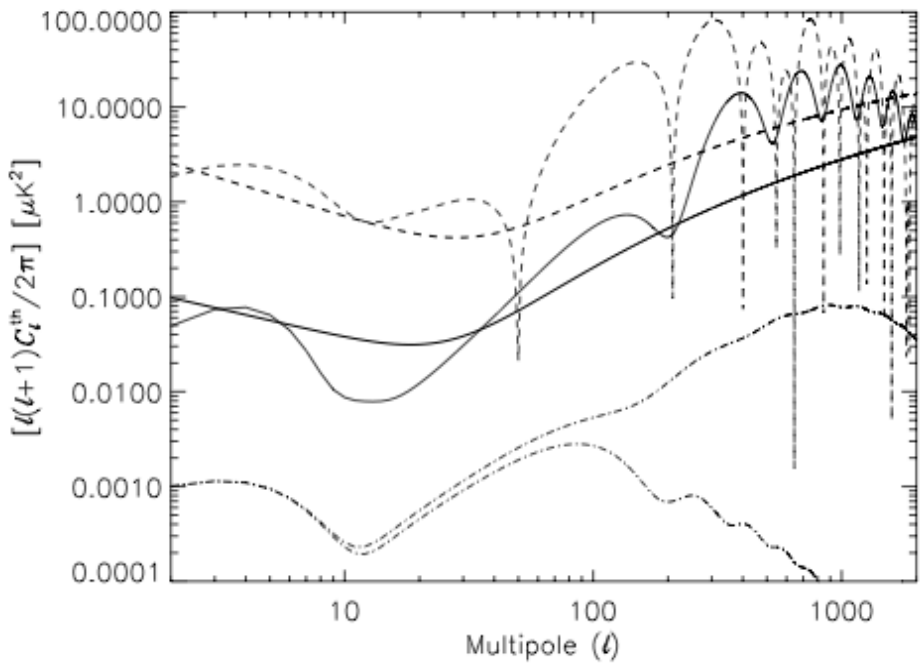

Comparison between our model of foreground residual in the *E mode (solid line) and in the TE mode (dashes) with a typical CMB angular power spectrum for the same modes and our fiducial B mode (i.e., with r = 0.0427) including (upper dash-dotted line) or not including (lower dash-dotted line) the contribution by lensing. Foreground residuals in the B modes are assumed equal to those in the E modes.*

From Burigana, Destri, de Vega, Gruppuso, Mandolesi, Natoli, Sanchez, 2010, ApJ, 724, 588

Cumulative three-channel marginalized likelihood distributions, including *B modes and foreground residuals, of the cosmological parameters for the ΛCDMr model. The fiducial ratio r = 0.0427.*
We plot the distributions in four cases:
(blue) without residuals,
(red dashes) with 30% of a toy model residuals in the TE and E modes and 16μK² in the T modes,
(violet dash-dots) with a toy model residuals in the TE and E modes and 160μK² in the T modes,
(green) with 65% of a toy model residuals in the TE and E modes and 88μK² in the T modes rugged by Gaussian fluctuations of 30% relative strength.

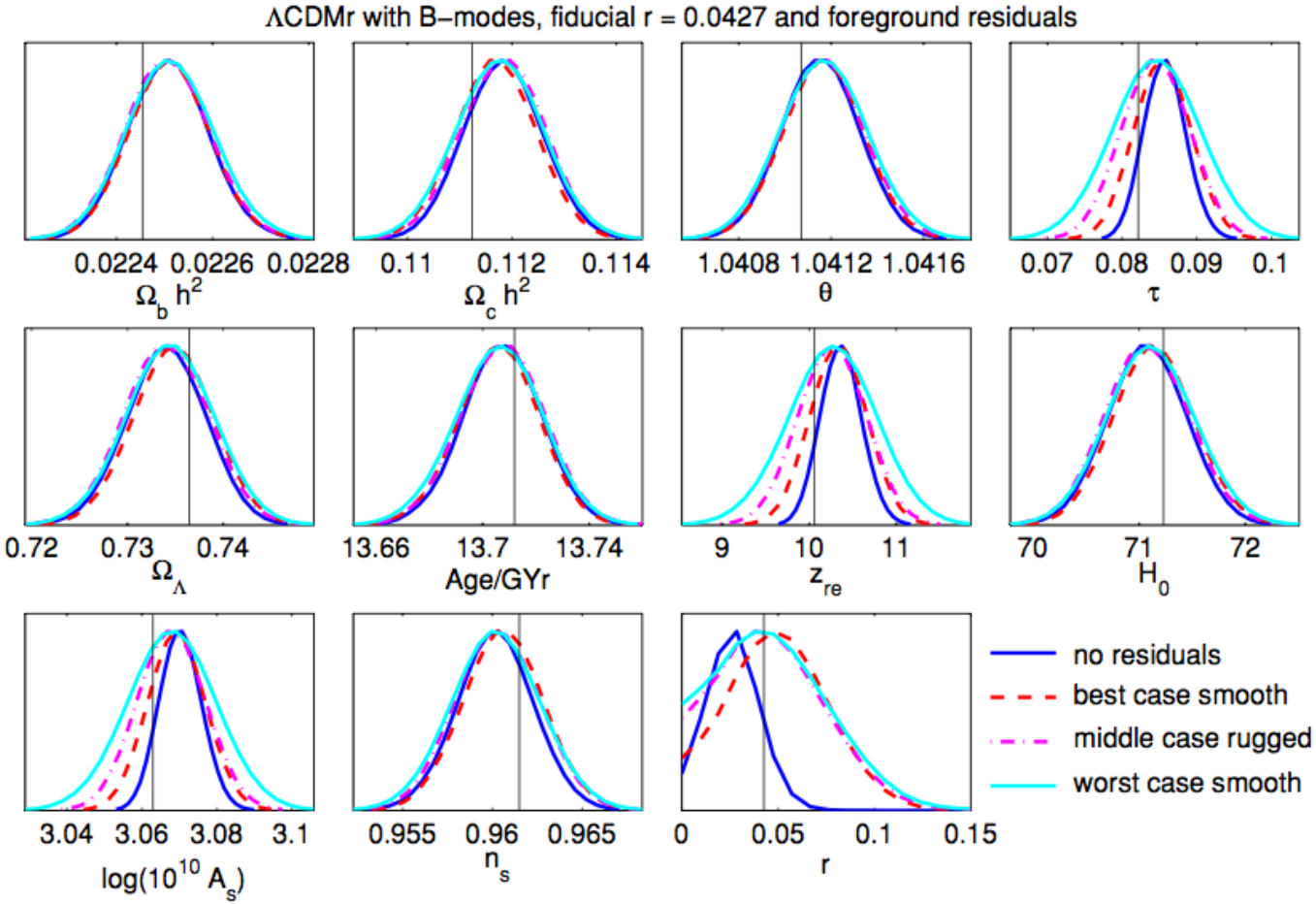

Planck
28 months
of integration

From
Burigana, Destri, de Vega,
Gruppuso, Mandolesi,
Natoli, Sanchez,
2010, ApJ, 724, 588

Cumulative marginalized likelihoods from the three channels for the cosmological parameters for the ΛCDM*rT model including B modes and fiducial ratio r = 0.0427 and the foreground residuals. We plot the cumulative likelihoods in four cases:*
(violet dash-dots) without residuals,
(blue) with 0.3 of the worst case residuals in the TE and E modes and 16μK2 in the T modes,
(red dashes) with the worst case residuals in the TE and E modes and 160μK2 in the T modes,
(green) with 65% of the toy model residuals in the TE and E modes displayed in Figure 2 and 88μK2 in the T modes rugged by Gaussian fluctuations of 30% relative strength.

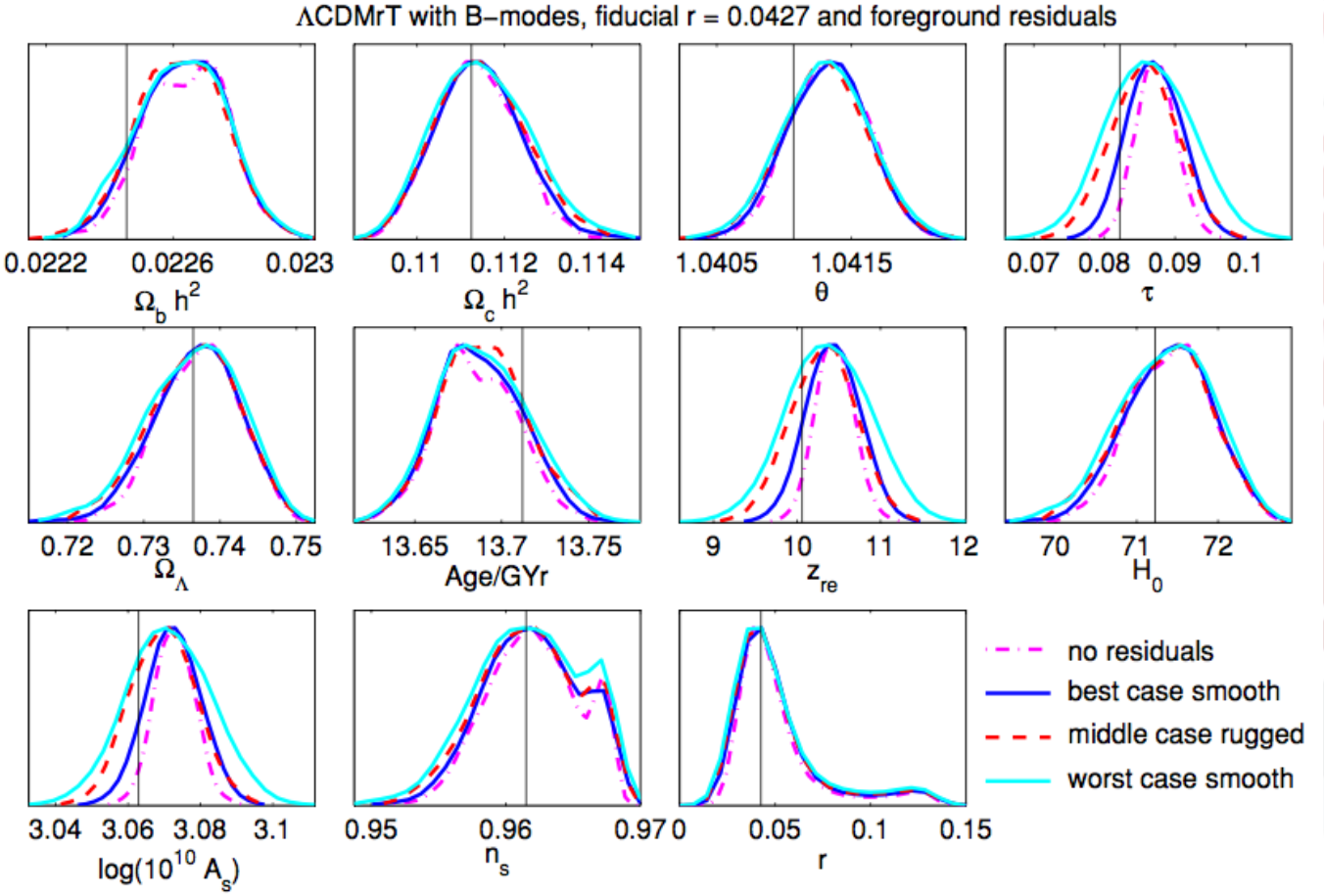

Planck
28 months
of integration

From
Burigana, Destri, de Vega,
Gruppuso, Mandolesi,
Natoli, Sanchez,
2010, ApJ, 724, 588

Conclusions

- ***Planck*** **is working as expected**
- **DPCs, instruments, CTs, WGs are working well & intensively to produce accurate TOD, frequency maps, component maps, source catalogs & to scientifically analyze data**

- ***Planck is probed to be a powerful "astrophysical surveyor" & we are working to deliver products (2013-2014) & cosmological results (2013-2014)***

- **So … the future will be bright for**
  - **CMB & cosmological "main" science**
  - **Galactic & extragalactic "secondary" science**

Thanks for your attention!

Acknowledgements

- **I warmly acknowledge the *Planck* Collaboration**

- ***Planck* is an ESA project with instruments funded by ESA member states (in particular the PI countries: France and Italy), and with special contributions from Denmark and NASA (USA)**